

Division of Molecular Therapeutics and Formulation,

School of Pharmacy

Children's Brain Tumour Research Centre,

School of Medicine

Nanotherapeutics as a localised drug delivery system for the treatment of GBM

Catherine Vasey

BSc

Thesis submitted to the University of Nottingham for the degree of

Doctor of Philosophy

September 2020

COVID-19 IMPACT STATEMENT

- Travel to UCLouvain, Belgium for completion of animal studies was due to take place in March 2020. This had been arranged in October 2019, and the dates finalised in January 2020. All materials were resynthesised at the start of the year and sent to Belgium for the study. The study was to consist of a dose escalation study, followed by a therapy study. This large section of work was set to comprise the final Results Chapter and prove or disprove the overarching PhD hypothesis.
- Regarding general experimental plans, due to University closure, completion of TEM, confocal microscopy, flow cytometry and clonogenic assays were unable to be completed as originally planned.
- I was offered a six month costed extension to complete the outlined work above. However, I was successful in securing a senior formulation scientist role at AstraZeneca, starting in September 2020 so declined the costed extension.

ABSTRACT

Glioblastoma multiforme (GBM) (recently classified by the World Health Organisation as glioblastoma isocitrate dehydrogenase wild-type or mutant), is the most common, malignant brain tumour in adults, mainly due to its rapid proliferation and ability to penetrate and diffusely infiltrate healthy brain parenchyma. Standard of care treatment consists of surgical debulking of the tumour, followed by an intense course of concomitant chemotherapy and radiotherapy. However, despite these multimodal treatment methods, and a greater understanding of disease biology, prognosis remains bleak with a median survival of 14 months from diagnosis.

This front-line treatment whereby tumours are neurosurgically-resected, poses a distinct opportunity for the consideration of localised, intracranial therapy for GBM patients, hereby overcoming the blood-brain barrier (BBB) and enabling the delivery of therapeutics directly to the site of the infiltrative disease left behind following surgical resection. The overarching aim of this thesis is to design and synthesise drug-loaded nanocarriers which can be incorporated into a pre-existing microparticulate paste to act as a localised drug delivery system for the treatment of GBM.

Chapter 2 details the design and synthesis of a library of these drug-loaded nanocarriers, optimising an established ring-opening

polymerisation (ROP) method to enable a user-friendly approach with a fast reaction time, resulting in polymers with highly predictable final molecular weights and narrow molar mass dispersities (Đ). The introduction of a functionalisable monomer enabled the conjugation of doxorubicin (DOX), a relevant chemotherapeutic, to the polymeric backbone. The resultant polymers were able to reproducibly self-assemble to form kinetically-trapped nanoparticles (NPs) with narrow polydispersity indexes (PDIs).

Chapter 3 details the cytotoxicity of the DOX-NPs on a range of GBM cell lines. Considering the inevitable recurrence of GBM is due to the infiltrative cells left behind following surgical removal of the original tumour, the NPs were tested upon a range of patient derived cell lines isolated from this infiltrative region, allowing a more clinically-relevant insight into the activity of the formulations.

Overall, the results from this thesis highlight the potential of incorporating drug-loaded NPs into a pre-existing microparticulate paste, for the first time in neuro-oncology, building a platform technology for future *in vivo* studies to investigate the potential efficacy of this delivery system as a localised treatment method for GBM.

OUTPUTS

PUBLICATIONS

- **C.E. Vasey*,** P. McCrorie*, S.J. Smith, M. Marlow, C. Alexander and R. Rahman. Biomedical engineering approaches to enhance therapeutic delivery for malignant glioma. *Journal of Controlled Release.* (2020) doi: 10.1016/j.jconrel.2020.11.022
- V. Taresco, T.F. Abelha, R.J. Cavanagh, **C.E. Vasey,** A.B. Anane-Adjei, A.K. Pearce, P.F. Monterio, K.A. Spriggs, P. Clarke, A. Ritchie, S. Martin, R. Rahman, A.M. Grabowska, M.B. Ashford and C. Alexander. Functionalized block co-polymer pro-drug nanoparticles with anti-cancer efficacy in 3D spheroids and in an orthotopic triple negative breast cancer model. *Adv. Therap.* (2020). doi: 10.1002/adtp.202000103
- C. Greco, V. Taresco, A.K. Pearce, **C.E. Vasey**, S. Smith, R. Rahman, C. Alexander, R.J. Cavanagh, F. Musumeci, and S. Schenone. Development of Pyrazolo[3,4-d]pyrimidine Kinase Inhibitors as Potential Clinical Candidates for Glioblastoma Multiforme. *ACS Med. Chem. Lett*. (2020). doi: 10.1021/acsmedchemlett.9b00530
- F. Sodano, R.J. Cavanagh, A.K Pearce, L. Lazzarato, B. Rolando, A. Fraix, T.F. Abelha, **C.E. Vasey**, C. Alexander, V. Taresco and S. Sortino. Enhancing doxorubicin anticancer activity with a novel polymeric platform photoreleasing nitric oxide. *Biomater. Sci.* (2020). doi:10.1039/C9BM01644A

- H. Phan, R.I. Minuet, P. McCrorie, **C.E. Vasey**, R.R. Larder, E. Krumins, M. Marlow, R. Rahman, C. Alexander, V. Taresco and A.K. Pearce. Role of self-assembly conditions and amphiphilic balance on nanoparticle formation of PEG-PDLLA copolymers in aqueous environments. *J. Polym. Sci. Part A Polym. Chem.* (2019). doi:10.1002/pola.29451
- **C.E. Vasey***, A.K. Pearce*, F. Sodano, R.J. Cavanagh, T.F. Abelha, V. Cuzzocoli-Crucitti, A.B. Anane-Adjei, M.B. Ashford, P. Gellert, V. Taresco and C. Alexander. Amphiphilic tri- and tetra-block co-polymers combining versatile functionality with facile assembly into cytocompatible nanoparticles. *Biomater. Sci.* (2019). doi:10.1039/c9bm00667b
- A.K. Pearce, **C.E. Vasey**, A.B. Anane-Adjei, F. Sodano, V. Cuzzocoli-Crucitti, D.J. Irvine, S. Howdle, C. Alexander and V. Taresco. Versatile, Highly Controlled Synthesis of Hybrid (Meth)acrylate–Polyester–Carbonates and their Exploitation in Tandem Post-Polymerization–Functionalization. *Macromol. Chem. Phys*. 2019, 220, 1900270. DOI: 10.1002/macp.201900270
- L.A. Ruiz-Cantu, A.K. Pearce, L. Burroughs, T.M. Bennett, **C.E. Vasey**, R. Wildman, D.J. Irvine, C. Alexander and V. Taresco. Synthesis of methacrylate-terminated block copolymers with reduced transesterification by controlled ring-opening polymerization. *Macromol. Chem. Phys*. 2019, 220, 1800459. DOI: 10.1002/macp.201800459

CONFERENCES

ORAL PRESENTATIONS

- 3 Minute Thesis, University of Nottingham. “Judges Choice Award”.
- The Macro Group UK Young Researchers Meeting, Nottingham, 2020.
- UK Paediatric Brain Tumour Symposium, Nottingham, 2018.
- CDT Colloquia: University of Nottingham, 2019 / AstraZeneca, Macclesfield, 2018 / UCL, London, 2018.

POSTER PRESENTATIONS

- Society for Neuro-Oncology and Society for CNS Interstitial Delivery of Therapeutics Joint Conference on Therapeutic Delivery to the CNS, Phoenix, 2019.
- Controlled Release Society Annual Meeting and Exposition, Valencia, 2019.
- UK and Ireland Controlled Release Society Research Symposium, Belfast, 2018.
- British Neuro-oncology Society, London, 2019.
- The Macro Group UK Young Researchers Meeting, Dublin, 2018.
- Second / Third / Fourth Annual Biomaterials Discovery Workshop, University of Nottingham, 2018 / 2019 / 2020.

ACKNOWLEDGEMENTS

First and foremost, I would like to thank my supervisors, Ruman, Cameron and Stuart. To Ruman, thank you for the weekly pep talks and confidence boosts, for being a general legend - even more so at conferences - and for your infinite knowledge and support. To Cameron, thank you for your infectious enthusiasm, for continually questioning and challenging me to help me grow and become a better scientist. To Stuart, thank you for providing me with an incredible insight to GBM patients and for reminding me why we do the research we do, a factor that has kept me motivated throughout my PhD journey.

To my fantastic post-doc, Dr. Vincenzo Taresco, thank you for taking me under your wing from the very beginning of my PhD journey, for training me in the realm of polymer chemistry, for all the opportunities you have allowed me, for the many, many beers on a Friday night and for being so supportive, caring and patient.

I have been most fortunate to be part of two excellent groups: the CDT in Advanced Therapeutics and Nanomedicine and the Children's Brain Tumour Research Centre. To my CDT family, Dr. Akosua Anane-Adjei, Dr. Sadie Swainson, Rachael, Addie, Paula, Issy, Ania, Steve and Ami, thank you for all the laughs, the much-needed tea breaks, and for generally keeping me sane(ish) throughout my PhD. To my CBTRC family, Hannah, Phoebe, Dr. Macha Aldighieri, Dr. Sophie Roper, Christine, Alice, Louisa, Alina and Louise, thank you for welcoming me into the world of biology, for your patience and guidance, and for sharing my love for food!

Thank you to the brilliant technical teams in both Boots and CBTRC; Colin, Paul, Esme and Doug, and Jonathan, Maria, Lisa, Becky and Franziska for your technical assistance and support. I would like to acknowledge the EPSRC, grant number EP/L01646X/1, for funding this project. To Claudia, our CDT 'Mum', thank you for being a genuinely wonderful human being; we are so lucky to have you within the CDT. Thank you for your continued support and care throughout the four years. Thank you to Carol, Julia and Amy Nairn, three lovely ladies I've had the pleasure of getting to know more over the four years. Thank you to Dr. Robert Cavanagh, for your endless cell knowledge and endless patience with all my questions. To Dr. Rabea Loczenski, thank you for your understanding and for never failing to make me laugh.

I would like to extend my gratitude to my amazing family, to whom I am forever grateful. To my three sisters, Helen, Becky and Sarah, thank you for being the best sisters I could wish for and for your unfailing love and support. To my parents, thank you for being the most incredible role models, for showing me how to "work hard and play hard", and for your never-ending, unconditional love, encouragement and guidance.

Finally, the biggest thank you to Dom. Thank you for allowing me to practise my presentations to you multiple times and not complaining (too much), for always being there to listen, for being my rock and supporting me in good time and bad times, for making sacrifices to come and live in Nottingham, and for (somehow) deciding you want to spend the rest of your life with me.

TABLE OF CONTENTS

Chapter 1 Introduction 1

1.1 Glioblastoma Multiforme 1

1.2 Diagnosis of GBM 3

1.2.1 Clinical presentation 3

1.2.2 Imaging 3

1.3 Management of GBM 4

1.3.1 Surgery 4

1.3.2 Adjuvant therapy 5

1.3.3 Palliative care 8

1.4 Treatment advances 9

1.4.1 Tumour Treating Fields 9

1.4.2 Local delivery 12

1.4.3 PLGA/PEG as a local delivery device 18

1.5 Polymers as drug delivery systems 20

1.5.1 Systemic delivery of NPs for brain tumour therapy 21

1.5.2 Targeting of NPs to GBM following systemic administration 25

1.5.3 Dual targeting of the BBB and GBM 27

1.5.4 Local delivery of NPs for brain tumour therapy 33

1.6 Ring Opening Polymerisation 35

1.6.1 Ring Opening Polymerisation of esters 35

1.6.2 Ring Opening Polymerisation of aliphatic carbonates 36

1.6.3 Catalysts for Ring Opening Polymerisation 36

1.7 Doxorubicin 39

1.7.1 DOX in the treatment of GBM 40

1.8 Project Rationale 47

1.8.1 Overarching hypothesis and aims of project 50

Chapter 2 Preparation of polymeric nanocarriers 51

2.1 Introduction..... 51

2.2 Chapter Hypotheses and Objectives 54

2.2.1 Hypotheses..... 54

2.2.2 Objectives: 54

2.3 Chapter Materials & Methods 54

2.3.1 Materials 54

2.3.2 Synthesis of tert-butyl (1,3-dihydroxypropan-2yl) carbamate (tert-butyl serinol, tBS)..... 55

2.3.3 Synthesis of tert-butyl (2-oxo-1,3-dioxan-5-yl) carbamate: (tert-butyl serinol carbonate, tBSC) 56

2.3.4 PEG Initiated Ring-Opening Polymerisation of Lactide and tert-butyl (2-oxo-1,3-dioxan-5-yl) carbamate (tBSC): Kinetics in Presence of DBU..... 57

2.3.5 BOC Deprotection Optimisation..... 58

2.3.6 DOX coupling procedure..... 59

2.3.7 Cy5 coupling procedure 60

2.3.8 Nanoparticle Preparation 60

2.3.9 Critical Aggregation Concentration (CAC) calculation 61

2.3.10 General Methods and Instrumentation 61

2.4 Results and Discussion 66

2.4.1 Monomer Synthesis and Purification..... 66

2.4.2 Ring Opening Polymerisation 68

2.4.3 Polymer side-chain derivatisation and drug coupling..... 72

2.4.4 Nanoparticle preparation..... 78

2.5 Conclusion..... 80

2.6 Chapter Acknowledgements..... 81

Chapter 3 *In vitro* evaluation of synthesised polymeric NPs for the treatment of GBM 82

3.1 Introduction..... 82

3.2 Chapter Hypotheses and Objectives 88

3.2.1 Chapter Hypotheses 88

3.2.2 Chapter Objectives: 88

3.3 Chapter Materials & Methods 88

3.3.1 Materials 88

3.3.2 Nanoparticle stability studies 90

3.3.3 Tissue culture of the cell monolayers 90

3.3.4 Cell lines 92

3.3.5 *In vitro* 2D cell viability assays 94

3.3.6 Cellular uptake of NPs 98

3.3.7 Preparation of PLGA/PEG matrix 99

3.3.8 Release studies 99

3.4 Results and Discussion 101

3.4.1 Nanoparticle stability studies 101

3.4.2 *In vitro* 2D cell viability 105

3.4.3 Cellular Uptake of NPs 122

3.4.4 Release studies 125

3.4.5 Systematic review of DOX-NPs 131

3.4.6 Representative Animal Glioma Cell Line 137

3.5 Conclusion 142

Chapter 4 Future Outlook and Summary 144

4.1 Future Outlook 144

4.1.1 Release Studies 144

4.1.2 Penetration studies 145

4.1.3 Further enhancement of polymeric formulation 146

4.1.4 Further enhancement of the PLGA/PEG drug delivery system 149

4.1.5 *In vivo* tolerability and efficacy study using a high-grade glioma rat allograft model 150

4.2 Summary 156

Chapter 5 References 159

Chapter 6 Appendices 199

LIST OF FIGURES

Figure 1-1 An image of the cerebral hemisphere of the brain, highlighting the four different lobes and the subsequent GBM incidence rates. This figure was created using Servier Medical Art templates, which are licensed under a Creative Commons Attribution 3.0 Unported License; https://smart.servier.com 2

Figure 1-2 A variety of patient MRI scans, obtained from the Queens Medical Centre Hospital, University of Nottingham, showing the typical characteristics of GBM, including the necrotic core (highlighted by the bold arrows) and the contrasting white rim, signalling gadolinium uptake (highlighted by the thin arrows)..... 4

Figure 1-3 Activation of Temozolomide to its active alkylating species, MTIC, at physiological pH..... 7

Figure 1-4 Mechanisms of action of TTFields in and around quiescent and dividing cells. Inside quiescent cells (A), the field is uniform, and the oscillating electric forces result only in “vibration” of ions and dipoles. In contrast, the nonuniform fields within dividing cells (B) induces forces pushing all dipoles toward the furrow. (C) TTFields exert directional forces and result in abnormal spindle formation and subsequent mitotic arrest or delay, possibly due to improper attachment of chromosomes to the spindle fibres. Cells can die in mitotic arrest or progress to cell division leading to abnormal aneuploid progeny. Abnormal daughter cells die in the subsequent interphase, undergo a permanent arrest or proliferate through additional mitosis where they will be subjected to further TTFields assault. (Adapted from[50])..... 11

Figure 1-5 Handling and implantation of Gliadel™ wafers during brain tumour surgery. (A) A single wafer is removed from its sterile packaging. (B) All 8 Gliadel™ wafers, from a complete pack, are removed and prepared for intracerebral implantation. (C) Gliadel™ wafers lining the wall of a GBM resection cavity. (D) Implanted wafers are covered with Surgicel to prevent dislocation and intracavitary movement. (Adapted from[57]) 14

Figure 1-6 Schematic of production of PLGA/PEG matrix. Adapted from [64][78]. 19

Figure 1-7 Images of the PLGA/PEG paste being administered (A), and sintered (B), in the brain of a sheep[84]. The sintered polymer conforms to the irregular-shaped lining of a pseudo-resection cavity, offering greater apposition than pre-formed Gliadel™ wafers. 20

Figure 1-8 A schematic representation of the BBB, highlighting the ability of small, lipophilic molecules to cross into the brain. 22

Figure 1-9 **Representation of functionalised liposome and polymeric NP systems**. Targeting moieties include proteins, antibodies, labelled antibodies, ligands and peptides. The lipophilic core of the liposome (left) can contain hydrophobic drugs, whilst hydrophilic drugs can become trapped within the hydrophilic bilayer. Hydrophobic drugs can become entrapped within the hydrophobic pockets of the polymeric NP (right) on self-assembly. This figure was created using Servier Medical Art templates, which are licensed under a Creative Commons Attribution 3.0 Unported License; https://smart.servier.com and BioRender.com. 26

Figure 1-10 Schematic presentation of preparation, conjugation and transportation of L-phenylalanine (PA)-SLNs. This figure was created using Servier Medical Art templates, which are licensed under a Creative

Commons Attribution 3.0 Unported License; https://smart.servier.com. Adapted from[142]. 29

Figure 1-11 Structures of the organobasic catalysts investigated for the ROP of lactide. 37

Figure 1-12 Proposed dual-action mechanism for the catalysis of the ROP of lactide by TBD. Adapted from[178]. 38

Figure 1-13 Two plausible routes involved in the DBU-catalysed ROP process of lactide with an alcohol initiator. 39

Figure 1-14 Chemical structure of doxorubicin. 40

Figure 1-15 **Catheter delivery using an Ommaya reservoir.** An Ommaya reservoir with the catheter placed in the tumour, allows regular injections of chemotherapeutics. The reservoir can also be placed into the lesion site post-surgery. This figure was created by Phoebe McCrorie using Servier Medical Art templates, which are licensed under a Creative Commons Attribution 3.0 Unported License; https://smart.servier.com. (Revised manuscript in prep; McCrorie*, Vasey* et al). 43

Figure 1-16 **Graphical abstract of project.** A representation of the lining of the resection cavity with the drug-loaded NP-embedded PLGA/PEG matrix. Figure was produced by Oran Maguire using Adobe Illustrator. 49

Figure 2-1 The Stokes-Einstein Equation. Combines the light scattering and diffusion behaviour of particles. 65

Figure 2-2 The synthetic scheme for the production of tert-Butyl (2-oxo-1,3-dioxan-5-yl)carbamate (tBSC)Ring Opening Polymerisation.. 67

Figure 2-3 Synthesis of monomer and PEG-initiated co-polymers of varying architectures. 69

Figure 2-4 A) general reaction scheme for the PEG-initiated ROP, B) ^{1}H NMR spectra of the five co-polymers (with random distribution of ester and carbonate units) and C) GPC traces of the polymers. 70

Figure 2-5 ^{1}H NMR spectra to show BOC deprotection on the carbonate unit in the polymer backbone. Spectra recorded after purification of the polymer from 0, 5, 10 and 30 minutes of reaction time. 73

Figure 2-6 A. Structure of the polymeric prodrug mPEG$_{5000}$-(LA)$_{50}$-(tBSC)$_{50}$-DOX. B. Stacked ^{1}HNMR spectra of the unmodified mPEG$_{5000}$-(LA)$_{50}$-(tBSC)$_{50}$ (bottom) and two modifications of mPEG$_{5000}$-(LA)$_{50}$-(tBSC)$_{50}$-DOX (middle and top spectra) at two different extents of functionalisation..... 75

Figure 2-7 Synthetic scheme for Cy5 conjugation to polymer backbone. 77

Figure 2-8 ^{1}H NMR showing coupling of Cy5 to the polymer backbone. 78

Figure 3-1 The mechanism of reduction of resezurin, a blue weak fluorescent indicator dye, to resofurin, a strong fluorescent pink dye, in response to irreversible chemical reduction. 94

Figure 3-2 DLS traces of formulations P1 – P5 in control conditions (PBS at 4°C; top row) and stimulated conditions (DMEM at 37°C; bottom row) after 0, 1, 24, 48 hrs and 1 week of incubation. No significant changes were observed for the NPs in control conditions. Breakdown of

each of the NPs was observed within 1 week of incubation in stimulated conditions. 103

Figure 3-3 In vitro U87 cell viability assay at 72h post treatment with different concentrations of the five NP formulations using PrestoBlue™ assay. Three independent repeats were carried out (n=4), across three different passages. Error bars show mean ± S.E.M. (A – E). The average size and PDI of each NP formulation tested in each repeat. Error bars show mean ± S.E.M (F). 106

Figure 3-4 In vitro cell viability assay at 72h post treatment with different concentrations of the P2 NP formulation on a human astrocyte cell line using the PrestoBlue™ assay. Four independent repeats (n = 4) were carried out. Error bars show mean ± S.E.M. [ns: p ≥ 0.05; ****: p < 0.0001, unpaired t-test with Welch's correction, comparing each data set to the control (negative control; medium) data set] 108

Figure 3-5 Effect of Culture Time and Seeding Density on PrestoBlue Fluorescence. Cell seeding density experiment for the PrestoBlue™ assay at 24, 48 and 72h. Four independent repeats were carried out (n=4) for the GIN-8 line and two independent repeats (n = 4) were carried out for the GIN-28 and GIN-31 cell lines. Error bars show mean ± S.E.M. 110

Figure 3-6 In vitro cell viability assay at 72h post treatment with different concentrations of the P2 NP formulation on primary glioma cell lines using the PrestoBlue™ assay. Three independent repeats were carried out (n=4) for the GIN-8 cell line whilst four independent repeats (n = 4) were carried out for the GIN-28 and GIN-31 cell lines. Error bars show mean ± S.E.M. [ns: p ≥ 0.05; *: p = 0.01-0.05; ****: p < 0.0001, unpaired t-test with Welch's correction, comparing each data set to the control (negative control; medium) data set] 113

Figure 3-7 Potency determination was achieved via measurement of cellular metabolic activity (PrestoBlue™ assay). DOX was diluted in DMEM containing 10% FBS and applied for 72 hours. U87, GIN-8 and GIN-28 cells were seeded at a density of $5x10^3$ cell/well and GIN-31 cells were seeded at a density of $3x10^3$ cell/well in 96 well plates. All cells were cultured for 24h prior to assaying. Data represent mean ± S.E.M and are quadruplets from four independent experiments. IC_{50} values are displayed in the key and are mean ± S.D and determined via GraphPad Prism. 115

Figure 3-8 P2-DOX formulation, showing average size obtained for each of the in vitro experiments carried out in this body of work. 116

Figure 3-9 In vitro cell viability assay at 72h post treatment with different concentrations of the P2-DOX NP formulation on glioma cell lines using the PrestoBlue™ assay. Five independent repeats were carried out (n=4) for the U87, GIN-28 and GIN-31 cell lines whilst four independent repeats (n = 4) were carried out for the GIN-8 cell line. Error bars show mean ± SEM. [ns: p ≥ 0.05; *: p = 0.01-0.05; **: p = 0.001-0.01; ***: p = 0.0001-0.001; ****: p < 0.0001, unpaired t-test with Welch's correction, comparing each data set to the control (negative control; medium) data set]..... 117

Figure 3-10 In vitro cell viability assay at 72h post treatment with different concentrations of the P2 NP and P2-DOX NP formulations on U87, GIN-8, GIN-28 and GIN-31 cell lines using PrestoBlue™ assay. Four independent repeats were carried out (n=4). Error bars show mean ± S.E.M. (ns: p ≥ 0.05; ****p ≤ 0.0001; two-way ANOVA with Sidak's multiple comparisons test)..... 119

Figure 3-11 U87 cells imaged on an inverted Nikon Eclipse TE 300 fluorescent microscope on DAPI (blue; nuclei) and Cy5 (magenta) filters.

Images were merged using ImageJ software. Uptake of NPs at t = 0.5, 1, 2 and 4 hours..... 124

Figure 3-12 Cumulative % and µg of DOX release from the DOX-loaded NPs over 44 days (A) and 24 hours (B). Release was carried out in PBS. Timepoints represent one independent repeat (n = 3) with error bars showing mean ± one SD..... 126

Figure 3-13 Cumulative % and µg of DOX-NP release from the PLGA/PEG microparticulate matrix over 63 days (A) and 24 hours (B). Release was carried out in PBS. Timepoints represent one independent repeat (n = 3) with error bars showing mean ± one SD. 129

Figure 3-14 Potency determination from DOX applied to the 9L rat glioma line was achieved via measurement of cellular metabolic activity (PrestoBlue™ assay). DOX was diluted in DMEM containing 10% FBS and applied for 72 hours. 9L cells were plated at 3 x 10^3 cells per well in 96 well plates. All were cultured for 24h prior to assaying. Data represent mean ± S.E.M and are quadruplets from three independent experiments. IC_{50} value is displayed in the key and are mean ± S.D and determined via GraphPad Prism. 139

Figure 3-15 In vitro cell viability assay at 72h post treatment with different concentrations of the P2 NP formulation (A) and P2-DOX NP formulation (B) on the 9L rat glioma cell line using the PrestoBlue™ assay. Three independent repeats were carried out (n=4). Error bars show mean ± SEM. [ns: $p \geq 0.05$; *: $p = 0.01$-0.05; ****: $p < 0.0001$, unpaired t-test with Welch's correction, comparing each data set to the control (negative control; medium) data set]..... 140

Figure 3-16 In vitro cell viability assay at 72h post treatment with different concentrations of the P2 NP and P2-DOX NP formulations on the 9L glioma rat cell line using PrestoBlue™ assay. Three independent

repeats were carried out (n=4). Error bars show mean ± SEM. (ns: p ≥ 0.05; ****p ≤ 0.0001; two-way ANOVA with Sidak's multiple comparisons test) 141

Figure 4-1 The chemical structure of Gemcitabine, indicating the free amine group on the chemotherapeutic. 147

Figure 4-2 The median-effect algorithm, used to determine the Combination Index (CI) where IC_{50} (A) and IC_{50} (B) are the IC_{50} values obtained from each drug separately. IC_{50} (A + B) is the IC_{50} value of both drugs in combination. 149

LIST OF TABLES

Table 1-1 Nanoparticles with dual targeting capabilities for both the BBB and GBM 30

Table 1-2 Examples of doxorubicin NPs used in the investigational treatment of GBM 45

Table 2-1 Chemical and physical characterisation of the PEGylated co-polymers. 71

Table 2-2 NP size distribution and zeta potential. 79

Table 2-3 Size, PDI and Zeta Potential values for P2, P2-DOX and P2-Cy5 NPs. 80

Table 3-1 Various Short and Long Term Cell Viability Assays 121

Table 3-2 Examples of DOX-NPs in oncology. 132

List of Abbreviations

[M]/[I]	Monomer : Initiator ratio
^{13}C NMR	Carbon Nuclear Magnetic Resonance Spectroscopy
^{1}H NMR	Proton Nuclear Magnetic Resonance Spectroscopy
3PEG	Trimethylopropane thoxylate
4PEG	Pentaerythritol ethoxylate
5-ALA	5-aminolevulinic acid
AEGFR	Anti-Epithelial Growth Factor
AM	Astrocyte Medium
ATR	Attenuated Total Reflectance
BBB	Blood Brain Barrier
BCEC	Brain Capillary Endothelial Cells
CAC	Critical Aggregation Concentration
$CDCl_3$	Deuterated Chloroform
CED	Convection Enhanced Delivery
$CHCl_3$	Chloroform
CI	Combination Index
CMC	Critical Micelle Concentration
CNS	Central Nervous System
CO_2	Carbon Dioxide
CSF	Cerebrospinal Fluid
CT	Computerised Tomography
Cy5	Cyanine 5
D	Diffusion Coefficient
Đ	Molecular Weight Distribution
DBU	Diazabicyclo[5.4.0]undec-5-ene
DCM	Dichloromethane
d_H	Hydrodynamic Diameter
DIPG	Diffuse Intrinsic Pontine Glioma
DLS	Dynamic Light Scattering
DMA	Dimethacrylate
DMEM	Dulbecco's Modified Eagle Medium

DMSO	Dimethyl Sulfoxide
DMSO-d_6	Deuterated Dimethyl Sulfoxide
DNA	Deoxyribonucleic Acid
DOX	Doxorubicin
DPBS	Dulbecco's Phosphate Buffer Saline
DRI	Differential Refractive Index Detector
DSC	N,N′-Disuccinimidyl Carbonate
DSC	Differential Scanning Calorimetry
ECS	Extracellular Space
EGFR	Epidermal Growth Factor Feceptor
ET_2O	Diethyl Ether
FBS	HyClone™ Bovine Growth Serum
FDA	Food and Drug Administration
FTIR	Fourier-Transform Infra-Red Spectroscopy
GBM	Glioblastoma Multiforme
GIN	Glioma INvasive
GMP	Good Manufacturing Practise
GPC	Gel Permeation Chromotagrophy
GSCs	Glioma Stem Cells
Gy	Grays
H&E	Hematoxylin and eosin
H_2O	Water
HA	Hyaluronic Acid
HBSS	Hank's Balanced Salt Solution
HCCs	Hydrophilic Carbon Clusters
HBMEC	Human Brain Microvascular Endothelial Cells
HPLC	High Performance Liquid Chromatography
Hz	Hertz
IC_{50}	Half Maximal Inhibitory Concentration
ILS	Increased Life Span
IV	Intravenous
κ	Boltzmann constant
LA	D,L-lactide

LAT1	Large Amino Acid Transporter 1
LiCl	Lithium Chloride
LMHP	Low Molecular Weight Heparin
LRP	Lipoprotein Receptor Related Protein
MeCN	Acetonitrile
MGMT	O-6-methylguanine methyltransferase
M_n	Molecular Weight
M_p	Peak Molecular Weight
mPEG	Poly(ethylene glycol) methyl ether
MRI	Magnetic Resonance Imaging
M_w	Weight Average Molecular Weight
NICE	National Institute for Health and Care Excellence
NLCs	Nanostructured Lipid Carriers
NP	Nanoparticle
PBS	Phosphate Buffered Saline
PCL	poly(caprolactone)
PDI	Polydispersity Index
PDX	Patient Derived Xenograft
PEG	poly(ethylene glycol)
PGA	poly(glycolide)
PLA	poly(lactic acid)
PLGA	poly(lactic-co-glycolic acid)
PMMA	Polymethylmethacrylate
PpIX	Protoporphyrin IX
ppm	Parts per million
PS	Polystyrene
RMT	Receptor-mediated transcytosis
RNA	Ribonucleic Acid
ROMP	Ring-Opening Metathesis Polymerisation
ROP	Ring-Opening Polymerisation
Serinol	2-amino-1,3-propanediol
SLNs	Solid Lipid Nanoparticles
$Sn(Oct)_2$	Tin octoate

TBD	1,5,7-Triazabicycle[4.4.0]dec-5-ene
tBS	tert-butyl serinol
tBSC	tert-Butyl (2-oxo-1,3-dioxan-5-yl)carbamate
TEA	Triethylamine
TFA	Trifluoroacetic acid
T_g	Glass Transition Temperature
TGA	Thermal Gravimetric Analysis
THF	Tetrahydrofuran
TMC	Trimethylenecarbonate
TMZ	Temozolomide
TNS	Trypsin Neutralization Solution
ToF-SIMS	Time-of-Flight Secondary Ion Mass Spectrometry
TTFields	Tumour Treating Fields
TWI	Tumour Weight Inhibition
VEGF	Vascular Endothelial Growth Factor
VEGFR2	Vascular Endothelial Growth Factor Receptor Type II
WHO	World Health Organisation

Chapter 1 Introduction

1.1 Glioblastoma Multiforme

Glioblastoma Multiforme (GBM) is classified as a grade IV tumour of the central nervous system (CNS) by the World Health Organisation (WHO)[1], described as, *"cytologically malignant, mitotically active, necrosis-prone neoplasms often associated with rapid pre- and post-operative disease evolution and a fatal outcome. Although not an essential feature, widespread infiltration of surrounding tissue and a propensity for craniospinal dissemination characterize some grade IV neoplasms.*[2]*"* GBM accounts for approximately 12 – 25% of all intracranial neoplasms and 60 – 75% of astrocytic tumours, making it the most common primary brain tumour[3,4]. The incidence rate is between three and four new cases per 100,000 population annually in most European and North American countries[4].

The terms primary and secondary GBM were first coined in 1940 by the German neuropathologist Hans Joachim Scherer[5–7]. Most GBMs (>90%) occur rapidly *de novo*, without recognisable precursor legions (primary GBMs), whilst a smaller number (<10%) develop slowly from pre-existing astrocytomas of a lower grade (secondary GBMs)[8]. GBM is commonly situated in the cerebral hemispheres of the brain. A large study conducted in the University Hospital of Zurich concluded that the most

frequently affected sites of the brain were the temporal (31%), parietal (24%), frontal (23%) and occipital lobes (16%)[9].

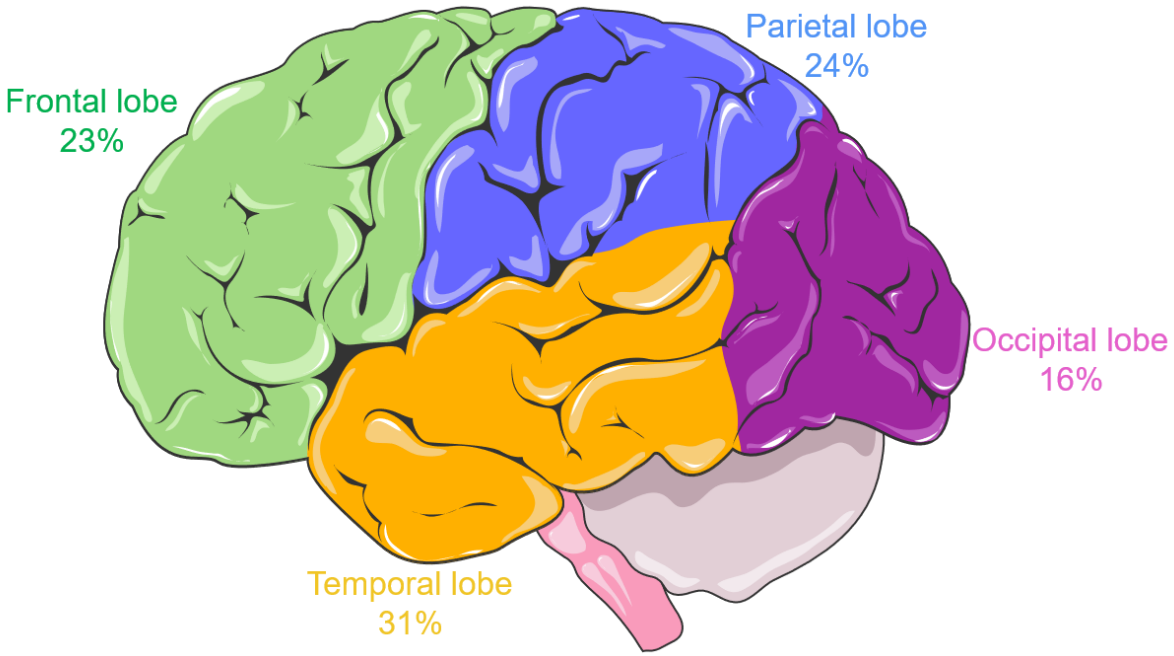


Figure 1-1 An image of the cerebral hemisphere of the brain, highlighting the four different lobes and the subsequent GBM incidence rates. This figure was created using Servier Medical Art templates, which are licensed under a Creative Commons Attribution 3.0 Unported License; https://smart.servier.com

As suggested from its name, glioblastoma "multiforme", the histopathology of GBMs are incredibly varied, leading to its highly heterogeneous nature. This aspect, coupled with the *"widespread infiltration of surrounding tissue"* result in the increased difficulty of treating this aggressive tumour type and ultimately the dismal prognosis, with a median survival of less than 15 months from diagnosis, for patients receiving multimodal treatment (median survival of 2 months for patients not receiving any treatment)[10].

1.2 Diagnosis of GBM

1.2.1 Clinical presentation

The presentation of a patient can vary significantly with newly diagnosed GBM. This is mainly dependent on the location and size of the tumour and thus the effect on the anatomical structures involved in the brain[11]. Often, patients present with symptoms of increased intracranial pressure, including headache and focal or progressive neurological deficits. Around one third of patients have a seizure, and this remains the most common symptom. At a later stage of the disease, this symptom can occur in as many as 50% of patients[12,13].

1.2.2 Imaging

Diagnostic imaging could initially include a Computerised Tomography (CT) or Magnetic Resonance Imaging (MRI) scan. Nearly all GBMs show areas of enhancement with gadolinium contrast on MRI, corresponding to regions of blood brain barrier (BBB) breakdown within the tumour, though other regions of the tumour may not enhance and are only visible as high signal on T2/FLAIR weighted MRI sequences. Necrosis is a characteristic feature of GBM[14] and can be observed through MRI, whereby an irregularly shaped mass with a hypointense centre of necrosis can be observed surrounded by a dense ring of enhancement[15], outlined in Figure 1-2.

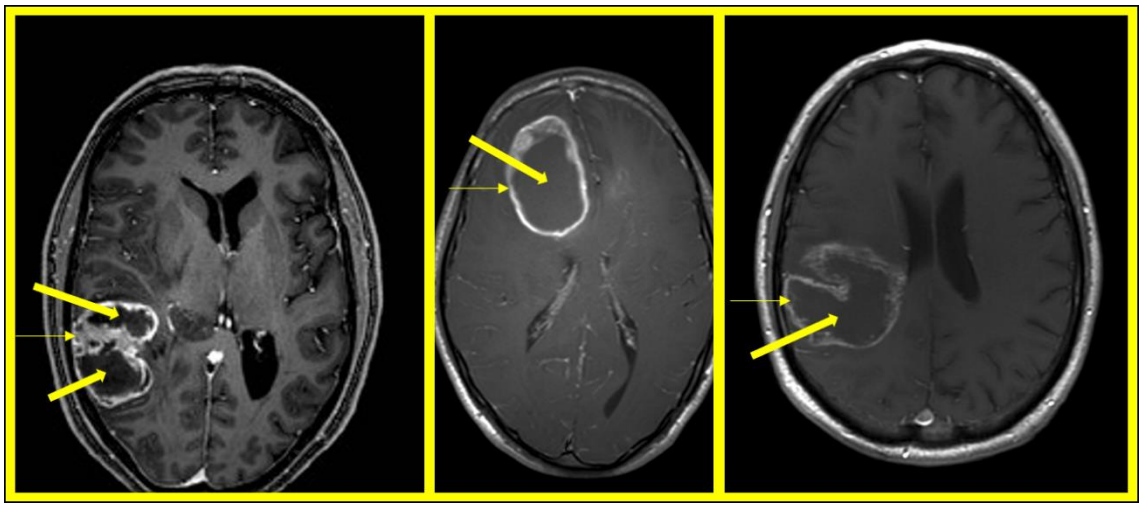


Figure 1-2 A variety of patient MRI scans, obtained from the Queens Medical Centre Hospital, University of Nottingham, showing the typical characteristics of GBM, including the necrotic core (highlighted by the bold arrows) and the contrasting white rim, signalling gadolinium uptake (highlighted by the thin arrows).

1.3 Management of GBM

1.3.1 Surgery

The use of MRI in preoperative planning, coupled with techniques such as ultrasound, CT scans and intra-operative MRI guided surgery during the maximal safe surgical resection of the tumour, allows a patient-specific multimodal neuronavigation of the tumour. Despite these techniques being used to distinguish between normal brain and tumour tissue, residual tumours continue to be a complex challenge.

Fluorescent-guided surgery was first introduced in malignant glioma patients in 1998 by Dr. Walter Stummer[16,17], who utilised the fluorescent pro-agent, 5-aminolevulinic acid (5-ALA), a natural human metabolite

with the intrinsic capability of crossing the BBB and penetrating the tumour interface in brain tumours[18]. Several hours before surgery, 5-ALA is administered orally to patients and leads to the preferential accumulation of protoporphyrin IX (PpIX) within glioma cells. PpIX emits light in the red region (625 - 740 nm) of the visible spectrum under blue-violet light conditions, leading to real-time fluorescence-guided surgery enabling the differentiation between tumour tissue and healthy brain[19–21]. This fluorescence-guidance surgery has been found to be more successful than traditional neuronavigational-guided surgery alone[22].

1.3.2 Adjuvant therapy

Following maximal safe surgical resection of the tumour, the intracranial wound of the patient is allowed to heal before starting further therapy, meaning the patient may have to wait for up to four weeks prior to beginning adjuvant therapy. Up until 2005, post-operative radiotherapy alone was standard treatment for GBM patients. However, following a pivotal phase III trial carried out by Dr. Roger Stupp *et al*, the standard of care treatment for GBM was updated. The trial concluded that external beam radiotherapy with concomitant oral temozolomide (TMZ) chemotherapy was more effective than radiotherapy alone[23]. It was found that patients who received radiotherapy plus TMZ had a median survival of 14.6 months compared to 12.1 months for those receiving radiotherapy alone. The cohort treated with radiotherapy plus TMZ had a higher proportion of long-term survivors than the radiotherapy alone cohort with 27% vs 11% at two years and 10% vs 2% at five years respectively[24].

This treatment strategy was soon coined the Stupp regimen and remains the standard of care treatment for GBM patients today. Patients receive a 6 week course of radiotherapy with a total dose delivered of 60 Grays (Gy), in 1.8-2 Gy fractions administered five days per week[25]. TMZ is typically administered at a dose of 75 mg/m^2 daily for the duration of the radiotherapy treatment. Following a rest period of approximately one month, the TMZ dose is increased to 150 mg/m^2 per day for five consecutive days for the first month, followed by an escalated dose (if tolerated) of 200 mg/m^2 for five consecutive days per month for the remainder of the treatment[15].

1.3.2.1 Temozolomide

TMZ is a pro-drug with the ability to cross the BBB[26]. When converted to its active form at physiological pH (Figure 1-3), it acts as an alkylating agent and methylates a range of sites of DNA, including the N-7 position and the O-6 position of guanine, and the N-3 position of adenine[27]. The primary site of DNA interaction responsible for TMZ's cytotoxicity is the O-6 position of guanine, which consequently triggers mispairing with thymine during DNA replication. This was concluded from studies whereby resistance was observed when tumours expressed high levels of the repair protein O-6-methylguanine methyltransferase (MGMT)[28–30]. Unless the mispairing between guanine and thymine was detected and repaired by MGMT, DNA strand breaks would occur, ultimately leading to cell cycle arrest and apoptosis. The methylation of the other two sites

in DNA are subsequently rapidly repaired by base excision repair enzymes[31].

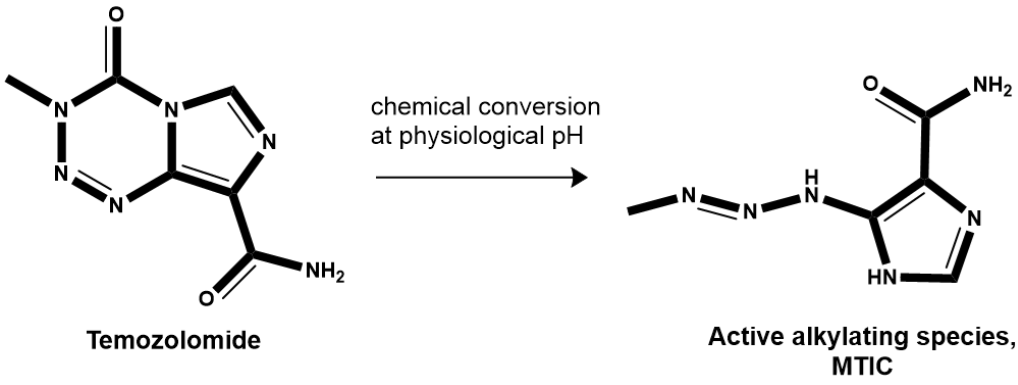


Figure 1-3 Activation of Temozolomide to its active alkylating species, MTIC, at physiological pH.

1.3.2.2 MGMT Status

Promoter methylation status of the MGMT gene is a powerful predictor of clinical outcome in GBM patients[32,33]. Promoter methylation is associated with longer survival in GBM patients as it reduces translation of the MGMT gene and henceforth the repair protein is unable to remove pro-mutagenic alkyl groups from the O-6 position of guanine in DNA[34,35]. Promoter methylation is common in GBM (45 – 75%)[36–38] and has been associated with longer survival of patients treated with TMZ[33]. Interestingly, secondary GBMs have shown a higher incidence of MGMT promoter methylation than primary GBMs[36,38].

1.3.3 Palliative care

Palliative care is described by the WHO as*, "An approach that improves the quality of life of patients and their families facing the problem associated with life-threatening illness, through the prevention and relief of suffering by means of early identification and impeccable assessment and treatment of pain and other problems, physical, psychosocial and spiritual*[39]*."*

Despite the multimodal treatment approach for GBM, the prognosis of patient's diagnosed with GBM is devastating, with an incredibly low median survival time[10]. Henceforth, when symptoms increase and anti-tumour treatment is no longer effective, patients will move into their end of life phase. During this period, patients will receive palliative care. Throughout palliative care, it must be considered that GBM patients have needs of both neoplastic disease and also neurological disease, since it affects the CNS[40]. Targets of palliative care include headache, nausea, vomiting, focal neurological deficits, drowsiness and prolonged sleep alongside post-surgical morbidities, radiation, chemotherapy and medical therapy adverse effects[41,42]. The overall aim of palliative care is to reduce symptom burden and to maintain quality of life for as long as possible, without inappropriately prolonging life[42].

1.4 Treatment advances

1.4.1 Tumour Treating Fields

Tumour Treating Fields (TTFields), a new treatment modality developed and pioneered by Novocure, was authorised for use by the U.S Food and Drug Administration (FDA) in 2011 after proving significant clinical benefit for GBM patients[43]. TTFields are alternating electric fields of low intensity and intermediate frequency with the ability to interact with rapidly dividing cancer cells and results in an anti-mitotic effect[44].

TTFields are administered to GBM patients through the Optune device. It is patient operated and consists of transducer arrays placed on the patient's shaved head which deliver the electric fields. This non-invasive treatment method was reported to substantially improve the patient's quality of life and furthermore, in a second phase III clinical trial for patients with newly diagnosed GBM, it was found that combinative treatment of TTFields with TMZ in the maintenance period of the Stupp protocol significantly improved overall survival (20.9 months) compared to patient's receiving TMZ alone (16.0 months)[45,46]. The two- and five-year survival rates for patients receiving TMZ alone was 31% and 5% respectively, compared with 43% and 13% for patients receiving TTFields treatment plus TMZ. These key data resulted in approval by the FDA in 2015 for treatment of newly diagnosed GBM patients to include TTFields in conjunction with TMZ.

Despite the significant benefit to patients receiving TTFields treatment, non-compliance was recorded for approximately 20% of patients in the first Phase III study (for recurrent gliomas)[43] and the main side effect of skin irritation was reported by 43% of the patients in the second Phase III trial (for primary gliomas)[45]. Consideration must be taken for patients administered the Optune device. The weight of the accompanying device of the second-generation Optune was reduced by approximately 1.5 kg, from 2.7 kg to 1.2 kg[47]. However, the transducers must be worn for a minimum of 18 hours per day, meaning that the patient must carry this accompanying treatment device with them during their daily routine. As already mentioned, the patient must shave their head to apply the transducers and skin irritation has been reported by approximately half of the patients treated with TTFields[48], resulting in discomfort for the patients regardless of alleviating invasive properties associated with other treatment options. Furthermore, TTFields have not yet been approved by The National Institute for Health and Care Excellence (NICE) for use in the U.K due to the astronomical cost of the device ($20,000 per month)[49].

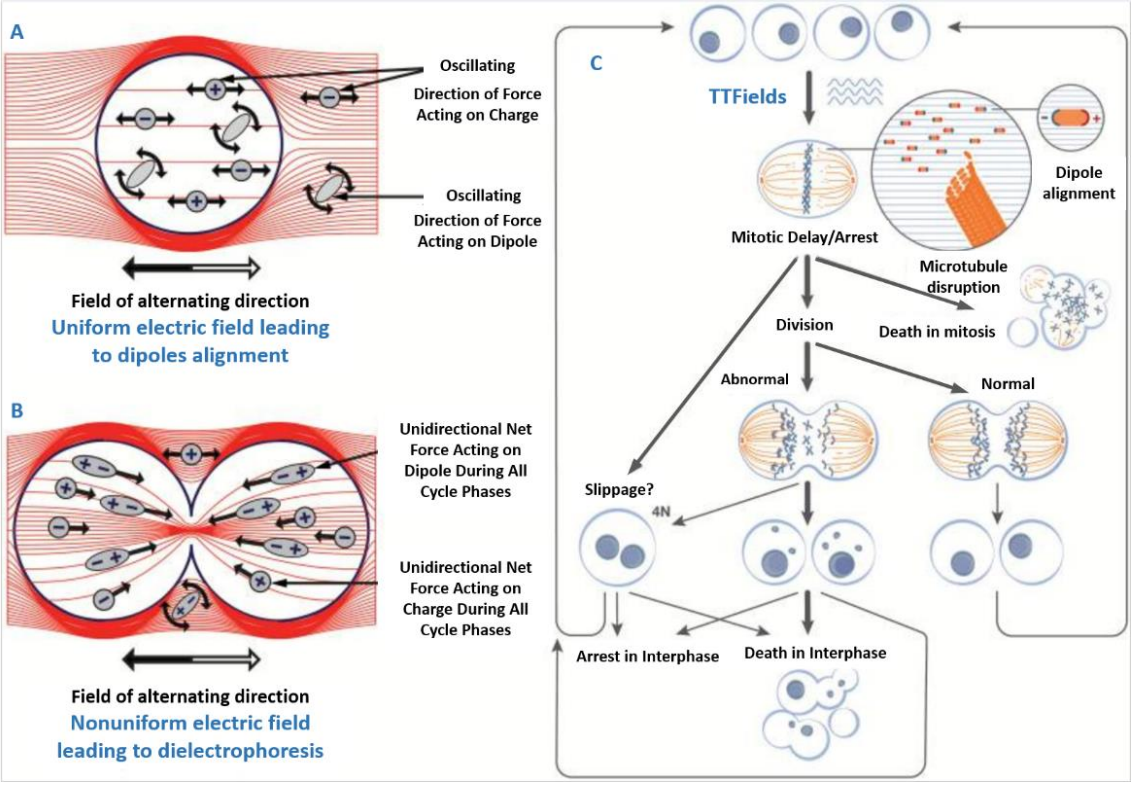


Figure 1-4 Mechanisms of action of TTFields in and around quiescent and dividing cells. Inside quiescent cells (A), the field is uniform, and the oscillating electric forces result only in "vibration" of ions and dipoles. In contrast, the nonuniform fields within dividing cells (B) induces forces pushing all dipoles toward the furrow. (C) TTFields exert directional forces and result in abnormal spindle formation and subsequent mitotic arrest or delay, possibly due to improper attachment of chromosomes to the spindle fibres. Cells can die in mitotic arrest or progress to cell division leading to abnormal aneuploid progeny. Abnormal daughter cells die in the subsequent interphase, undergo a permanent arrest or proliferate through additional mitosis where they will be subjected to further TTFields assault. (Adapted from[50])

1.4.2 Local delivery

Despite standard of care treatment for GBM shifting from singular radiotherapy to chemoradiation combination therapy following surgical debulking of the tumour, there remains significant limitations to the systemic delivery of chemotherapeutics in the treatment of GBM. The main obstacle is that of the BBB, rendering most commonly-used chemotherapy agents futile in the treatment of GBM as they are unable to cross the BBB[51]. Local, intracranial drug delivery has been developed over the last two decades, in order to circumvent the BBB. Ideal systems used to deliver drugs via this route should be biodegradable so as not to necessitate a second surgery for device removal and to lessen the prospect of a foreign body immune response.

1.4.2.1 Gliadel™ wafers

Currently, there is only one formulation authorised for local drug delivery by the FDA and NICE for GBM: Gliadel™ wafers, approved in 1996. The wafer is a biodegradable co-polymer composed of 1,3-bis-(p-carboxyphenoxy)propane and sebacic acid in a 20:80 ratio, which is impregnated with carmustine, a cytotoxic drug[52]. The wafers (typically 6-8) are inserted into the cavity after surgical resection of the tumour and carmustine is subsequently released over a three-week time frame. Despite this novel treatment method, the overall median survival is only improved by two months, and GBM continues to reoccur[53–55]. This is due to several reasons including: i) the rigid structure of the Gliadel™ wafers,

rendering them unable to conform to the irregularly-shaped cavity lining and are thus incapable of delivering drug to the entire cavity area; ii) the wafers can dislodge from the cavity wall and fall to the bottom of the cavity, minimising contact with the brain parenchyma, causing a reduction in the effective diffusion distance of carmustine; iii) the therapeutic agent is unable to penetrate far enough into brain parenchyma to eradicate remaining residual cells; iv) the delivery system was designed as a mono-therapeutic approach, purely for the single drug carmustine. The heterogeneous nature of GBM cells makes treatment with a single therapeutic agent poorly effective, since drug resistant tumour sub-clones can rapidly overcome pharmacological interference with a single molecular pathway. Furthermore, the half-life of carmustine is only 15 minutes[56], which is too short a time for the active drug to diffuse across large distances before drug degradation/metabolism occurs. Nevertheless, the development and approval of Gliadel™ wafers has provided a proof-of-concept that intra-cavity drug delivery, reliant on diffusion, can lead to significant survival benefits for patients with primary and recurrent GBM. This has opened the field to developing more treatment methods of this nature.

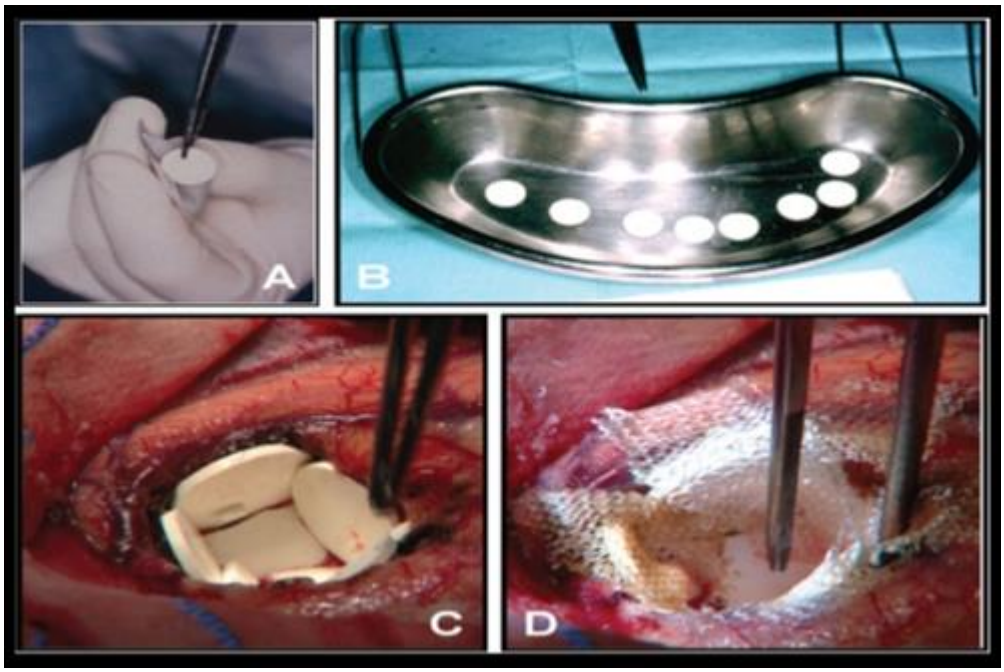


Figure 1-5 Handling and implantation of Gliadel™ wafers during brain tumour surgery. (A) A single wafer is removed from its sterile packaging. (B) All 8 Gliadel™ wafers, from a complete pack, are removed and prepared for intracerebral implantation. (C) Gliadel™ wafers lining the wall of a GBM resection cavity. (D) Implanted wafers are covered with Surgicel to prevent dislocation and intracavitary movement. (Adapted from[57])

1.4.2.2 Convection Enhanced Delivery

An additional investigational localised treatment strategy for brain tumours is convection enhanced delivery (CED), which was introduced in 1994 by Bobo *et al*[58]. It consists of a direct, continuous infusion of a therapeutic in the brain parenchyma using a micro-catheter connected to a pumping device. Through this device, a pressure gradient is created to allow the infusion of drug into the brain and surrounding interstitium.

A major issue facing CED is the short half-life of many chemotherapeutic drugs within the brain and the subsequent fast clearance post infusion.

Studies have been carried out which enhance the CED method through the incorporation of drug loaded nanocarriers[59]. It was hypothesised that through encapsulation, consistent exposure of the drug would be achieved, prolonging the half-life of the chemotherapeutic, and henceforth increasing tumour cytotoxicity. Encapsulation was also anticipated to contribute towards a reduction in neurotoxicity and an increase in tissue retention, improving the prognosis for patients with GBM. Each study utilised poly(lactic-co-glycolic acid) (PLGA) nanoparticles (NPs) encapsulating carboplatin[60], paclitaxel[61] and camptothecin[62] and showed improved sustained drug release over free drug alone. Some groups have also engineered NPs with capacity for dual functionality for delivery via CED, whereby NPs carrying drug cargo also contain a magnetic core, allowing the NPs to be detected via MRI, permitting tracking *in vivo*[63,64].

Coupling CED with NPs has the potential to considerably improve the outlook for patients with malignant glioma, as it capitalizes on strong elements of two powerful drug delivery strategies. Consequently, there is currently an active Phase I clinical trial using CED to deliver a gold NP-based formulation containing panobinostat (MTX110) to diffuse intrinsic pontine glioma (DIPG), an inoperable childhood brain tumour located in the brain stem [ClinicalTrials.gov ID: NCT03566199].

However, infection, catheter obstruction, and inadequate drug distribution have limited the success of this delivery method. Furthermore, CED is only able to deliver a therapeutic over a fixed period

of time, that being when a temporary catheter is in place[65]. It is believed that more sustained and effective treatment may require continuous treatment with a chronically infused agent and this concept has been explored in primate models, demonstrating safety and feasibility of CED for long periods of time in large animal brains[66].The neurouinfuse™ system provides a potentially permanent catheter device with low infection rates[67]. However, there are major concerns surrounding the effects of infusing fluid under pressure into tissue with pre-existing raised interstitial pressure and the adverse effects on tissue perfusion this may have, potentially leading to hypoperfusion of brain tissue and neurological deficits[68]. This concept has also been well reviewed by Lewis *et al*, addressing the requirement for increased volumes and infusions of rapidly cleared chemotherapies to brain tumours[69]. Later work has shown a significant reduction in tumour volume when chronically infusing carboplatin using robot-guided implantation of catheters on a patient with recurrent GBM[67]. Applying NP technology to this promising delivery device could be well received in the field, utilising NPs to increase the potency, specificity and diffusion of the chemotherapies.

1.4.2.3 Polymeric hydrogel systems

Hydrogels are three-dimensional networks, which retain a physically viscoelastic structure while containing large amounts of water. Hydrogels can be synthesised to respond to several physiological stimuli including

temperature, pH and ionic strength, making them appealing matrices for controlled drug delivery.

The ReGel™ system consists of a triblock thermosensitive co-polymer (PLGA-PEG-PLGA) which is water soluble at 2 - 15°C but converts to a viscous, biodegradable, water insoluble, controlled-release gel at body temperature[72]. Oncogel™ is a non Cremaphor EL based formulation of paclitaxel in ReGel™, designed for the local delivery of paclitaxel to solid tumours, thus avoiding the systemic toxicities associated with conventional systemic paclitaxel delivery[73]. Oncogel™ provides a depot for the continuous release of paclitaxel directly to the tumour and surrounding tissue for six weeks. A study assessing the safety and efficacy of intracranial injected Oncogel™ into rats with 9L gliosarcomas, concluded that when combined with radiotherapy, this treatment method was more effective than either ReGel™ or radiotherapy alone[74]. Ultimately however, a subsequent human clinical trial was discontinued.

More recently, a hydrogel composed of lipid nanocapsules loaded with lauroyl-gemcitabine (GemC12-LNC), an amphiphilic derivative of gemcitabine, has been developed for the localised treatment of GBM, showing a significant survival benefit in pre-clinical studies[75,76]. The same laboratory has further enhanced this hydrogel system through loading a second chemotherapeutic, paclitaxel, into the hydrogel and *in vitro* studies in GBM models showed a promising efficacious and synergistic effect of the dual drug delivery system[77].

The systems detailed shed light on the treatment potential of local drug delivery devices in the treatment of GBM. As maximal safe resective surgery is usually the first stage in GBM treatment, the rationale for intracranial drug delivery is based upon a unique treatment window immediately adjuvant to neurosurgery, delivering drugs directly to the site of the tumour, thus commencing neuro-oncological treatment at a time when residual disease burden is relatively minimal.

1.4.3 PLGA/PEG as a local delivery device

Poly(lactic-co-glycolic acid)/poly(ethylene glycol) (PLGA/PEG) microparticle-based matrices have been developed, which acts as a paste at room temperature when mixed with saline and which sinters (solidifies) at 37°C (i.e. body temperature) when the microparticles fuse, as outlined in Figure 1-6 [78–80]. Both PLGA and PEG polymers have been authorised for use by the FDA for drug release applications, further promoting them as a desirable material[81–83]. The chemical properties of polyesters such as PLGA, derived from β-hydroxycarboxylic acids or other short chain hydroxyalkylacids, allow hydrolytic degradation through de-esterification. The monomeric components, lactic acid and glycolic acid, are then removed by natural biochemical pathways following degradation[84,85].

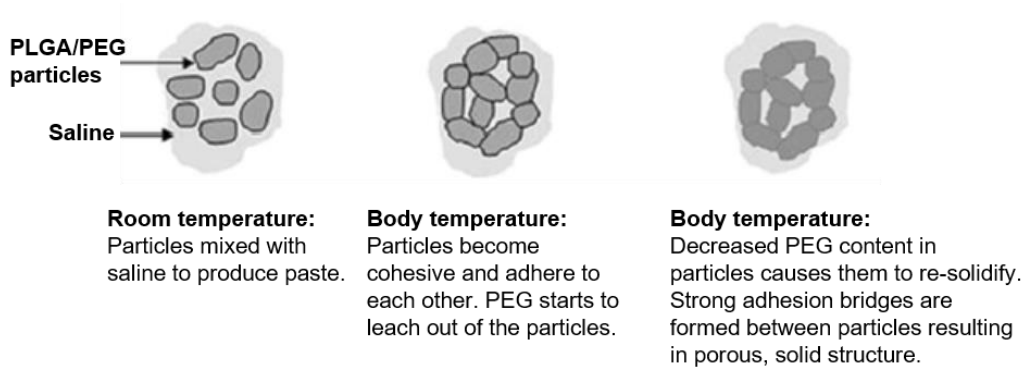


Figure 1-6 Schematic of production of PLGA/PEG matrix. Adapted from [64][78].

PLGA/PEG co-polymers have been investigated and adapted by our laboratory to be used as a novel microparticulate matrix to line the tumour cavity post-surgery and act as a carrier for locally applied chemotherapeutics. It has been demonstrated that the PLGA/PEG paste caused no toxicity or surgical morbidity to the animals tested; *ex vivo* brain scans (i.e. MRI and CT scans) showed that polymer could be delineated from brain tissue (a vital aspect for post-surgery follow-up in the clinical setting) and furthermore, the paste was able to withstand fractioned radiotherapy *in vitro*, with no disruption to the polymer structure and therefore no expected interference with drug release[86]. The release of three different drugs, trichostatin A, etoposide and methotrexate from the PLGA/PEG paste was initially tested *in vitro*. A burst release was observed for each of the three drugs, followed by sustained release for up to 28 days[86]. Significant overall survival benefit was observed *in vivo* using an orthotopic allograft model of high-grade glioma, when control animals receiving standard of care treatment were compared to animals receiving surgery + PLGA/PEG + etoposide and temozolomide.

Histological results confirmed over half of the animals were disease-free, long-term survivors[87,88].

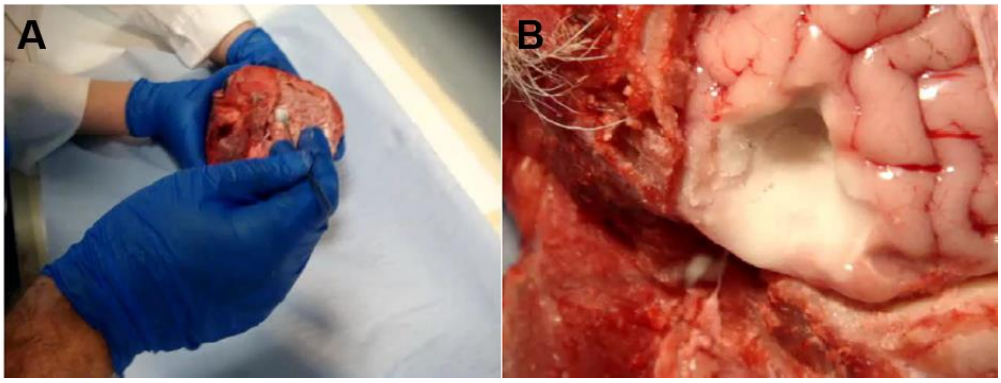


Figure 1-7 Images of the PLGA/PEG paste being administered (A), and sintered (B), in the brain of a sheep[86]. The sintered polymer conforms to the irregular-shaped lining of a pseudo-resection cavity, offering greater apposition than pre-formed Gliadel™ wafers.

These initial studies provided a proof of concept: chemotherapeutic drugs can be incorporated into the PLGA/PEG paste and released gradually through diffusion from the matrix leading to efficacy in brain tumour animal models, and thus provides a platform technology for future work.

1.5 Polymers as drug delivery systems

Synthetic and biomimetic drug-carriers which are of similar sizes to viruses have been extensively investigated for anti-cancer applications[89,90]. It has been hypothesised that materials in this size range (typically 60-180 nm) may enhance the concentrations of drugs in cancerous cells and tissues when compared to administration of the free drugs. This is because virus-sized particles distribute through the body in

a different manner to small molecule drugs, and can be internalised by specific cells via pathways which are not accessible to conventional drug molecules[91–93]. In addition, particles in the 'nano-sized' range i.e. 10-1000 nm, can accumulate in areas of inflammation, or of poorly-formed vasculature, and their transport away from blood vessels and into tumours can be increased by physical disruption of endothelial barriers[94,95].

Many NPs have been reported in the controlled release literature, with increasing numbers of examples in the field of GBM[96–108]. In most cases, these NPs have been designed to overcome non-cellular and cellular based mechanisms of resistance and increase selectivity of drugs towards cancer cells whilst reducing toxicity to healthy tissue[109]. NPs offer the prospect of encapsulating poorly soluble drugs, shielding therapeutic molecules from degradative processes and enhancing blood circulation and tissue distribution, thus increasing bio-distribution and improving the efficacy of drugs of low biological stability[110]. NPs also provide the opportunity to repurpose redundant chemotherapeutics that have previously been deemed too toxic or which have failed clinical development due to stability or solubility issues.

1.5.1 Systemic delivery of NPs for brain tumour therapy

Chemotherapeutics are predominantly administered intravenously (IV), often leading to a destructive treatment modality as only 0.7% of the administered dose accumulates within cancerous cells[111], inducing many

side effects as the drugs are distributed throughout the body, resulting in dose-limiting undesirable toxicities and a reduced quality of life for the patient. A problem when attempting to treat neuro-oncological diseases such as GBM, is the presence of the BBB, which acts as a physical protective layer for the brain but thus also as a physical obstacle for systemic therapy to penetrate the brain. The BBB is composed of a layer of tightly packed endothelial cells and supporting cells such as pericytes, which acts as a "barrier" whereby only small (<500 Da) lipophilic (logP = 1.5 – 2.7[112,113]) molecules can easily penetrate into the CNS[114,115]. For chemotherapeutics which do not have these properties to reach a target site in the brain, and to ensure site-selective release of the drugs in their active form, appropriate drug formulations are needed.

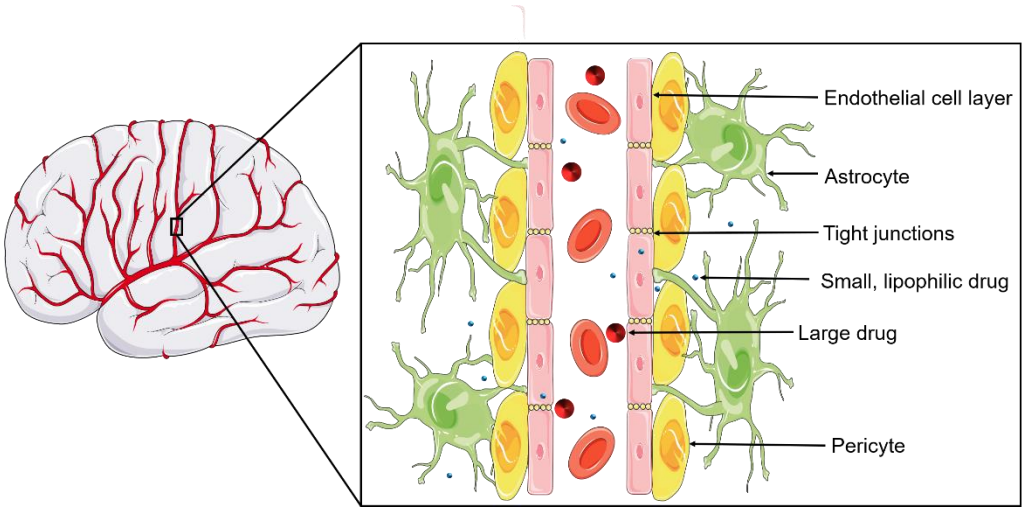


Figure 1-8 A schematic representation of the BBB, highlighting the ability of small, lipophilic molecules to cross into the brain.

Henceforth, through incorporating therapeutics into a NP carrier, the distribution of the drug and its accumulation in tissues can be altered.

Lipophilic drugs, which otherwise would not be soluble enough for injection, can be incorporated in, or conjugated to, a hydrophilic carrier. Larger biomolecules such as proteins and nucleic acids can also be formulated with ligand-conjugated carriers in order to use active transporters at the BBB to enable delivery into the brain. Many studies have concluded that particular hydrophilic polymers, for example PEG[116], can be used in formulations to enhance solubility of small molecule drugs and to extend the circulation time of therapeutics in the body. Polymers such as PEG can, when suitably conjugated to a drug or a particle, also act as a steric and entropic barrier to minimise associative interactions of the drug, or particle surfaces, with plasma proteins or cell membranes. These PEGylation and related NP carrier strategies thus reduce the early clearance of therapeutics and can be combined with ligand-receptor targeting and external physical stimuli such as focused ultrasound, to further enhance the transport of drugs into the brain[117–119].

Another exciting prospect of NPs is that they offer the potential of repurposing chemotherapeutics that have previously been discarded due to their inability to cross the BBB and/or resulting in dose-limiting systemic toxicities to healthy organs and tissues. One example is the NP incorporation of camptothecin, previously deemed ineffective in the treatment of GBM due to the rapid hydrolysation from its active form to a less active, more toxic form which undergoes rapid clearance once bound to plasma proteins[120]. The study showed that PLGA NPs containing camptothecin were able to cross the BBB in an orthotopic murine GBM

model, leading to a significant increase in survival compared to controls[121]. PLGA NPs stabilised with poloxamer 188 were loaded with doxorubicin (DOX) and were shown to cross the BBB of rats at therapeutically effective concentrations[122]. Paclitaxel was loaded into PEGylated poly(trimethylene carbonate) NPs and used to treat xenograft tumour-bearing mice, whereby median survival was significantly increased when compared to taxol[123].

In vitro cell-based models can be complementarily used to assess the potential of carriers to cross the BBB. One example of a well-known model utilises a monolayer of hCMEC/D3, a well-characterised brain microvascular endothelial cell line, which mimics the *in vivo* phenotype, as discussed in depth in a review by Weksler *et al*[124]. This model was used by Battaglia *et al*, which demonstrated that bevacizumab loaded solid lipid NPs (SLNs) enhanced the permeation of the drug across this BBB mimic, showing greater diffusion through the monolayer and into the collection chamber below, compared to free drug alone (80% versus 10%, respectively)[125]. SLNs were also loaded with DOX and observed to increase drug permeation through primary human brain microvascular endothelial cells (HBMEC), which also retain some properties of the BBB *in vitro*. The DOX released from the NPs was found to be efficacious against two primary human GBM cell lines, demonstrating the cytotoxic effects of encapsulated DOX on clinically relevant cells[126]. Another study showed an increased permeability coefficient for propidium iodide and etoposide across the BBB through using HBMEC/U87 (endothelial/GBM)

co-culture as an *in vitro* model[127]. It is however important to emphasise the limitations of current *in vitro* BBB models utilising cell monolayers, including restricted numbers of relevant cell types and lack of blood circulation and immune components.

1.5.2 Targeting of NPs to GBM following systemic administration

Several small molecule ligands, peptides and antibodies have been conjugated to NPs and drugs to target GBM, as depicted in Figure 1-9. For example, monoclonal antibodies have been used to exploit the overexpression of vascular endothelial growth factor (VEGF) and its receptor type II (VEGFR2) in core tumour cells and migrated glioma cells[128–130]. Other studies have targeted the epidermal growth factor receptor (EGFR), which is overexpressed in many types of tumours including GBM[131], through conjugating peptides[132] or antibodies[133,134] to NP surfaces. A study conducted by Nilewski *et al* synthesised PEGylated hydrophilic carbon clusters (PEG-HCCs), whereby the EGFR binding peptide, GE11, was conjugated to surface PEG chains. The resultant "nanosyringes" could be loaded with a wide range of hydrophobic dyes and drugs, including paclitaxel and DOX[132], with efficacy in both U87-EGFR cells and primary human GBM culture. *In vivo* studies investigating flank and intracranial xenograft mouse models found a strong accumulation of the nanosyringes in the subsequent tumour sites, despite differences between rodent and human BBB.

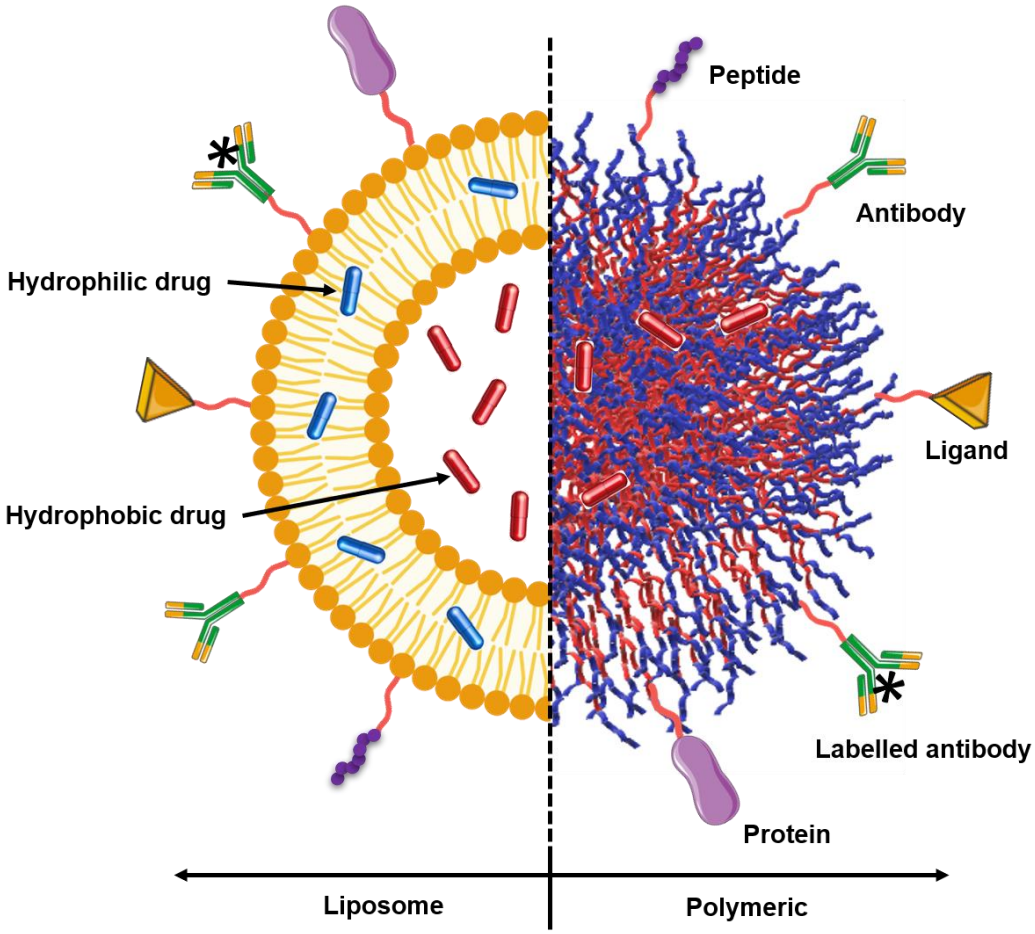


Figure 1-9 ***Representation of functionalised liposome and polymeric NP systems****. Targeting moieties include proteins, antibodies, labelled antibodies, ligands and peptides. The lipophilic core of the liposome (left) can contain hydrophobic drugs, whilst hydrophilic drugs can become trapped within the hydrophilic bilayer. Hydrophobic drugs can become entrapped within the hydrophobic pockets of the polymeric NP (right) on self-assembly. This figure was created using Servier Medical Art templates, which are licensed under a Creative Commons Attribution 3.0 Unported License; https://smart.servier.com and BioRender.com.*

A recent study reported the use of a canine model with late stage *de novo* brain tumours to deliver bacterially derived minicells loaded with DOX, whereby the surface of the minicells were decorated with bispecific antibodies targeting EGFR. The study reported that this delivery method was safe and extremely well tolerated by canines, with no adverse effects

observed. In comparison to murine and rodent models, the large size of the canine brain offers a useful model for the assessment of dose volumes and thus effectiveness of brain tumour therapies in a clinically relevant manner. This study, coupled with other preclinical data, formed the design basis of a Phase I clinical trial of EGFR-minicell-DOX in human recurrent GBM[135].

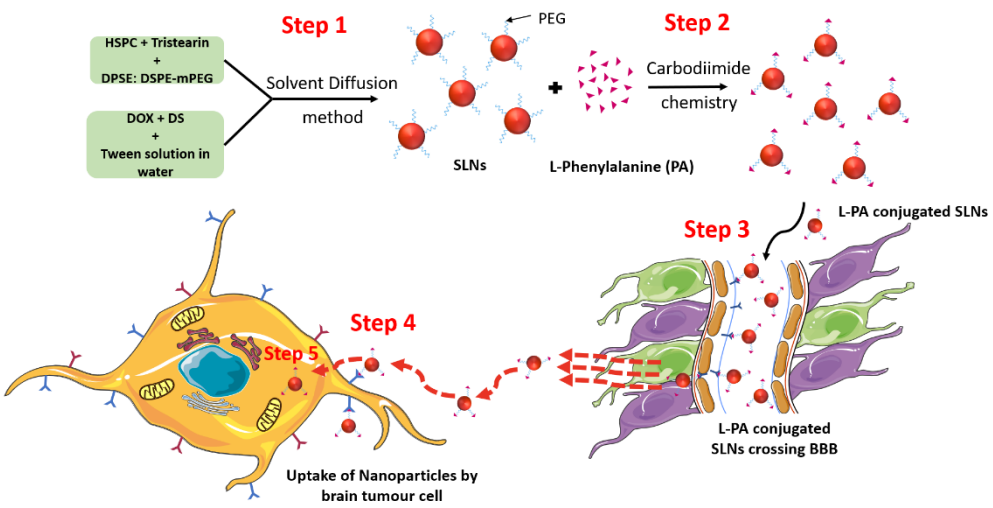
Antibodies have also been used to target the transferrin receptor[136], overexpressed in many cancerous cells, particularly GBM. One study used PLGA NPs to deliver TMZ, where the polymer surface was decorated with the monoclonal antibody OX26. Two different glioma cell lines were investigated and the prepared nanocarriers enhanced the anticancer activity of TMZ. In particular, the functionalisation of the nanocarrier was advantageous in enhancing cellular internalisation in GBM cells[136].

A considerable challenge for all targeted therapy efforts to date, is the sub-clonal nature of GBM, where only a minority sub-population of cells within a tumour may express molecular targets such as EGFR or VEGF. This warrants the need for targeting strategies which can deliver combination therapeutic moieties.

1.5.3 Dual targeting of the BBB and GBM

Researchers are attempting to target the biological properties of both GBM and the BBB by increasing the sophistication and targeting ability

of the nanocarriers, and a number of these studies are outlined in Table 1-1. Several targets are simultaneously overexpressed on both the BBB and GBM cells, potentially allowing NPs bearing a single targeting moiety to cross the BBB more effectively and to enhance internalisation into GBM cells. These targets include the low density lipoprotein receptor related protein (LRP)[137–139], transferrin receptor[140,141] and large amino acid transporter 1 (LAT1)[142–144] (Figure 1-10). Conjugating a single targeting moiety to the NP surface has the additional advantage of reducing the complexity of the formulation process, a major issue facing the clinical adoption of NPs[145].



Step 1: Preparation of SLNs using solvent diffusion method.

Step 2: Conjugation of ligand with SLNs using carbodiimide chemistry.

Step 3: Intravenously administered PA-SLNs reach brain blood capillaries and cross the BBB with help of carrier mediated transport system (L-type amino acid transport system (LAT1)) of BBB.

Step 4: Ligand receptor interaction between PA present on surface of SLN and PA receptor on brain tumour cell.

Step 5: Internalisation of PA-SLNs by brain tumour cell.

Figure 1-10 Schematic presentation of preparation, conjugation and transportation of L-phenylalanine (PA)-SLNs. This figure was created using Servier Medical Art templates, which are licensed under a Creative Commons Attribution 3.0 Unported License; https://smart.servier.com. Adapted from[144].

Table 1-1 Nanoparticles with dual targeting capabilities for both the BBB and GBM

NP material used	Target for BBB	Target for GBM	Targeting moiety used	Drug incorporated	*In vitro* model	*In vivo* model	Conclusion of Study	Reference
	Both							
Poly(caprolactone)	Low-density lipoprotein receptor		Angiopep-2	Paclitaxel	3D spheroids, Brain capillary endothelial cells (BCEC)	Nude mice bearing intracranial tumours	- Post IV treatment, penetration, distribution and accumulation higher than PEG-PCL control - No acute toxicity observed	Xin *et al,* 2012[146].
PLGA	Transferrin receptor		CRT peptide	Paclitaxel	3D spheroids; BCEC cells	Nude mice bearing intracranial tumours	- CRT-NP significantly prolonged median survival compared to Taxol	Kang *et al, 2015*[147].
Liposome	Transferrin receptor		Anti-transferrin single chain antibody fragments	Temozolomide	U87 (Temozolomide resistant and non-resistant lines) and U251	Nude mice bearing intracranial tumours	- Significantly increased survival compared with free temozolomide	Kim *et al,* 2015[148].
Liposome	Large amino acid transporter 1 (LAT1)		l-3,4-dihydroxyphenylalanine (l-DOPA)	WP1066 (JAK2 inhibitor)	GL261 cells (mouse GBM cells)	C57BL/ 6J mice bearing intracranial tumours	- Significantly increased survival compared with free WP1066	Bhunia *et al,* 2017[149].
Solid lipid NPs	α-subunit of insulin receptor	Anti-epithelial growth factor (AEGFR)	83-14Mab	Etoposide	U87 GBM cells and HBMECs	----	- Dual targeted NPs showed increased antiproliferation efficiency over single targeted and etoposide loaded NPs. - 83-14Mab effectively increased BBB permeability	Kuo *et al,* 2016[150].
PLGA	Lactoferrin receptor	Folate receptor	Lactoferrin and folate	Etoposide	U87 GBM cells and HBMECs	----	- Dual targeted NPs showed increased antiproliferation efficiency	Kuo *et al,* 2015[151].

							over single targeted and etoposide loaded NPs.	
Solid lipid NPs	Lactoferrin receptor	Multi-drug resistance proteins (MRPs)	Tamoxifen and lactoferrin	Carmustine	U87 GBM cells and HBMECs	----	- Dual targeting system increased the permeability of the BBB and resulted in greater inhibition of U87 cell growth.	Kuo *et al,* 2016[152].
Super paramagnetic iron oxide NPs	Transferrin receptor	Nestin (stem cell marker specific to GBM)	Transferrin/ polysorbate-80 and antibody against nestin	Temozolomide	----	Nude mice bearing intracranial tumours	- Transferrin coated NPs demonstrated greater tumour regression than polysorbate-80 coated NPs.	Prabhu *et al*, 2017[153].
Immunoliposomes	Low-density lipoprotein receptor	CD133 glycoprotein	Angiopep-2 and CD133 Mab	Temozolomide	U87 GBM cells and glioma stem cells (GSCs)	Nude mice bearing intracranial tumours	- Significant increase in survival observed relative to free temozolomide	Kim *et al,* 2018[154].
Liposomes	Transferrin receptor	Folate receptor	Transferrin and folate	Doxorubicin	C6 glioma cells and bEND3 BBB model	Rats bearing intracranial tumours	- Dual targeting effect was observed - NP was less toxic than doxorubicin solution	Gao *et al,* 2013[155].

Receptor-mediated transcytosis (RMT) via the transferrin receptor pathway has been investigated, with one study showing that transferrin-conjugated self-assembled NPs incorporating zoledronic acid increased the anti-tumour efficacy of the drug in mice bearing intracranial xenografts, due to an increased ability to cross the BBB. This was shown by tumour weight inhibition (TWI) from transferrin conjugated NPs of 41% compared to non-targeted NPs at 31% TWI and an increased life span (ILS) of 23% compared to 10% respectively; in contrast, free drug alone showed only a 20% TWI and an ILS of 10%[156].

Once the BBB has been crossed, NPs encounter the problem of traversing the parenchyma to reach the target site of infiltrative cells, which is required to inhibit the otherwise inevitable tumour reoccurrence. Recent seminal work has investigated the effect of NP size on the ability to penetrate through brain tissue[157,158]. Predominant opinion suggested that materials with diameter ranges of up to 64 nm could traverse at substantial rates across the brain extracellular space (ECS), confirmed by a study utilising 35 nm quantum dots and dextran in rat ECS and modelling the diffusion in ECS and fluid filled pores[159]. The effectiveness of many therapies is therefore limited, as most particulate drug delivery systems carrying therapeutic genes or viruses, as previously discussed, are too large for efficient penetration at this quoted size range. However, the study estimated that human ECS contains some pores larger than 200 nm, and that more than one quarter of the pores are ≥100 nm. These findings were confirmed *in vivo* using mice, where 40 and 100 nm

polystyrene (PS) NPs spread rapidly within the brain tissue, if densely coated with PEG. In contrast, 200 nm PEG coated PS NPs did not penetrate the brain tissue. Further work showed that model PS-PEG-coated NPs of 114 nm in diameter were able to rapidly diffuse into normal brain tissue[158] and that paclitaxel-loaded, PLGA-co-PEG block co-polymer NPs, with an average diameter of 70 nm, were able to diffuse 100-fold faster than similarly sized paclitaxel-loaded PLGA particles without a PEG coating[157]. The hydrophilic PEG coating acts as a flexible hydrated cloud, creating a barrier which minimises adhesive interactions with cell surfaces, allowing the NPs to pass further into the brain. In short, despite PEGylation being utilised originally for improved circulation time during systemic delivery, it has been shown that PEGylation also improves the penetration of biological barriers, leading to enhanced overall delivery, even locally[160].

1.5.4 Local delivery of NPs for brain tumour therapy

Most localized nanotherapeutic delivery systems that have been explored in the field of GBM are administered through CED, as previously described. The only case of a drug-loaded NP depot device is that of a PEG-dimethacrylate (DMA) photopolymerisable hydrogel system, developed at Université Catholique de Louvain in Belgium[161,162]. Originally, the PEG-DMA hydrogel was loaded with TMZ-loaded polymeric micelles to treat GBM. The micelles were composed of PEG_{750}-block-poly(ε-caprolactone-co-trimethylenecarbonate) [PEG-p-(CL-co-TMC)][163,164]. *In vivo* studies demonstrated that the photopolymerisable

hydrogel was well tolerated, and the efficacy study showed that the tumour weight of the mice treated with the TMZ-micelle loaded hydrogel drastically decreased in comparison with the control groups 7 days post-surgery. The *in vivo* study was carried out on nude mice bearing a human U87MG xenograft[161]. The PEG-DMA hydrogel was also loaded with paclitaxel-encapsulated PLGA NPs, and similar *in vivo* studies were carried out. Incredibly, more than 50% of the mice treated with paclitaxel-loaded PLGA NPs hydrogel were still alive 150 days after the injection of tumour cells, resulting in long term survival[162]. More recently, the same photopolymerisable hydrogel-based local drug delivery system was utilised for the codelivery of paclitaxel and TMZ[96]. In this study, the same paclitaxel-loaded PLGA NPs were investigated but the TMZ was embedded directly into the hydrogel. The median survival time of mice with paclitaxel-loaded PLGA NPs or TMZ-loaded hydrogels was significantly prolonged, but the combination treatment showed even higher significance levels compared to the control groups. Only 22% of the mice had tumour recurrence within 110 days after tumour implantation. The other mice showed no sign of tumour recurrence, and this was analysed through both MRI and Hematoxylin and eosin (H&E) staining of the sacrificed mouse brains at day 110.

1.6 Ring Opening Polymerisation

The different mechanisms of Ring Opening Polymerisation (ROP) include radical, cationic, anionic and Ring-Opening Metathesis Polymerisation (ROMP) and largely refers to the type of initiator in the polymerisation process[165]. The monomers consist of ring structures, and it is this ring strain and accompanied steric conditions that act as the driving force behind ROP[166]. For anionic ROP, commonly used initiators are materials with hydroxyl end groups, for example PEG, and the polymerisation can also be initiated with amine-based materials.

Lactide is a frequently used starting material for ROP, resulting in the formation of poly(lactic acid) (PLA), a biodegradable material. Due to the ease of ROP, the hydrophobic chain length can be controlled, enabling the polymeric carrier to be prepared at the most beneficial size.

1.6.1 Ring Opening Polymerisation of esters

Access to a wide range of biodegradable, bioassimilable and renewable polymeric materials is provided through the ROP of cyclic esters. This technique leads to the production of polyester polymers, and growing these into large macromolecular frameworks provides enhanced control over polymer characteristics[167]. ROP is the preferred method for preparation of polyesters over polycondensation due to the high temperature and long reaction times required for polycondensation, also in addition to the side reactions and necessity to remove small molecular

weight by-products such as H_2O, CO_2 etc[168]. It has been observed that the ROP of lactide enables a more precise control of the final molecular weight of the subsequent polymer; whereby a linear relationship between monomer conversion and final molecular weight was yielded, resulting in a narrow Polydispersity Index (Đ). Conversely, polycondensation has been found to limit the accessible range of molecular weights, resulting in broad Đs of 2[169].

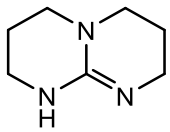
1.6.2 Ring Opening Polymerisation of aliphatic carbonates

Aliphatic poly(carbonate)s have gained a broad interest for biomedical application, mainly due to their biocompatibility, biodegradability and low toxicity[170]. They also offer the possibility of incorporating functionalities to the polymeric backbone. This can be achieved through post polymerisation functionalisation; however, this method can result in polymer degradation due to the harsh conditions applied[171]. Alternatively, functionality in the polymer backbone can be achieved through the copolymerisation of functional cyclic monomers (often poly(carbonates)) and simple cyclic esters[171–174]. However, not all functional groups are compatible with the ROP process and can inhibit the polymerisation efficiency in some cases[172].

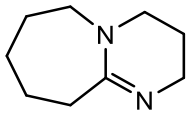
1.6.3 Catalysts for Ring Opening Polymerisation

The selection of the catalyst for ROP is of upmost importance to promote the thermodynamically favourable ring opening of the monomer over

transesterification and other side reactions. Tin octoate [$Sn(Oct)_2$)] is a standard catalyst used in the ROP of lactide[175,176] but should be avoided for biomedical applications due to toxicity concerns from the metallic residues of the reactions. Alongside these toxicity concerns, removing metal-based catalysts also evades issues in large scale manufacture surrounding the cost and supply for precious metals[177]. These reasons have driven scientists to explore new catalysts for ROP reactions, enabling safer, more appropriate formulations to be utilised in the medical field. This move was pioneered by Hedrick and Weymouth in 2002, whereby they introduced N-heterocyclic carbenes as alternative catalysts for living ROP of cyclic esters, generating polymers with predictive molecular weights, reflecting the initial monomer-initiator ratio and narrow polydispersities[178]. Two examples of the N-heterocyclic carbenes are 1,5,7-Triazabicycle[4.4.0]dec-5-ene (TBD) and 1,8-Diazabicyclo[5.4.0]undec-5-ene (DBU), and their structures are shown in Figure 1-11.



1,5,7-Triazabicycle[4.4.0]dec-5-ene (TBD)



1,8-Diazabicyclo[5.4.0]undec-5-ene (DBU)

Figure 1-11 Structures of the organobasic catalysts investigated for the ROP of lactide.

TBD was first introduced as a catalyst for the ROP of cyclic esters in 2006[179], and is believed to undergo a bifunctional nucleophilic mechanism[180]. It is this bifunctionality which enables the simultaneous activation of both the cyclic ester monomer and the alcohol group of the initiator, leading to excellent control over the polymerisation. It is a highly active catalyst and has been proven to effectively catalyse the ROP of large ring catalysts[181] (Figure 1-12).

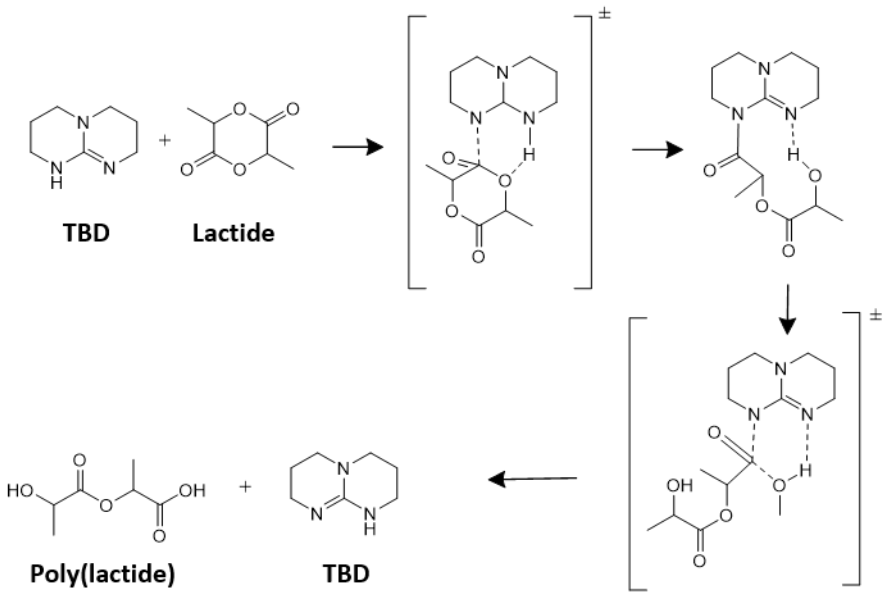


Figure 1-12 Proposed dual-action mechanism for the catalysis of the ROP of lactide by TBD. Adapted from[180].

DBU has been shown to be inactive for the ring opening of large ring lactones, but has shown to have promise for 6-membered rings such as lactide[181], and works in a monomodal fashion (Figure 1-13)[169].

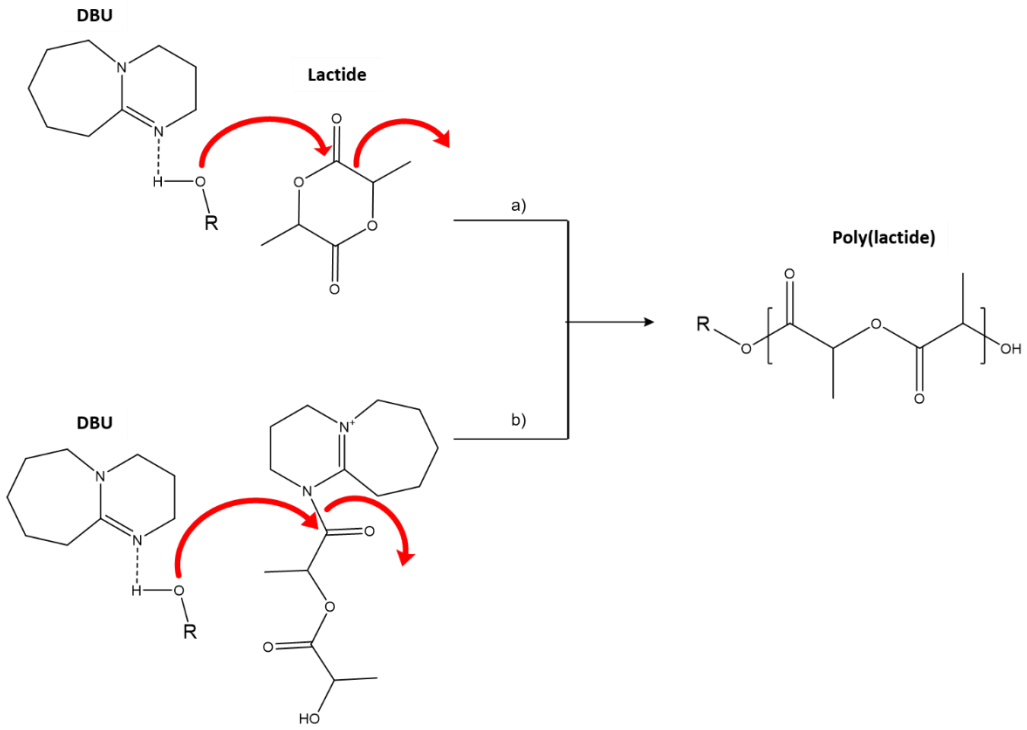


Figure 1-13 Two plausible routes involved in the DBU-catalysed ROP process of lactide with an alcohol initiator.

Through appropriate catalysts, this work is progressing toward the overall goal of producing medically friendly, biodegradable drug delivery systems.

1.7 Doxorubicin

DOX, it's structure outlined in Figure 1-14, is an anthracycline antibiotic and is one of the most widely used anti-cancer agents[182]. Yet, the mechanism of DOX is not wholly understood. It is most often described as a topoisomerase II inhibitor[183] but this mechanism of action does not fully explain the scope of cytotoxicity exhibited by DOX[184]. The unwinding of DNA for transcription and replication is catalysed by the family of

topoisomerase enzymes. DOX inhibits this enzyme by forming complexes with DNA by intercalation with base pairs, stabilising the DNA-topoisomerase II complex and thus leading to double stranded DNA breaks[185,186]. However, it is also proposed that there are other targets for DOX-induced cell death including inhibition of RNA and DNA synthesis[187,188], the production of free radicals[189] and the formation of DOX-DNA adducts, mediated by formalehyde[190,191].

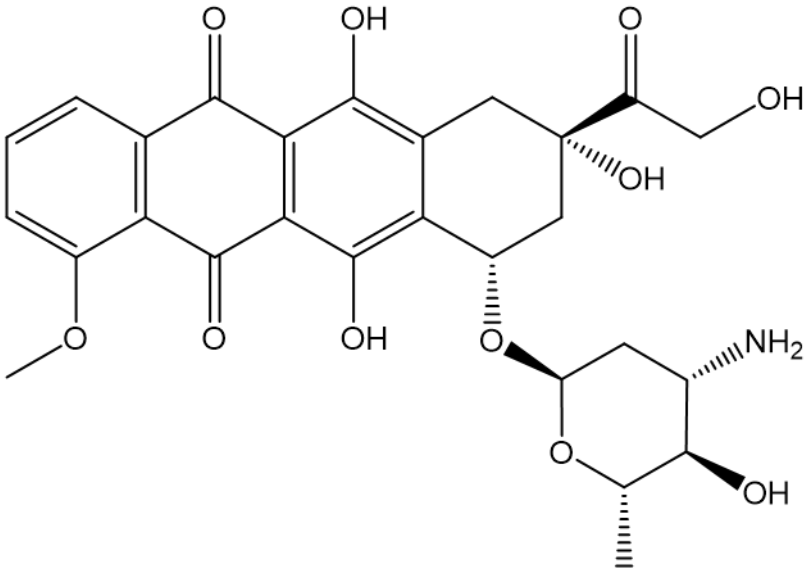


Figure 1-14 Chemical structure of doxorubicin.

1.7.1 DOX in the treatment of GBM

DOX has been explored in the treatment of GBM with very limited success. Despite *in vitro* data validating the cytotoxicity of DOX against a variety of GBM cell lines[192–195], *in vivo* data advocating DOX as a strong anti-glioma agent[15–29] and even clinical data confirming DOX's potential as a treatment for GBM patients[211–213], there remains strong concerns

surrounding the use of DOX in the treatment of GBM. All chemotherapeutics have toxicities and adverse effects associated with their use, due to their “unspecific” action, but DOX also has a significant increase in the risk of potentially fatal cardiotoxicity[214,215], resulting in a serious concern for prescribing medical staff. Alongside this, DOX has very poor penetration across the BBB[216,217], therefore very high doses are needed and have been proven to be ineffective[218–221]. A potential solution to these problems is to incorporate DOX into a nanocarrier formulation[222–225], and/or to deliver DOX locally.

1.7.1.1 Local delivery of DOX in GBM

As described earlier, Gliadel™ wafers are the only local drug delivery treatment method currently used to treat patients with GBM. They were invented and developed by Prof. Henry Brem and colleagues at Johns Hopkins University. Following the success of Gliadel™ in the treatment of both primary and recurrent GBM, the team explored replacing the original drug, carmustine, with DOX to explore the efficacy of locally delivered DOX as a monotherapeutic agent against malignant brain tumours in rats[209]. Rats bearing intracranial tumours were treated with the polymeric wafers containing 3% DOX and 5% DOX and were compared against rats with blank polymer (0% DOX) and no polymer (control). Compared to both the control arms, rats treated with DOX had significantly increased survival (21 days vs 34 days vs 45 days for control, 3% DOX and 5% DOX respectively). This study was able to conclude that

when delivered locally, DOX showed promise as a monotherapeutic agent for the treatment of GBM.

A small preclinical trial, consisting of ten patients with recurrent glioma who had not responded to radiation therapy, was completed whereby patients were administered DOX via an Ommaya pump[211]. At the time of the second craniotomy, the Ommaya reservoir and catheter were placed in the resection site allowing delivery of DOX intratumourally. Ommaya pump delivery is a catheter-based therapy which relies on diffusion of drugs from the reservoir into the tumour cavity as a result of a concentration gradient[226]. It was originally developed for ventricular drainage in 1963[227].

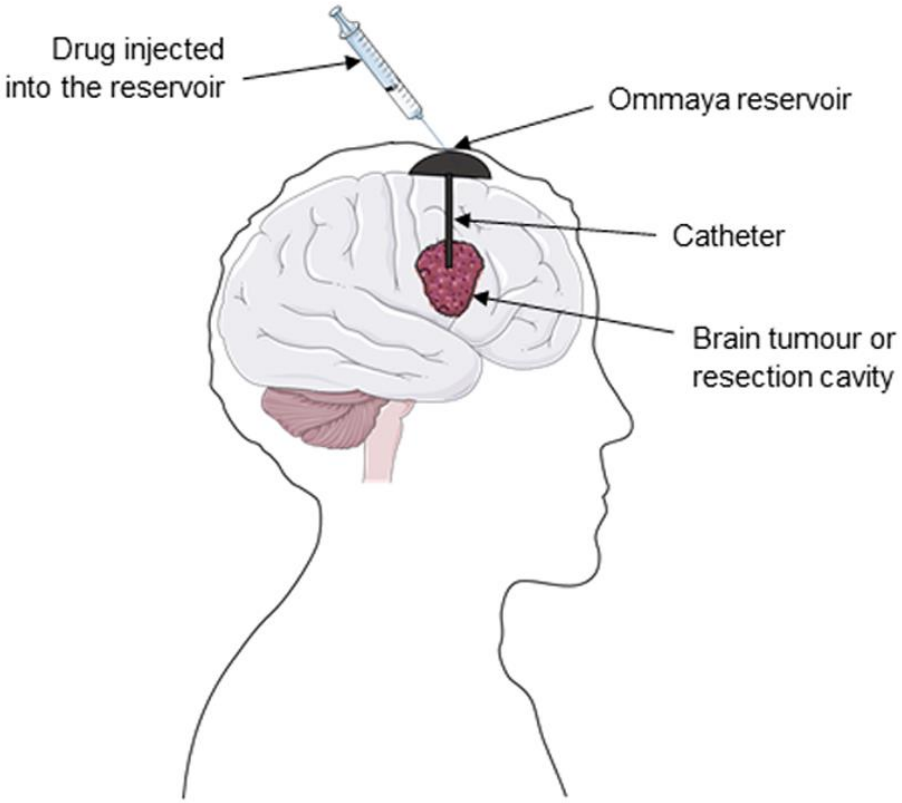


Figure 1-15 ***Catheter delivery using an Ommaya reservoir.*** *An Ommaya reservoir with the catheter placed in the tumour, allows regular injections of chemotherapeutics. The reservoir can also be placed into the lesion site post-surgery. This figure was created by Phoebe McCrorie using Servier Medical Art templates, which are licensed under a Creative Commons Attribution 3.0 Unported License; https://smart.servier.com. (Revised manuscript in prep; McCrorie*, Vasey* et al).*

This method of drug delivery shows great promise, as the drugs can be delivered directly to the site of tumour, reducing adverse side effects from the drugs. In this study, patients were administered 0.5 mg DOX daily on days one to ten of treatment, and six out of the ten patients showed clinical improvement[211]. Importantly, the study reported that *"there were no other clinically significant adverse reactions either in the brain or systemically"* easing previous concerns of the adverse toxicity caused by DOX, and again, further promoting DOX as a potential chemotherapeutic

in the treatment of GBM when delivered locally.

1.7.1.2 Delivery of DOX via NPs for GBM

NPs have been used to investigate the systemic delivery of DOX to treat GBM as outlined in Table 1-2 below. All the NPs described utilised a polymer coating to enable successful delivery of DOX across the BBB.

Table 1-2 Examples of doxorubicin NPs used in the investigational treatment of GBM

NP material used	Coating material used	Size (nm)	*In vitro* model	*In vivo* model	Conclusion of Study	Reference
LGA	Poloxamer-188	120 ± 1	U87MG	--	Cell uptake within one hour, with the poloxamer coating improving the internalisation efficiency.	Malinovskaya *et al*[228]
Poly(butyl cyanoacrylate)	Polysorbate 80	250	---	Rats bearing intracranial 101/8 GBM tumours	The polysorbate-coated NPs produced considerable doxorubicin concentrations in the brain, the uncoated NPs did not reach a level above the limit of detection. Efficacy study showed that IV administration of the NPs led to 40% cure.	Jörg Kreuter[229]
PLGA	Poloxamer 188 / Polysorbate 80	243.4 / 239.9	---	Wistar rats bearing intracranial 101/8 GBM tumours	Poloxamer 188 coated NPs had higher efficacy than polysorbate 80-coated NPs following IV administration.	Gelperina *et al*[230]
Poly(butyl cyanoacrylate)	Polysorbate 80		---	Wistar rats bearing intracranial 101/8 GBM tumours	Polysorbate-coated NPs showed an increase in long term survival compared to uncoated-NPs and doxorubicin alone following IV administration.	Steiniger *et al*[208]
PLGA	Poloxamer 188	250	---	Wistar rats bearing intracranial 101/8 GBM tumours	Poloxamer 188-coated PLGA nanoparticles enable delivery of doxorubicin across the BBB in the therapeutically effective concentrations following IV administration	Wohlfart *et al*[231]
PLGA	Glutathione-PEG	331.6 ± 9.1	Rat glioma cell line, RG2. BBB model made up of Transwell™ with a 0.4µm pore size	---	The glutathione-coating showed significantly higher rates cellular uptake increased the permeability rate across the *in vitro* BBB model compared to their uncoated counterparts.	Geldenhuys *et al*[232]

Clinical studies involving PEGylated liposomal DOX have been conducted for the treatment of malignant glioma[212,213,233]. This formulation is now better known as Caelyx™ or Doxil®, and was the first "nano-drug" formulation to be approved by the FDA, in 1995[214]. It is used to treat breast cancer, ovarian cancer, other solid tumours and AIDS-related Kaposi's sarcoma[234]. Clinical studies in the treatment of breast carcinoma therapy reported that approximately half of the dose of DOX-PEG liposomes compared with conventional DOX-liposomes resulted in the same clinical response[235,236], leading to a strong rationale for the PEGylation of these liposomes to increase efficacy.

Pre-clinical data of this formulation in an intracranial xenograft mouse model showed that concentrations of DOX in tumour tissue and cerebrospinal fluid (CSF) increased when stabilised liposomes were administered[237] and increased even further when the formulation was PEGylated[238]. In the first Phase II clinical trial, a dose escalation study was completed whereby patients received liposomal DOX through IV administration at 20 mg/m^2 every two weeks. This dose was increased to 40 mg/m^2 if patients were able to receive it. The study concluded that the optimal dosage was 20 mg/m^2 every two weeks and a prolonged median survival of 20 months was observed, which was found to be superior to other second-line treatments for recurrent glioma[233].

The successful results of the Phase II trial led to a second clinical trial with a two-part aim; to assess the efficacy of the PEGylated formulation

(Caelyx™) alone and in combination with tamoxifen, a known modulator of tumour resistance[212]. The study found that there was no statistical significance between the two groups of patients in terms of efficacy, but they were both well-tolerated and moderately effective for patients with recurrent high-grade gliomas.

Another Phase I/II clinical trial investigated the treatment of Caelyx™ with the usual TMZ/radiotherapy regime[213]. In Phase I, Caelyx™ was administered in a 3-by-3 dose-escalation regime. In Phase II, 20 mg/m^2 Caelyx™ was administered once prior to radiotherapy and on days one and 15 of each 28-day cycle, commencing four weeks after radiotherapy. TMZ was administered daily during radiotherapy and on days one to five of each 28-day cycle. It was found that the combination treatment of Caelyx™, TMZ and radiotherapy was well tolerated; however, no significant improvement of the patient's outcome was observed as compared to the standard of care treatment.

1.8 Project Rationale

Given the reported success of local delivery in the treatment of GBM, this project aims to incorporate aspects of both an established localised delivery system with a novel drug delivery approach *via* nanocarriers to potentially enhance the treatment of GBM. As surgery is a first-line intervention for almost all patients diagnosed with malignant brain cancer such as GBM, considerations for local, interstitial delivery of nanotherapeutics are particularly clinically relevant for this disease. This

project will incorporate nanotherapeutics into an established microparticle-based localised delivery system (PLGA/PEG). To the best of our knowledge, this is the first attempt to incorporate nano-scale therapeutics with micro-scale delivery systems, to produce a multi-component platform for neuro-oncology and indeed oncology in general. Localised delivery also circumvents the BBB, thus alleviating the problems associated both with therapeutic drug concentrations crossing the BBB and dose-limiting toxicities associated with systemic delivery.

However, brain penetration of these delivered agents once released from this drug delivery system still presents a major challenge to effective treatment. Polymer therapeutics offer a solution to this problem, whereby anticancer agents can be conjugated to macromolecules or encapsulated within NPs and subsequently formulated with the PLGA/PEG particles. The polymeric nanocarrier system is predicted to diffuse away from the drug depot before releasing its drug payload, thus potentially enabling delivery of the drug, in its active form, further into the brain parenchyma than is currently possible with direct release of drug from the PLGA/PEG microparticles.

It is believed that the use of nanocarriers will offer a two-fold benefit to the drug delivery system as opposed to releasing a chemotherapeutic directly from the PLGA/PEG paste: i) the nanocarrier will act as a “protective casing” for the drug, leading to a longer half-life of the drug and ii) the nanocarriers will enable the drug to have a greater degree of penetration across the brain parenchyma, due to transcellular transport

mechanisms[239]. In turn, this will lead to the drug-loaded NP diffusing further through the brain than drug alone from the PLGA/PEG matrix, and thus also a higher concentration of active drug, having avoided degradation in the brain. Furthermore, it has been reported that PEGylating these types of systems leads to more enhanced penetration properties of biological barriers, in both healthy tissue[160,240] and tumour models[241].

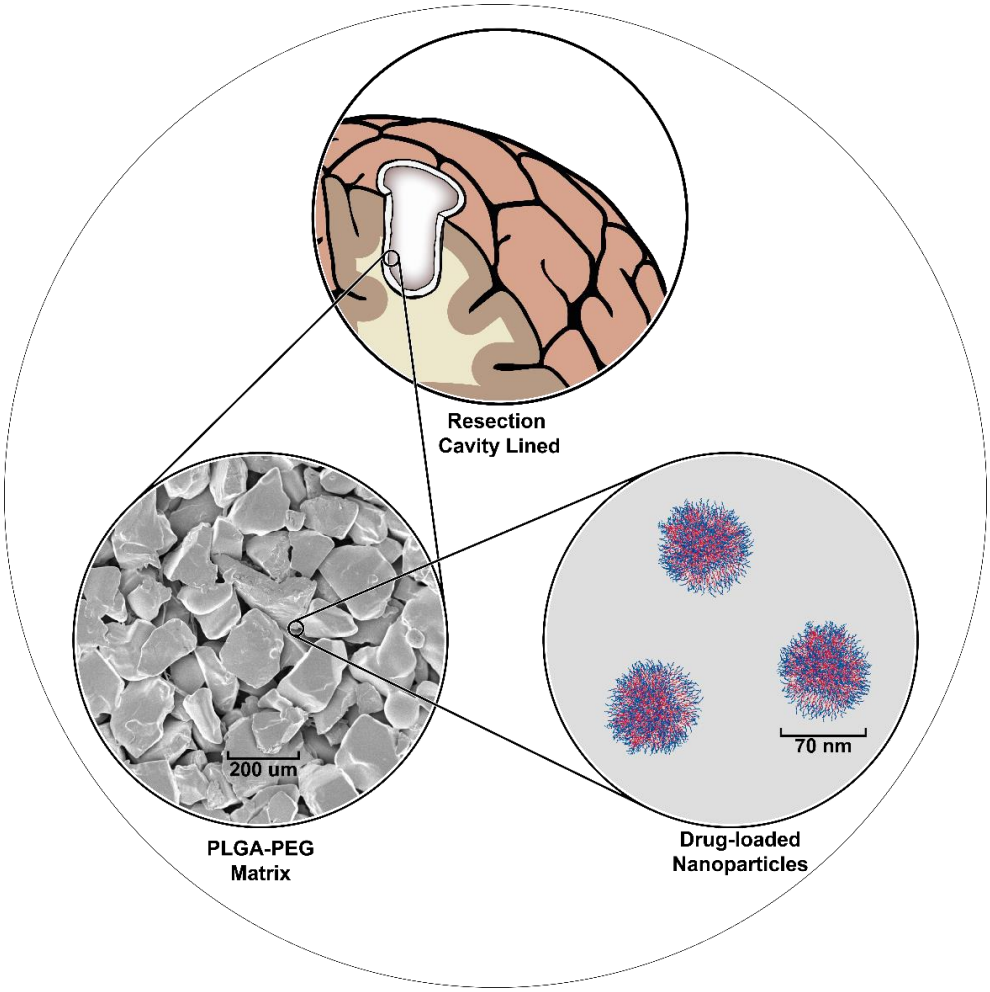


Figure 1-16 ***Graphical abstract of project.*** *A representation of the lining of the resection cavity with the drug-loaded NP-embedded PLGA/PEG matrix. Figure was produced by Oran Maguire using Adobe Illustrator.*

1.8.1 Overarching hypothesis and aims of project

Overarching project hypothesis: “Polymeric nanocarriers are compatible with, and can be released from, PLGA/PEG matrices for local delivery of chemotherapeutics, resulting in enhanced survival benefit in the treatment of GBM *in vivo.*”

Aims:

- Synthesise a library of biodegradable, biocompatible polymers, based on linear and star structures.
- Incorporate DOX, a relevant chemotherapeutic, into the formulation.
- Perform *in vitro* cytotoxicity studies with formulated NPs on a range of patient-derived GBM cell lines.
- Measure the release of the NPs from the PLGA/PEG microparticle matrix and release of DOX from the NPs.
- Complete *in vivo* studies using an orthotopic high-grade glioma rat allograft model, to assess the tolerability and efficacy of the formulations.

Chapter 2 Preparation of polymeric nanocarriers

2.1 Introduction

Biodegradable synthetic polymer-drug conjugates have been under active investigation as macromolecular therapeutics for over 40 years, yet there are still relatively few marketed drugs of this type[242–245]. One major reason for this lack of commercial and clinical translation has been the difficulty in matching the conflicting demands of high therapeutic efficacy with ease of preparation and characterisation. For example, there have been many examples of synthetic polymer-drug conjugates which show high activity *in vitro* and in pre-clinical *in vivo* studies[246–249]. However, inspection of the structures of some of these materials suggests they would be challenging to synthesise from a scale-up, commercial standpoint, or would require extensive toxicological investigations to ensure Good Manufacturing Practice (GMP)-compliance prior to use which would slow their development[250,251]. Accordingly, there remains a focus on aliphatic polyesters for pharmaceutical applications, as there are many flexible routes for their synthesis, and the metabolites produced upon their breakdown in the body are largely known and are removed via natural excretory pathways[168,252,253]. Poly(lactide) (PLA), poly(caprolactone) (PCL) and poly(glycolide) (PGA) and their copolymers are the most widely used polyesters in the health care sector, owing to their accessibility from

readily-available monomers, favourable mechanical properties, hydrolytic degradation and cytocompatibility[254–257].

Of particular interest are PLAs and associated co-polymers which can be easily synthesised via ring-opening polymerisation (ROP) of D,L-lactide (LA), a cyclic ester available from naturally occurring materials. PLA is already used in drug delivery as the hydrophobic block of GenexolP10®, a PEG-PLA co-polymer formulation of the anti-cancer drug Paclitaxel[258], currently in the clinic in Korea. However, a major drawback with lactide-type polymers in advanced therapeutic applications is the lack of functional 'handles' on the monomer units, resulting in a limited capability to conjugate drug molecules to the polymer backbone, reducing the overall drug loading in the formulation and ultimately the dose which can be delivered. In addition, limitations in the ability to control degradation rate, as well as concerns over the long-term biological effects of tin-based catalysts typically used in their production[179,259], are driving research efforts towards the development of more 'functional' and adaptable PLA-analogue polymer therapeutics.

Modification of the starting lactide monomers can be employed to introduce addressable functionalities along the polymer main chain[260]. However, this strategy often requires many synthetic steps as well as inefficient purification steps resulting in low yields. Additionally, not all introduced functionalities are compatible with the ROP process. Free nucleophiles such as hydroxyls, amines or thiols cannot be present during polymerisation, and therefore protection/deprotection and post-

polymerisation modifications may need to be employed if drugs are to be linked to the polymers. In this regard, aliphatic poly(carbonate)s are advantageous, as there are a range of methods for their derivatisation, and the central polymer backbone has appropriate properties for biomedical applications, being well-tolerated in the body, including the brain[261], and also biodegradable[262]. In addition, main-chain substituted poly(carbonate)s can be synthesised from functionalised cyclic carbonate monomers through relatively simple chemistry, thus allowing ready access to covalently-linked polymer-drug conjugates[170].

There are now several reports that both lactide and cyclic carbonate monomers can be ring-opened under ambient conditions with organocatalysts, such as DBU[263–266], thus negating the need for metal catalysts or high temperatures which might otherwise generate toxic or degraded components in the final polymer product. These data suggest that functionalised materials which are a) biodegradable and b) adaptable for a variety of therapeutic formats might be produced through ROPs of carbonates under mild reaction conditions. These chemistries might also serve to generate ‘platform’ polymer-drug conjugates which can be optimised for specific drug delivery applications by further end-group or side-chain modifications.

2.2 Chapter Hypotheses and Objectives

2.2.1 Hypotheses

Hypothesis 1 - A variety of polymers, based on both linear and star structures, will be synthesised and have the ability to form nanoparticles (NPs).

Hypothesis 2 - A chemotherapeutic drug will be incorporated to the formulations, resulting in drug-loaded nanocarriers, relevant for the future application of a drug delivery method for GBM.

2.2.2 Objectives:

1. Synthesise a variety of polymers, based on linear and star structures.
2. Conjugate a relevant chemotherapeutic to the polymer backbone.
3. Formulate nanoparticles with polymeric formulations.

2.3 Chapter Materials & Methods

2.3.1 Materials

All chemicals were used as obtained without additional purification unless otherwise stated. Poly(ethylene glycol) methyl ether (mPEG, M_n = 5000/2000 Da), trimethylolpropane ethoxylate (3PEG, 4/15 EO/OH, M_n =

1014 Da), pentaerythritol ethoxylate (4PEG, 15/4 EO/OH, M_n = 797 Da), 1,8-Diazabicyclo[5.4.0]undec-5-ene (DBU, 98%), Triethylamine (TEA, ≥ 99%), di-tert-butyl dicarbonate (99%), ethyl chloroformate and extra-dry dimethyl sulfoxide (DMSO) were purchased from Sigma-Aldrich. Polyethylene glycol (PEG, Average M_n = 4000 Da), tetrahydrofuran (THF, ≥99.8%), hexane and diethyl ether (Et_2O) were purchased from Fisher Chemical. 2-amino-1,3-propanediol (Serinol, 98%), dichloromethane (DCM, 99.8%, extra dry over molecular sieve, stabilised, Acroseal) and acetonitrile (MeCN, 99.9%, extra dry anhydrous, AcroSeal) were purchased from AcrosOrganics. Trifluoroacetic acid (TFA, 99%) was purchased from VWR Chemicals. Ethylchloroformate and N,N′-Disuccinimidyl Carbonate (DSC, > 95%) were purchased from Merck KGaA.

2.3.2 Synthesis of tert-butyl (1,3-dihydroxypropan-2yl) carbamate (tert-butyl serinol, tBS)

Serinol (10 g, 110 mmol) was dissolved in a mixture of water and THF (100 ml, 4:1 v/v) and the solution was cooled to 0°C. Following addition of TEA (22.5 mL, 162 mmol) to this mixture, di-tert-butyl dicarbonate (29 g, 131.5 mmol) pre-dissolved in THF (20 mL) was added dropwise over 1h. The reaction mixture was left stirring overnight at room temperature. Subsequently, THF was removed under reduced pressure and the residue was extracted with ethyl acetate (4 x 100 mL). The colourless organic phase was dried over anhydrous magnesium sulphate and concentrated under reduced pressure. The crude product was

recrystallized in ethyl acetate (yield 70%, 14.7 g). ^{1}H NMR (400 MHz, CDCl3, ppm): δ 5.30 (s, 1H), 3.86-3.63 (m, 5H), 2.60 (s, 2H), 1.45 (s, 12H). Observed chemical shifts and integrals were in agreement with previous reports[267].

2.3.3 Synthesis of tert-butyl (2-oxo-1,3-dioxan-5-yl) carbamate: (tert-butyl serinol carbonate, tBSC)

Tert-butyl (1,3-dihydroxypropan-2yl) carbamate (26.0 g, 136 mmol) and ethyl chloroformate (32.0 g, 295 mmol) were dissolved in THF (140 mL) and the solution was cooled to 0°C. TEA (47.0 mL, 338 mmol) was then added dropwise over 1h. Subsequently, the reaction mixture was left stirring overnight at room temperature. The precipitated salts were filtered off and the filtrate was concentrated under reduced pressure to afford the product as a white solid. The product was left drying in a vacuum oven overnight and subsequently washed with a mixture of THF:Et_2O (2:8, v/v) to remove traces of unreacted starting materials (yield 65%, 19.20 g). ^{1}H NMR (400 MHz, $CDCl_3$, ppm): δ 5.30 (s, 1H), 4.55 (d, 2H), 4.45 (d, 2H), 4.10 (s, 1H), 1.45 (s, 9H). Observed chemical shifts and integrals were in agreement with previous reports[267,268].

2.3.4 PEG Initiated Ring-Opening Polymerisation of Lactide and tert-butyl (2-oxo-1,3-dioxan-5-yl) carbamate (tBSC): Kinetics in Presence of DBU

A predetermined amount of PEG chain initiator ($mPEG_{2000}$; 111 mg, 0.055 mmol, $mPEG_{5000}$; 277 mg, 0.055 mmol, PEG_{4000}; 222 mg, 0.055 mmol, 3PEG; 56 mg, 0.055 mmol or 4PEG; 44 mg, 0.055 mmol), lactide (399 mg; 2.77 mmol) and tBSC (601 mg; 2.77 mmol) were weighed out in a glass vial (dried in an oven at 100°C overnight) and capped with a rubber stopper. [M]/[I] was adjusted in order to maintain a constant length of hydrophobic chains across the different final architectures. Dry DCM (5 mL), was added and the mixture was allowed to dissolve at room temperature. An aliquot was taken of the monomer-initiator mixture at this point: this sample was denoted as time point t0. DBU (3 % mol/mol compared to the total amount of monomers) was dissolved in DCM (1 mL) and added to catalyse the ring-opening process. After reaction, the catalyst was deactivated through adding the polymer mixture, dropwise, to cold hexane (30 mL) and the polymer was purified via multiple precipitation steps and dried in a vacuum oven (conversion of monomer into polymer ~ 75-80% w/w; ~ 800 mg). The purified materials were analysed by NMR and GPC. ^{1}H NMR ($mPEG_{5000}$-$(LA)_{50}$-$(tBSC)_{50}$ as model) (400 MHz, CDCl3, ppm): δ 5.19 (broad m, 104H), 4.26 (broad m, 249H), 3.66 (broad s, 492H), 3.39 (s, 3H), 1.82-1.46 (2 asymmetric broad s, 429+35H), 1.59 (broad m, 314H). ^{13}C NMR (101 MHz, CDCl3, ppm) δ

= 169.76, 154.50, 70.57, 69.00, 67.97, 65.58, 30.93, 28.33, 25.61, 16.65, 15.28.

2.3.5 BOC Deprotection Optimisation

A predetermined amount of PEGylated co-polymer ($mPEG_{5000}$-$(LA)_{50}$-$(tBSC)_{50}$, 100 mg, 0.46 mmol in carbonate-BOC monomer) was dissolved in extra dry DCM (3 mL). Varying amounts of TFA, with respect to the calculated tBSC units (2.3 mmol, 263 mg), was added slowly to the polymer mixture at 0°C. The reaction mixture was left stirring for varying amounts of time (5, 10 and 30 mins) and following precipitation in cold hexane, was washed with cold Et_2O and analysed by ^1H NMR. Different degrees of deprotection were achieved by simply varying the amount of TFA used and the reaction time. The optimum amount of TFA was found to be 5 eq, when the reaction time of 20 minutes was undertaken. These optimised parameters resulted in successful deprotection (~40%) whilst avoiding degradation of the main polymer backbone. ^1H NMR (t = 0 min) (400 MHz, DMSO-d6) δ = 5.26 – 5.10 (m, 80H), 4.17 – 4.01 (m, 168H), 3.52 (s, 492H), 1.48 (s, 240H), 1.39 (s, 370H). ^1H NMR (after 30 mins and post purification and drying) (400 MHz, DMSO-d6) δ = 8.42 (bs, 30H), 7.18 – 7.02 (m, 34H), [approx. 10 units deprotected] 5.24 – 5.11 (m, 62H), 3.51 (s, 492H), 1.55 – 1.41 (m, 204H), 1.38 (s, 320H).

2.3.6 DOX coupling procedure

DSC (1.5 eq. with respect to the amount of DOX, 0.125 mmol, 32 mg) pre-dissolved in anhydrous MeCN (3 mL) was added to a solution of DOX.HCl (1.0 eq., 0.083 mmol, 48 mg) in dry DMSO (3 mL) at 0 °C. TEA (2.5 eq. with respect to the amount of DOX, 0.21 mmol, 30 µL) was added slowly to the reaction mixture and left stirring for 4-5 hours. Deprotected polymer ($mPEG_{5000}$-$(LA)_{50}$-$(tBSC)_{50}$; 1.0 eq., 0.083 mmol, 15 mg; equivalents were calculated to be in high excess when compared to each repeating tBSC unit) was dissolved in a mixture of anhydrous MeCN/ dry DMSO (50/50, v/v, 3 mL) and TEA (2.0 eq. with respect to the amount of deprotected polymer, 0.166 mmol, 23 µL) was added, and the solution was subsequently added dropwise to the previous reaction mixture. The reaction was left stirring for a further 3 hours at 0 °C. The resultant conjugated polymer was purified through multiple precipitation steps in cold hexane:Et_2O (1:5 v/v) mixture and dialysed against water:methanol (5:1 v/v) mixture for 24 h. Finally, the purified aqueous suspension was freeze-dried for 48 h and stored at -22°C. The conjugation efficiency was found to be ~72%. A final NMR spectrum of the product ($mPEG_{5000}$-(LA)50-(tBSC)50-DOX) post purification and completely dried was recorded. ^{1}H NMR (400 MHz, DMSO-d6) δ = 14.08 (s, 4H), 7.93 (d, J = 4.3 Hz, 8H), 7.69 – 7.65 (m, 4H), 7.63 (s, 4H), 7.07 (d, J = 7.1 Hz, 21H), 5.34 (d, J = 8.7 Hz, 8H), 5.24 – 5.11 (m, 78H), 4.86 (d, J = 5.9 Hz, 4H), 4.61 – 4.56 (m, 4H), 4.50 (d, J = 10.1 Hz, 8H), 4.36 (d, J = 4.0 Hz, 12H), 4.16 – 3.93 (m, 205H), 3.81 – 3.74 (m, 8H), 3.71 – 3.66 (m, 4H), 3.51 (s,

492H), 3.24 (s, 4H), 3.07 – 3.01 (m, 8H), 2.94 (d, J = 5.9 Hz, 4H), 2.23 (d, J = 3.8 Hz, 4H), 1.50 – 1.41 (m, 200H), 1.38 (s, 290H).

2.3.7 Cy5 coupling procedure

Polymer ($mPEG_{5000}$_LA_tBSC; 100 mg), TEA (excess; 10 µL) in dry MeCN (0.5 mL) and DSC (excess; 5 mg) in dry MeCN (1 mL) were added to a dry glass vial under continuous stirring at 0°C and left for 3 hours. A stock solution of dye-TEA was made up in dry MeCN. The dye was at 1% wt/wt to the polymer and the TEA was in excess of the dye. Henceforth, 1 mg Cy5 and 10 µL TEA were dissolved in 2 mL dry MeCN. This was then added to the reaction under constant stirring at 0°C and left for a further 3 hours. Subsequently, the resultant conjugated polymer was purified through multiple precipitation steps in cold hexane: Et_2O (3:5 v/v) and left to dry in a vacuum oven to yield Cy5-conjugated polymer.

2.3.8 Nanoparticle Preparation

A nanoprecipitation method was used to form NPs, whereby the polymers (10 mg) were dissolved in acetone (1 mL), then the polymeric solution was added dropwise to deionized water (10 mL, final concentration of 1 mg/mL), under constant stirring at 550 rpm. The polymers rapidly formed NP suspensions through solvent exchange between water and acetone. The final suspension was then left stirring overnight at room temperature in order to reach complete acetone evaporation.

2.3.9 Critical Aggregation Concentration (CAC) calculation

The Critical Aggregation Concentration (CAC) was calculated using a Zetasizer Nano ZS as described in Malvern application note AN101104 (http://www.malvern.com/en/support/resource-center/application-notes/AN101104SurfactantMicelleCharacterization.aspx). In brief, a constant attenuator was selected and the intensity of the scattered light (count rate in kcps) was monitored for a range of diluted NP suspensions (100–0.05 µg/mL)[269]. The intensity increases linearly with concentration above the CMC, while below the CMC the count rates reach a plateau. The CMC was then calculated by intersecting the two lines.

2.3.10 General Methods and Instrumentation

2.3.10.1 Nuclear Magnetic Resonance (NMR)

NMR spectroscopy is an analytical chemistry technique used to determine the content and purity of a sample, alongside its molecular structure[270]. In NMR measurements, a magnetic field is applied to the atomic nucleus of stable isotopes, such as ^{1}H and ^{13}C in this body of work. The resonant frequency of the atomic nucleus is characterized through radio frequency pulses in accordance with its chemical or environmental surroundings. The electrons of the atom circulate in the direction applied by the magnetic field, which causes a small opposing magnetic field at the nucleus. The “chemical shift” (ppm or Hz) is observed for each nucleus whereby the static and opposing magnetic fields differ. Further analysis of the inter-relations between protons in the

molecule can be determined based on a principle called “spin-spin coupling” whereby nuclei that are three or less bond lengths apart exert an influence on each other’s opposing magnetic field[271].

Bruker AV400 and AV3400 NMR spectrometers operating at 400 MHz (^{1}H) and 101 MHz (^{13}C) at ambient temperature were used to perform nuclear magnetic resonance (NMR) analysis. Chemical shifts were assigned in parts per million (ppm). ^{1}H NMR chemical shifts (δH) are reported with the shift of C<u>H</u>Cl$_3$ (δ = 7.26 ppm) as the internal standard when CDCl$_3$ was used. ^{13}C Chemical shifts (δC) are reported using the central resonance of <u>C</u>HCl$_3$ (δ = 77.0 ppm) as the internal standard. All spectra were obtained at ambient temperature (22 °C ± 1 °C). MestReNova 6.0.2 copyright 2009 (Mestrelab Research S. L.) was used for analysing the spectra.

2.3.10.2 Fourier-Transform Infra-Red (FTIR) Spectroscopy.

FTIR is a form of vibrational spectroscopy used to determine the molecular structure of a compound based on its characteristic absorption of infrared radiation[271]. Each organic compound has a specific infrared spectrum, based on its molecular structure known as a “fingerprint”[272,273]. Attenuated total reflectance (ATR) is a method that directly analyses the sample through intimate contact between the crystal attached to the ATR-FTIR and the sample surface. During a measurement, the beam of electromagnetic radiation travels through the crystal and excites the surface of the sample. The subsequent emitted photons are recorded,

and those which correspond to the resonant mode frequencies in the sample are absorbed. Since the absorption bands relate to specific functional groups within the molecule, identification of these bands leads to the identification of the functional groups within the molecule[273].

FTIR spectroscopy was performed in the range of 4000–650 cm^{-1}. This was carried out using a Bruker Tensor 27 FT-IR spectrophotometer using an ATR attachment. Spectra were analysed using MicroLab software.

2.3.10.3 Gel Permeation Chromatography (GPC).

GPC is a size exclusion technique which characterises the molecular weight and molecular weight distribution of a polymer or macromolecule[274]. The sample is dissolved in a solvent and passed through a highly porous column which separates the particles based on size. Low molecular weight particles get trapped in the pores and travel slowly through the column, leading to a high retention time, whilst high molecular weight particles pass quickly through the column and thus elute from the column first[274]. When coupled with a refractive index detector, the molecular weight and size distribution can be determined[275].

GPC was used for determination of number average molecular weight (M_n), weight average molecular weight (M_w), peak molecular weight (M_p) and molecular weight distribution (polydispersity, Đ, M_w/M_n). The analysis was performed using an Agilent 1260 Infinity Series HPLC (Agilent Technologies, USA) fitted with two Agilent PL-gel Mixed-E columns in

series at a flow rate of 1 mL min^{-1} using THF (HPLC grade, Fisher Scientific) as eluent at room temperature and a differential refractive index detector (DRI); or a PL50+ Polymer Laboratories system equipped with a refractive index detector, employing 2 mixed bed (D) columns at 50°C and using a solution of DMF 0.1% LiCl as mobile phase at a flow rate of 1 mL min^{-1}. Poly(methyl methacrylate) standards (M_n range: 1,800,000-505 g mol^{-1}) and polycaprolactone standards were used for calibration.

2.3.10.4 Differential Scanning Calorimetry (DSC).

DSC is a thermoanalytical technique to determine phase transitions, such as the glass transition temperature (T_g). Briefly, the sample is heated against a reference material and the changes in heat flow required to heat the two samples at a constant rate is recorded[271]. Thermal properties of the materials (5 - 10 mg) were studied by DSC (Q2000, TA Instruments, Leatherhead, UK) at a heating rate of 10 °C/min.

2.3.10.5 Thermal Gravimetric Analysis (TGA).

TGA is a thermoanalytical technique whereby changes in the mass of a sample is monitored isothermally (as a function of time) or dynamically (as a function of increasing temperature at a constant rate)[271]. TGA analysis of the materials (20 mg) was performed in the temperature range of 30-400^{o}C at 10^{o}C/min (TGA5500). The data were analysed using Thermal Analysis Software (TRIOS).

2.3.10.6 Dynamic Light Scattering (DLS).

DLS is a non-invasive technique used for the rapid determination of the hydrodynamic diameter of particles in suspension (typically in the sub-micron range) through measuring the speed at which the particles diffuse due to Brownian motion[276]. The Stokes-Einstein equation (Figure 2-1) is then used to correlate the velocity of Brownian motion, the translational diffusion coefficient, to the size distribution profiles of the particles[277,278].

Stokes-Einstein Equation

$$d_H = \frac{\kappa T}{3\pi\eta D}$$

d_H = hydrodynamic diameter (m)
κ = Boltzmann constant (J/K)
T = temperature (K)
η = solvent viscosity (kg/m.s)
D = diffusion coefficient (m^2/s)

Figure 2-1 The Stokes-Einstein Equation. Combines the light scattering and diffusion behaviour of particles.

In DLS measurements, a light source shines a beam of focused light at the particles in solution, causing it to scatter in all directions and the intensity of the scattered light is measured by a detector. A detectable signal is produced when the scattered light results in mutually constructive phases which are then correlated by the digital autocorrelator to determine the diffusion behaviour of the particles[277].

The particle size was analysed by DLS using a Zetasizer Nano ZS at 25°C, with a scattering angle of 173° and laser wavelength of 633 nm (Malvern Instruments Ltd). Particle size for the Cy5-NPs were analysed by DLS at 25°C using a Viscotek 802 DLS, with a laser wavelength of 830 nm (Malvern Instruments Ltd). Measurements were taken in triplicate of NPs suspensions at 1 mg/mL in milli-Q water and used to calculate average intensity particle size distributions.

2.3.10.7 Zeta Potential Measurements

Measurements of zeta potential were performed using a Zetasizer Nano ZS (Malvern Instruments Ltd). The laser doppler velocimetry technique was used to measure the velocity of the particles in suspension, whereby this electrophoretic mobility is used to obtain the zeta potential using the Henry equation[279]. Measurements were taken in triplicate of NP suspensions at 1 mg/mL in milli-Q water and used to calculate average zeta potentials.

2.4 Results and Discussion

2.4.1 Monomer Synthesis and Purification

The key steps in the syntheses were preparation of a side-chain functional cyclic carbonate monomer, and ROPs with organic catalysts under mild conditions to generate materials with a range of architectures and self-assembly properties. The cyclic carbonate monomer was

prepared by adapting a previously reported two-step synthesis[267]. The key modification was the removal of chromatographic purification steps in the monomer synthesis by a simple solvent/non solvent (THF/Et_2O) wash step. The final non optimised yield of pure monomer was 65% after this rapid and simplified synthetic route (Figure 2-2).

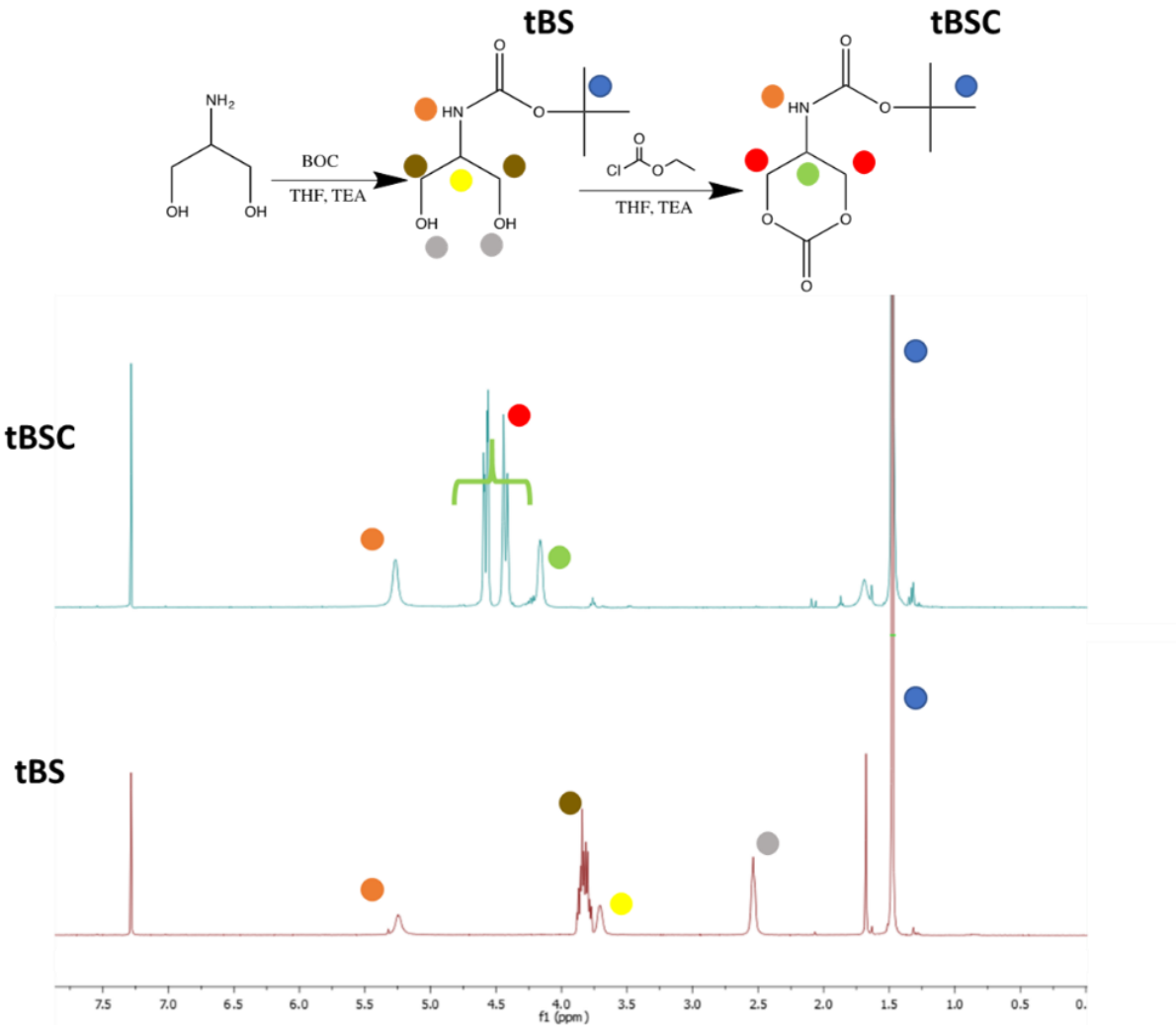


Figure 2-2 The synthetic scheme for the production of tert-Butyl (2-oxo-1,3-dioxan-5-yl)carbamate (tBSC).

2.4.2 Ring Opening Polymerisation

Five different PEGylated initiators were adopted to produce polymers with different final architectures, but with the same overall length of hydrophobic unit, which in this case was a random co-polymer of lactide and tBSC. It was observed via NMR kinetics experiments that both monomers were consumed to >90% conversion within 15 minutes (Figure A 1), and therefore this was chosen as the reaction time for all the PEG-initiated polymerisations. As depicted in Figure 2-4, all the final polymers showed the characteristic NMR peaks of polymerised lactide and tBSC, with good agreements in the feed ratios of both monomers and the initiator (Figure A 2**,** $mPEG_{5000}$-$(LA)_{50}$-$(tBSC)_{50}$ as model, P2 entry). In addition, in the ATR-IR spectra, all the characteristic transitions of both ester and carbonate moieties were observed (Figure A 3), further confirming the successful co-polymerisation. There was no observed difference in reactivity across the series of PEGylated initiators, as demonstrated by the final molecular weights and monomer ratios reached post-purification (Table 2-1).

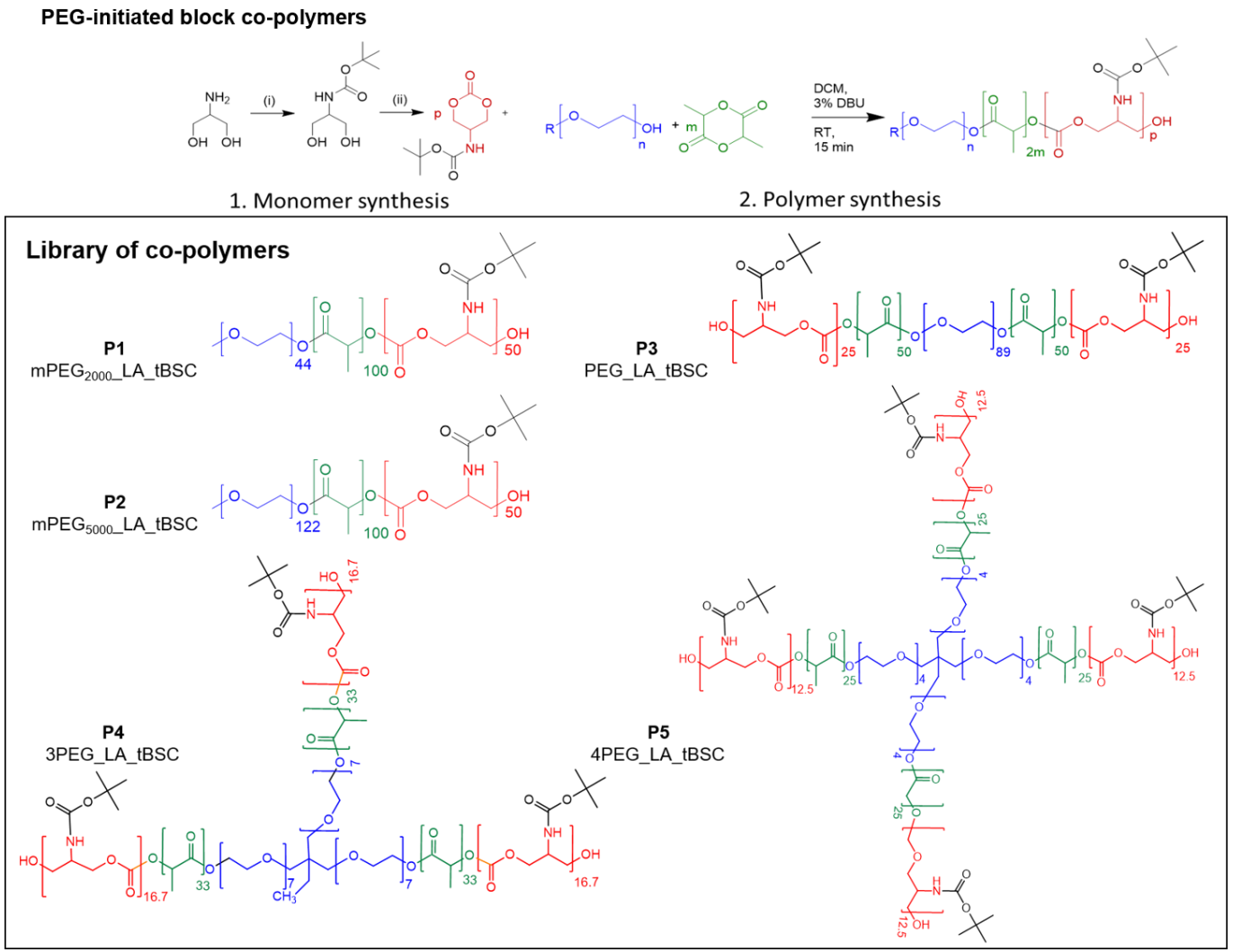


Figure 2-3 Synthesis of monomer and PEG-initiated co-polymers of varying architectures.

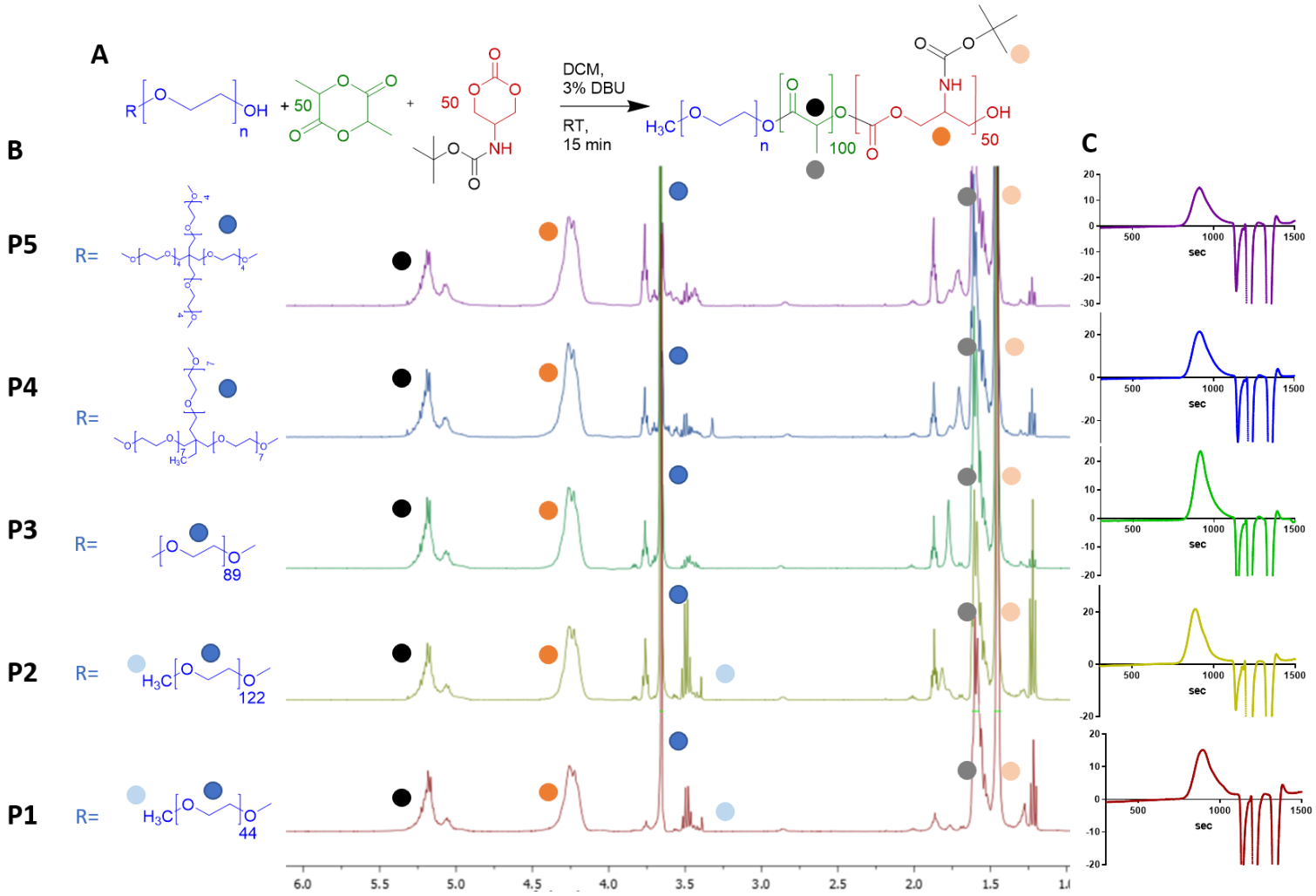


Figure 2-4 *A) general reaction scheme for the PEG-initiated ROP, B) ^{1}H NMR spectra of the five co-polymers, whereby the colour coding refers to the monomers constituting the polymeric backbone and C) GPC traces of the polymers.*

Table 2-1 Chemical and physical characterisation of the PEGylated co-polymers.

**compared to PMMA standards.*

	LA-tBSC units (targeted)	LA-tBSC units (exper)	M_n (NMR)	M_n (GPC) kDa	Đ	T_g (°C)	T_{m1} (°C)	T_{m2} (°C)	ΔH (J/g)
P1 $mPEG_{2000}$_LA_tBSC	60 – 53	55 – 48	20330	20.3	1.26	43.1	39.6	-	5.5
P2 $mPEG_{5000}$_LA_tBSC	55 - 50	52 - 50	23200	23.3	1.15	18.6	45.2	-	31.7
P3 PEG_LA_tBSC	50 -50	50 – 45	20960	17.0	1.22	20.6	42.1	-	25.6
P4 3PEG_LA_tBSC	55 – 53	52 – 49	19135	16.4	1.21	46.4	-	-	-
P5 4PEG_LA_tBSC	55 – 55	55 – 55	20650	16.3	1.22	42.1	-	-	-

In the DSC thermograms, as reported in Table 1, the polymers synthesised using crystalline PEG initiators showed a melting point (with different values of enthalpy) in the first cycle, while no melting transition could be observed in subsequent cooling and heating cycles within the temperature range explored. Glass transition temperatures (T_g) were observed for all the polymeric samples indicating the presence of amorphous structures as previously reported for similar co-polymers such as PEG-PLGA and PLGA[280,281]. The inability of the PEG chain to recrystallise can be attributed to the interaction with the ester-carbonate hydrophobic chains, hindering the chain-packing nucleation steps during cooling cycles[282]. Interestingly, the T_g of P2 and P3 was found to be below 37°C, and hence would be in emulsion form, rather than suspension form, meaning a different drug release could be expected and stealth properties of the NPs would likely be enhanced. In addition, it was found that the polymers synthesised from PEG initiators which were liquid at room temperature (i.e. the 3 and 4 arms PEG, P4 and P5 entries) had no determinable melting point.

2.4.3 Polymer side-chain derivatisation and drug coupling

2.4.3.1 BOC Deprotection

The intended use of the polymer family as delivery agents was also envisaged whereby drugs were covalently attached as well as, or in place of, encapsulated therapeutics. Accordingly, polymer P2 was chosen as the exemplar material from the small library and activated for drug attachment by removal of the BOC group. It was important for this step to occur without causing degradation of the polyester and polycarbonate backbone, thus the reaction was performed at 0^{o}C. In experiments to evaluate the optimal timing of the reactions, it was found that consistent deprotection of up to 40% of the initial BOC functionality was reached within 20 minutes of reaction, without degradation of the polymer backbone as shown by NMR (Figure 2-5). It was also found that removal of the BOC group and formation of free amine groups on the side-chains reduced the solubility of the polymer in $CDCl_3$, thus all the deprotected materials were analysed in DMSO-d_6 (for clarity the unfunctionalised polymer was also analysed in both the deuterated solvents as shown in Figure A 4). As depicted in Figure 2-5, the NH proton of the carbamide and the protons of the new produced ammonium moieties were clearly visible in the spectra between 7.0 and 8.6 ppm thus allowing simple calculation of the extent of BOC deprotection and conversion to free amine groups on the side chains.

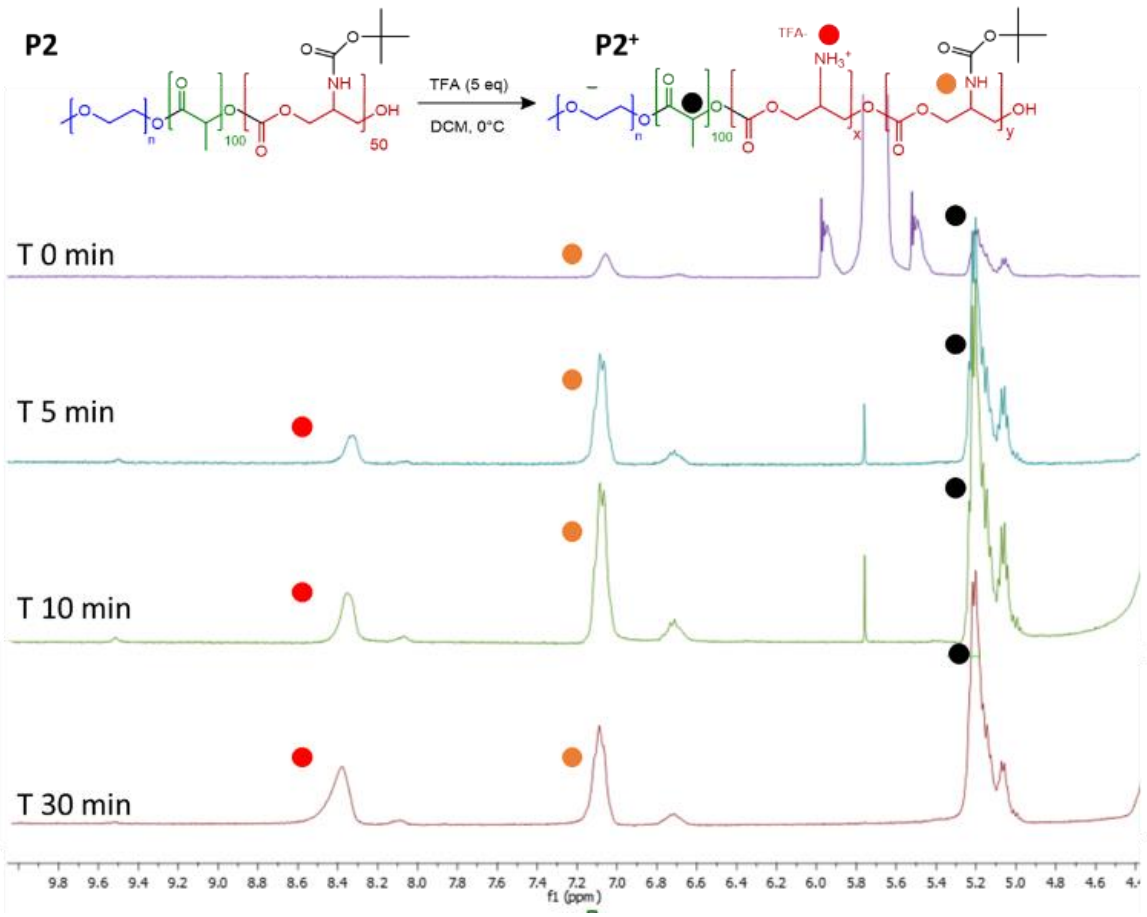


Figure 2-5 *^{1}H NMR spectra to show BOC deprotection on the carbonate unit in the polymer backbone. Spectra recorded after purification of the polymer from 0, 5, 10 and 30 minutes of reaction time.*

2.4.3.2 Drug Conjugation

Following the formation of the amine groups on P2, coupling of the widely-used anticancer agent, DOX, was carried out using N,N'-disuccinimidyl-carbonate (DSC) as the coupling-agent, thus linking the drug to the polymer via a stable urea linkage. The resultant polymer prodrug P2-DOX contained ~10 molecules of DOX based on NMR analysis, indicating a coupling yield of ~ 80 % based on the 12-13 free NH_2 units available per chain following BOC deprotection (Figure 2-6).

DOX was selected as the drug of choice for conjugation to the polymeric backbone in part due to the availability of a primary amine group, which we hypothesised would be an accessible group for conjugation to the amine groups on the polymeric backbone. Alongside this, DOX has shown promising *in vitro*[126] and *in vivo*[122,135,155] results and has been used in clinical trials in the treatment of GBM (systemic delivery)[213,283]. In particular, it has been shown to be efficacious in the treatment of GBM through local delivery[209].

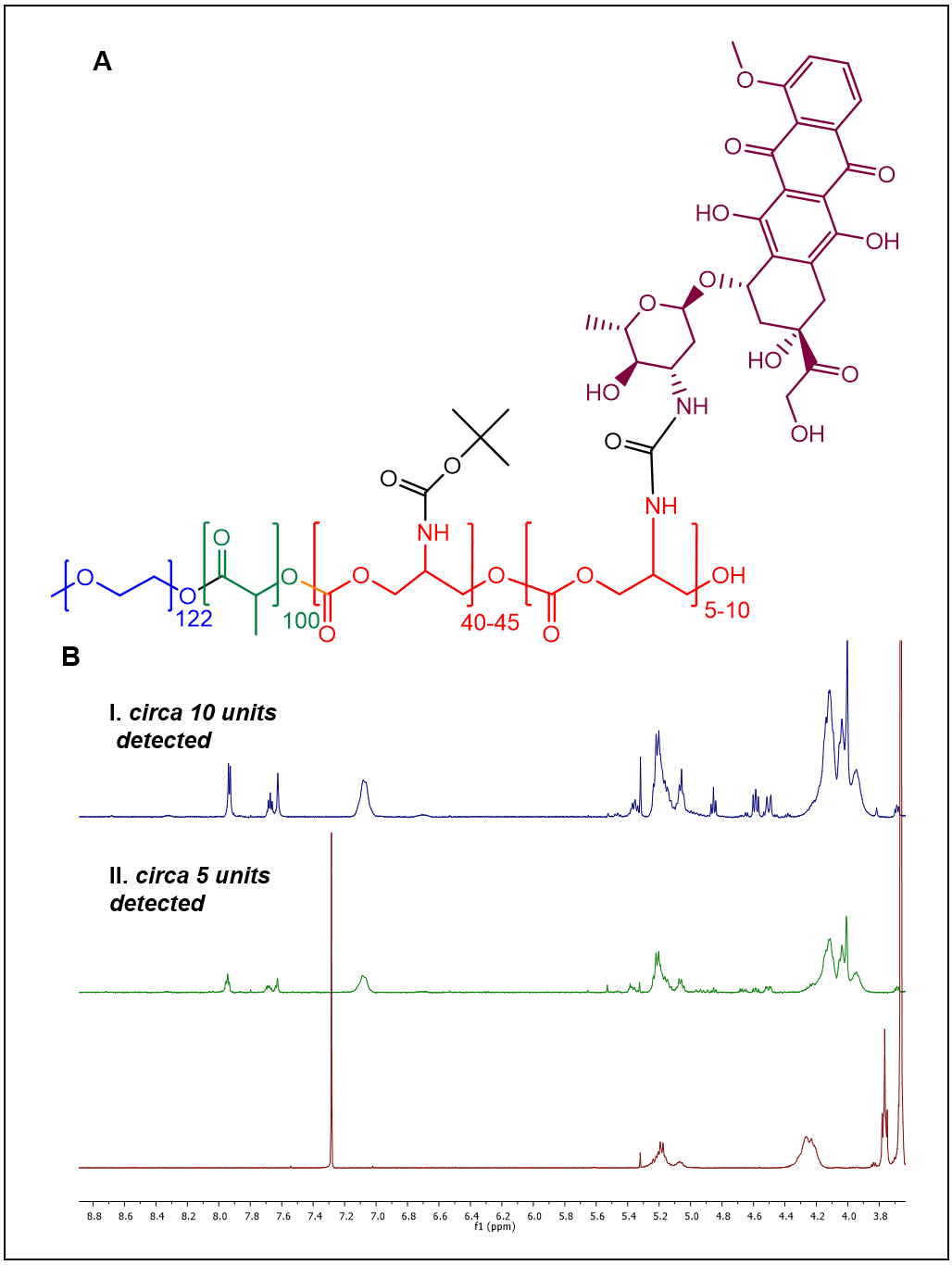


Figure 2-6 *A. Structure of the polymeric prodrug mPEG$_{5000}$-(LA)$_{50}$-(tBSC)$_{50}$-DOX. B. Stacked ^{1}HNMR spectra of the unmodified mPEG$_{5000}$-(LA)$_{50}$-(tBSC)$_{50}$ (bottom) and two modifications of mPEG$_{5000}$-(LA)$_{50}$-(tBSC)$_{50}$-DOX (middle and top spectra) at two different extents of functionalisation.*

2.4.3.3 Cy5 Dye conjugation

Cy5, a near-IR labelling agent, was selected as the dye of choice for imaging purposes due to its low limits of detection, accessible wavelength fluorescence emission and common use in biodistribution studies *in vivo*[284]. The hydroxyl group present on Cy5 would form a carbamate bond upon conjugation, and DSC was investigated as the coupling agent[285–287] (Figure 2-7). The presence of broadened peaks in the aromatic region of the ^{1}H NMR (Figure 2-8) indicates the successful coupling of Cy5 to the hydroxyl end of the polymer. Fluorescence spectroscopy experiments are required to quantify the amount of dye present per polymer chain.

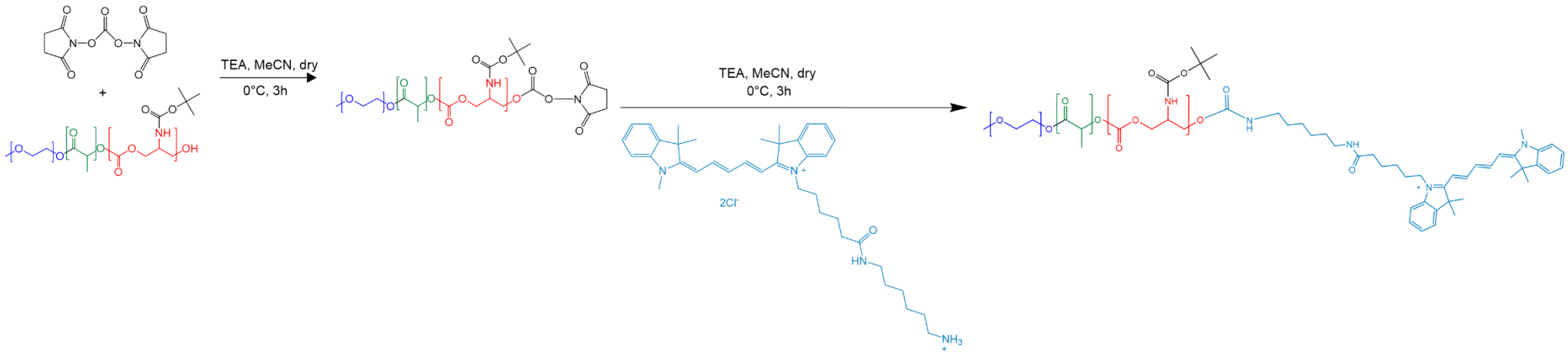


Figure 2-7 *Synthetic scheme for Cy5 conjugation to polymer backbone.*

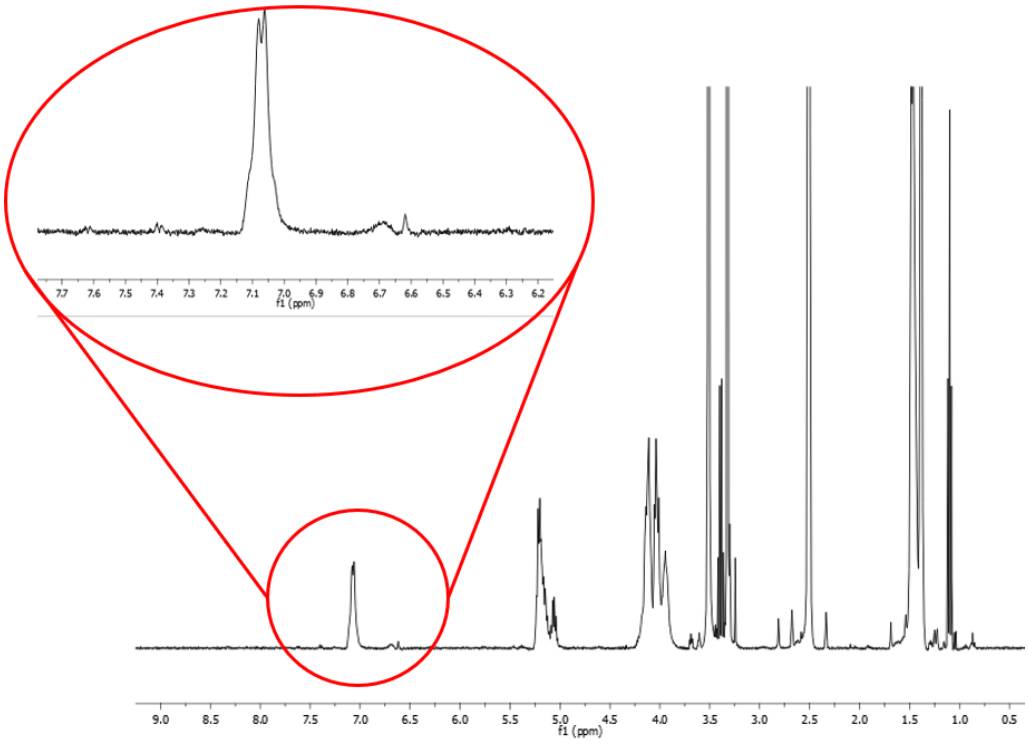


Figure 2-8 *^{1}H NMR showing coupling of Cy5 to the polymer backbone.*

2.4.4 Nanoparticle preparation

Self-assembling amphiphilic PEG-polylactide and PEG-polycarbonate materials have been widely investigated as NP carriers in drug and gene delivery assays[288,289]. Therefore, the ability of the varying polymeric architectures synthesised above to self-assemble into well-defined NPs using the standard formulation technique of nanoprecipitation (solvent displacement)[290] was evaluated. Rapid precipitation of the block polymers from acetone solutions into deionised water resulted in formation of NPs with sizes varying from 65 – 120 nm (Table 2-2**;** Figure A 5). The zeta potentials of all these NPs were negative, below -10 mV, as expected based on the presence of a hydrophilic PEG corona shell, with weak lone-pair interactions at the oxyethylene units with solution

cations and the corresponding association of solution anions to form the outermost layers (Table 2-2). The length of the hydrophobic fragments was kept constant across the range of co-polymers, and thus the differences in size and zeta potential can be attributed to the different PEG initiators adopted. CAC values were calculated by exploiting the light scattering count rate intensity variation according to serial dilution experiments. The resulting values were in the range of 8.5 to 12.7 µg/ml which indicated that NPs were present at low concentration in the final suspensions and required high dilution before disaggregation occurred.

Table 2-2 NP size distribution and zeta potential.

Average values from at least 3 sample replicates produced from 3 batches: measurements in milliQ water

	Size (nm) (At 1 mg/mL)	PDI	Z-potential (mV)	Critical Aggregation Concentration (CAC) (µg/mL)
P1 $mPEG_{2000}$_LA_tBSC	68.6 ± 1.1	0.1 ± 0.0	-26.9 ± 2.5	9.5
P2 $mPEG_{5000}$_LA_tBSC	61.4 ± 1.0	0.1 ± 0.0	-23.5 ± 4.5	8.5
P3 PEG_LA_tBSC	68.1 ± 1.9	0.1 ± 0.0	-10.7 ± 3.5	12.7
P4 3PEG_LA_tBSC	118.9 ± 3.8	0.1 ± 0.0	-29.2 ± 5.5	11.5
P5 4PEG_LA_tBSC	119.6 ± 3.1	0.1 ± 0.0	-30.1 ± 5.5	12.1

DLS was the only method used to determine the size profiles of the various NP formulations. TEM is a microscopy technique used to determine the size and morphology of NPs and is often used as an orthogonal method to DLS. In TEM measurements, a beam of high energy electrons is transmitted through a sample and an image is

subsequently formed based on the interactions of the electrons with the sample[291]. The morphologies and sizes of polymeric NPs can thus be determined. For further characterisation of these NP formulations, TEM should be performed.

The incorporation of Cy5 or DOX onto the polymeric backbones did not have an impact on the size of the NPs, as they were only slightly larger with the additional components, and the PDI remained narrow for each formulation, as can be observed in Table 2-3. Zeta potential measurements for the P2-Cy5 and P2-DOX NP formulations should be carried out to clarify whether the additional dye/drug components affected the stability of the NPs, and thus alter the characteristics of the subsequent NPs.

Table 2-3 Size, PDI and Zeta Potential values for P2, P2-DOX and P2-Cy5 NPs.

Formulation	Size (nm)	PDI	Zeta Potential
P2	61.4 ± 1.0	0.10 ± 0.00	-23.5 ± 4.5
P2-DOX	66.9 ± 2.0	0.09 ± 0.02	---
P2-Cy5	65.2 ± 23.6	0.13	---

2.5 Conclusion

In this body of work, the design, synthesis and characterisation of five PEGylated poly(lactide)-poly(carbonate) co-polymers with varying architecture and balance of amphiphilic components has been

presented. It has been demonstrated that these potential biomedical polymers suggest a number of advantages compared to existing methodologies for biomaterial synthesis. Firstly, the use of DBU as catalyst for controlled ROP enabled a range of polymers to be formed with good retention of functionality, and these materials were easily accessible through reactions under ambient and readily-achievable conditions. Secondly, PEGylated co-polymers could be generated with minimal purification steps, preserving the key functionalities along the polymeric backbone allowing for further modifications with drug molecules and labels for desired pharmaceutical and medical applications. Finally, the polymers could be designed for particular architectures or self-assembly properties without requiring multiple reactions steps, and their association into drug delivery NPs was easily demonstrated.

2.6 Chapter Acknowledgements

I would like to acknowledge Valentina Cuzzucoli Crucitti for carrying out the DSC and TGA measurements, and Vincenzo Taresco for completing the CAC and GPC measurements.

Chapter 3 *In vitro* evaluation of synthesised polymeric NPs for the treatment of GBM

3.1 Introduction

Glioblastoma multiforme (GBM) is the most common, malignant and aggressive brain tumour in adults, mainly due to its rapid proliferation and ability to penetrate and diffusely infiltrate healthy brain parenchyma. Standard of care treatment currently involves a combination of surgery, radiotherapy and chemotherapy. Yet, despite this multimodal treatment method, the median survival remains less than 15 months[23]. Local, intracranial drug delivery has been developed over the last two decades in order to exploit the low transport of drugs across the BBB, and thus ensure locally-delivered drugs remain in the brain. As surgery is the usual first step in the treatment of GBM, the rationale for intracranial drug delivery is based upon a unique treatment window immediately adjuvant to neurosurgery, in this case by delivering drugs directly to the site of minimal volume residual tumour following surgery. However, better treatment methods are necessary to eradicate residual tumour cells which remain beyond the resection cavity lining post-surgery, as GBM recurrence is almost certain unless these cells are eradicated.

A PLGA/PEG matrix, consisting of PLGA/PEG microparticles, has been designed and developed by our laboratory to act as a localised drug delivery system in the treatment of GBM[86,87]. The microparticles are

mixed with saline at room temperature to form a paste, enabling the surgeon to line the resection cavity site following the removal of the tumour. The microparticles then sinter at 37°C when the microparticles fuse, retaining the cavity lining shape. Initial studies have provided a promising proof of concept whereby chemotherapeutic drugs can be embedded into the drug delivery matrix and released gradually, via diffusion, away from the original resection site in the brain, efficaciously targeting the residual infiltrative cells remaining beyond the resection site[88].

Brain penetration of delivered agents once released from the drug delivery depot still presents a major challenge to effective treatment. Polymer therapeutics offer a solution to this problem, whereby anticancer agents are conjugated to macromolecules or encapsulated within nanoparticles. When subsequently formulated within the PLGA/PEG microparticles prior to releasing their drug payload, it is hypothesised that enhanced delivery of the therapeutic further into the brain parenchyma would be achieved compared to what is currently possible with direct release of the drug from the microparticles. The direct release of drugs relies on passive diffusion and unspecific uptake in healthy cells, as well as cancer cells[292], which restricts the tissue penetration of the drug. Conversely, the release of polymeric nanocarriers relies on active transport mechanisms[293–296], increasing the ability of the nanocarrier to travel further away from the drug depot site.

NPs can be internalised by two major endocytosis pathways: phagocytosis and pinocytosis. Pinocytosis accounts for the cellular uptake of smaller NPs (<500 nm) and can be further distinguished by clathrin-dependent, caveolae-dependent and clathrin/caveolae-independent pathways[297]. Clathrin-dependent endocytosis occurs via receptor-specific uptake or by receptor-independent uptake, and takes place in clathrin-rich areas of the plasma cell membrane[298]. Caveolae-dependent endocytosis plays a vital role in many biological processes, including cell signalling and transcytosis. Importantly, in terms of drug delivery, particles entering the cell through this pathway can circumvent lysosomal degradation, leading to improved efficacy[299]. Where cells are devoid of both clathrin and caveolae, nanoparticles may be internalised via the clathrin/caveolae-independent pathway[300], and there are many examples of nanoparticles exploiting this internalisation pathway through the utilisation of folic acid as a targeting agent[301]. Furthermore, less major transport mechanisms are known to enable the uptake of NPs into cells, for example, passive diffusion, direct microinjection and electroporation[293].

NPs can be released from cells via exocytosis, which is distinguished by two main mechanisms: regulated exocytosis and constitutive exocytosis. Regulated exocytosis occurs when the contents of an intracellular vacuole are secreted from the cell in response to a specific signal, whereas constitutive exocytosis does not require a signal to secrete the macromolecules[302]. Cell internalisation and exocytosis pathways are of

importance when considering the design and future application of drug-loaded nanocarriers[303]. For instance, the various endocytosis routes can transport the drug-loaded nanocarrier to different internal sites within the cell. In the case of this project, it would be ideal for the NPs to avoid lysosomes and subsequent degradation to thus afford further penetration through brain parenchyma.

Localised drug delivery for GBM has major advantages over delivering drugs systemically, mainly that high therapeutic drug concentrations can be achieved at the malignant tumour site, whilst avoiding systemic dose-limiting side effects. This method is proposed to enable the controlled and sustained release of the chemotherapeutic drug(s) over a number of weeks, thus filling the current oncological treatment gap between surgery and radiotherapy/chemotherapy (typically 3 – 4 weeks).

The previous chapter introduced the PEGylated poly(lactide)-poly(carbonate) co-polymers, where the main polymeric platform was based upon a commercially-available polymeric formulation, GenexolP10®, a PEG-lactide polymeric backbone with paclitaxel incorporated, approved for use in the clinic in South Korea for the treatment of breast cancer and non-small cell lung cancer[258]. A second monomer with functionalising capability was introduced to the system to enable the conjugation of DOX, a relevant chemotherapeutic in the treatment of GBM[304,305]. A library of five polymers was synthesised with different PEG initiators, leading to materials with varying macromolecular

architectures. Each polymer formulation displayed self-assembling properties, and all were able to form NPs of varying sizes.

DOX was selected as the drug candidate of choice, not only for the availability of a primary amine group offering a possible conjugation point to the polymeric backbone, but also for its use in multiple *in vitro*[192–195], *in vivo*[195-206] and clinical trials[211,213,214], indicating its relevance in the treatment of GBM. DOX, however, has been shown to be inefficient at crossing the BBB[306,307], and despite the development of DOX-loaded NPs capable of traversing the BBB, DOX is an exemplar of a favourable drug choice for localised delivery in the treatment of GBM.

It was hypothesised that incorporating drug loaded NPs, which are capable of transcytotic 'hopping'[241,308–312], into the pre-existing biodegradable microparticulate paste, would lead to efficacious local delivery in the treatment of GBM. Through the use of polymer-drug conjugate NPs, there is the possibility of avoiding drug metabolism and degradation, potentially leading to a higher delivered dose.

A major problem with existing treatment approaches for GBM includes the increased intrinsic resistance to chemotherapeutic drugs, caused by the heterogeneity of the tumour micro-environment and subsequent genetic and epigenetic variation in tumour sub-clones as a result of variable selective pressures. Based on an increasing understanding of brain intra-tumour heterogeneity, the capability to evaluate prospective treatment on primary derived cell lines from the invasive region of the

tumour, is clinically-relevant for the treatment of GBM. Most commercial GBM cell lines have been historically derived from the MRI contrast-enhanced core region of tumours, which does not allow a realistic, phenotypically accurate representation of the infiltrative cells which remain post-surgery and ultimately result in the inevitable recurrence of GBM[313]. Significantly, residual cells at the tumour margin are responsible for the 85% of GBMs that relapse locally (typically within 2 cm^3 of the infiltrative margin) after maximal safe surgical resection followed by the standard combination protocol of temozolomide and radiotherapy[314]. Therefore, the discovery of chemotherapeutics active against invasive GBM cells represents a crucial step in the development of therapies for the treatment of this pathology[315].

This body of work utilises cell lines derived from the infiltrative margin of adult patients, including those undergoing 5-ALA fluorescence-guided neurosurgical resection, at the Queen's Medical Centre, University of Nottingham[88]. In this chapter, the effect of the synthesised NPs (described in Chapter 2) on the metabolic activity of these primary cell lines and the traditionally-used commercial glioma cell line, U87, derived from the tumour core, was evaluated. The release profile of the DOX-loaded NPs from the PLGA/PEG matrix and DOX release from NPs was also evaluated.

3.2 Chapter Hypotheses and Objectives

3.2.1 Chapter Hypotheses

Hypothesis 1 – Non-drug-loaded NPs (control NPs) are cytocompatible with patient-derived glioblastoma cell lines.

Hypothesis 2 – DOX-loaded NPs will release from PLGA/PEG paste *in vitro* over several weeks.

3.2.2 Chapter Objectives:

1. Perform metabolic cell viability assays with non-drug-loaded control NPs on a panel of GBM cell lines.
2. Perform metabolic cell viability assays with DOX-loaded NPs on a panel of GBM cell lines and calculate IC_{50} concentrations.
3. Measure drug release from the DOX-loaded NPs.
4. Measure release of the DOX-loaded NPs from the PLGA/PEG matrix.

3.3 Chapter Materials & Methods

3.3.1 Materials

All materials were used as obtained unless otherwise stated. Dulbecco's Phosphate Buffered Saline (PBS; modified without calcium chloride and magnesium chloride; sterile-filtered), Dimethyl Sulfoxide (DMSO,

>99.7%; sterile-filtered) and sterile water (sterile-filtered) were purchased from Sigma Life Science. Astrocyte Medium (AM; sterile filtered), Poly-L-Lysine (1 mg/mL; sterile filtered), Trypsin/EDTA solution (T/E; 0.25%; sterile-filtered) and Trypsin Neutralization Solution (TNS; sterile filtered) were purchased from ScienCell Research Laboratories. Hank's Balanced Salt Solution (HBSS; sterile-filtered), Dulbecco's Phosphate Buffer Saline (DPBS; supplemented with calcium chloride and magnesium chloride), Dulbecco's Modified Eagle Medium (DMEM; supplemented with 1 g/L D-Glucose L-Glutamine and pyruvate), phenol red-free DMEM (with 4500 mg/L glucose and sodium bicarbonate and without L-glutamine, sodium pyruvate and phenol red) and FluoroBrite DMEM were purchased from Gibco™ by ThermoFisher Scientific. PrestoBlue™ Cell Viability Reagent and Hoechst 33342 were purchased from Invitrogen™ by ThermoFisher Scientific. HyClone™ Bovine Growth Serum (FBS; GE Healthcare) was purchased from Fisher Scientific by ThermoFisher. Acetone (>99.8%) was purchased from Fisher Chemical. Dimethyl Sulfoxide (DMSO) was purchased from Honeywell. Poly(ethylene glycol) (PEG; M_n = 400 Da) was purchased from Aldrich Chemistry. Poly(lactic-co-glycolic acid) Resomer® (P_{DL}LGA; Select 85:15 DLG 4CA; technical grade) was purchased from Evonik. Doxorubicin (hydrochloride) (DOX.HCl) was purchased from Cayman Chemical company.

3.3.2 Nanoparticle stability studies

Nanoparticles (NPs) were formed as described in the previous chapter. In brief, a nanoprecipitation method was used to form kinetically-trapped, 'micellar-like' NPs, whereby the polymers (10 mg) were dissolved in acetone (1 mL), and the polymeric solution was added dropwise to deionized water (10 mL, final concentration of 1 mg/mL) under constant stirring at 550 rpm. The polymers rapidly formed NP suspensions through solvent exchange between water and acetone. The final suspension was subsequently dialysed in a 3.5 kDa molecular weight cut-off pleated snakeskin tubing against PBS overnight in order for complete exchange between water and PBS. The resultant sizes of the NPs were derived via DLS measurements following filtration using a 0.22 µm filter. Control NPs (final conc. 500 µg/mL) were stored at 4°C, whilst another set were mixed 1:1 with DMEM (final conc. 500 µg/mL) and stored at 37°C, to provide a "stimulated" environment. The particle sizes were determined by DLS at time points 1, 4, 24, 48 and 168 h using a Zetasizer Nano ZS (Malvern Instruments Ltd). Measurements were taken in triplicate of NPs suspensions at 500 µg/mL and used to calculate mean intensity particle size distributions.

3.3.3 Tissue culture of the cell monolayers

3.3.3.1 Routine cell maintenance

The cells were cultured in 75 cm^2 flasks at 37°C in a humidified incubator with 5% CO_2 until they reached confluence. Once confluent, cells were

passaged using Trypsin/EDTA. Media was removed from the flask and cells were washed gently with HBSS. Trypsin/EDTA (3 mL) was added to the flask and incubated for two – three minutes, until the cells had detached from the bottom of the flask by enzymatic dissociation. This was checked using a light microscope. Warmed DMEM (supplemented with 1 g/L D-Glucose L-Glutamine and pyruvate; 8 mL) was added to the flask to deactivate the trypsin. The resultant suspension was centrifuged at 800 rpm for five minutes. The supernatant medium was removed, replaced with fresh DMEM (5 mL) and the cells were resuspended. An aliquot of cell suspension was added to a fresh flask containing DMEM (12 mL). Splitting ratios between 1:2 and 1:8 were used dependent on cell type (doubling rate) and confluency.

3.3.3.2 Frozen Storage of Cells

Cells were cultured to confluency and detached using the previously described method. Freezing medium was made up of FBS : DMSO (9:1; 1 mL per cryovial). Following centrifugation and removal of the supernatant, the cells were resuspended in freezing medium and transferred to a labelled sterile cryovial and placed in a ‘Mr Frosty’ container which was subsequently placed in a -80°C freezer in order to achieve a controlled cooling rate of 1°C per minute. For longer term storage, the cryovials containing the frozen cells were transferred to vapour phase liquid nitrogen storage tanks.

3.3.3.3 Revival of frozen cells

The cells were removed from cold storage and rapidly thawed at 37°C in a water bath. The cell suspension was added to a newly labelled flask containing warmed DMEM (at least 13 mL) and placed in an incubator. The medium was changed within 24 hours in order to remove all cryoprotectant. Following revival, cells were passaged at least twice before carrying out any assays.

3.3.4 Cell lines

3.3.4.1 U87 glioma cell line

The U87 GBM cell line was obtained from ATCC and cultured within a passage window of 13 splits. Cells were cultured in Dulbecco's Modified Eagle Medium (DMEM) supplemented with 10% (v/v) Foetal Bovine Serum (FBS) at 37°C in a humidified incubator with 5% CO_2.

3.3.4.2 Primary GBM cell lines

GIN-8 (Glioma INvasive margin cells) were isolated from medial front invasive margin (54y Female, Wild type IDH (primary GBM), intact ATRX, 0% MGMT promoter methylation, 90% resection plus Gliadel wafers; Treatment 60Gy radiotherapy, concurrent and adjuvant temozolomide; patient died 5months after surgery), GIN-28 were isolated from 5-ALA fluorescence-positive invasive margin (71y Male, Wild type IDH (primary GBM), intact ATRX, 0% MGMT promoter methylation 99% resection; no

adjuvant therapy (patient choice); died 3 months after surgery)[316] and GIN-31 were isolated from 5-ALA fluorescence-positive invasive margin (57y Female, Wild type IDH (primary GBM), intact ATRX, 0% MGMT promoter methylation, 100% resection; Treatment 60Gy radiotherapy, concurrent and adjuvant temozolomide; patient died 16.1 months after surgery) by our laboratory, and were used at passages of 24-50, 26-41 and 28-55 respectively. Single tandem repeat (STR) genotyping is detailed in Figure A 6. Cell lines were cultured in Dulbecco's Modified Eagle Medium (DMEM; Sigma-Aldrich) supplemented with 10% FBS, 1g/L Glucose and 2 mM L-glutamine (Sigma-Aldrich) at 37°C with 5% CO_2.

3.3.4.3 Human Astrocyte cell line

A primary human astrocyte cell line was used as a comparator of healthy brain cells. This was obtained from ScienCell Research Laboratories (catalogue #1800) and cultured between passage three and ten. Cells were cultured in Astrocyte Medium (AM) supplemented with 2% FBS (v/v), 1% penicillin-streptomycin (v/v) and 1% Astrocyte Growth Medium (v/v) at 37°C in a humidified incubator with 5% CO_2. Cells were cultured in flasks previously coated with poly-l-lysine (150 µL; 10 mg/mL) and sterile water (10 mL; final concentration 2 µg/cm^2) for a minimum of one hour to promote adhesion of the cells. Prior to plating the cells, the flasks were washed twice with sterile water.

3.3.4.4 9L Rat Glioma cell line

The 9L rat glioma cell line was used as a model for future *in vivo* work. It was received as a gift from Prof. Henry Brem and Dr. Betty Tyler from Johns Hopkins University. The cell line was cultured in DMEM supplemented with 10% FBS, 1g/L Glucose and 2 mM L-Glutamine at 37°C with 5% CO_2.

3.3.5 *In vitro* 2D cell viability assays

The PrestoBlue™ assay is a cell viability assay based on enzymatic reduction of a resazurin indicator dye by metabolically active cells[317]. The enzymatic reduction occurs in the mitochondria by enzymes such as flavin mononucleotide dehydrogenase, flavin adenine dinucleotide dehydrogenase, nicotinamide adenine dehydrogenase, and cytochromes[318]. The red resorufin is subsequently excreted to the surrounding medium of the cells resulting in a visible colour change from blue to pink.

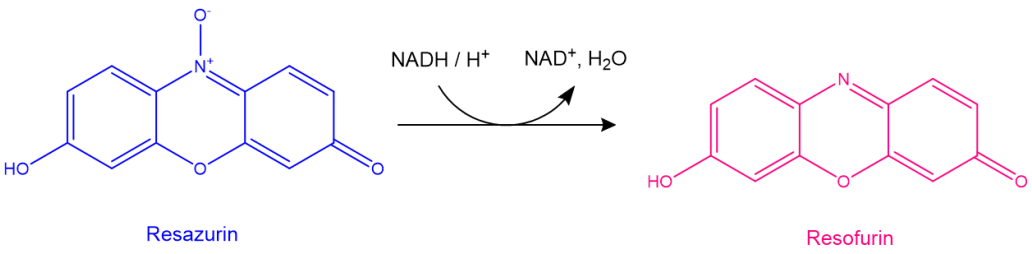


Figure 3-1 The mechanism of reduction of resezurin, a blue weak fluorescent indicator dye, to resofurin, a strong fluorescent pink dye, in response to irreversible chemical reduction.

The rate of reduction, which can be quantified colourimetrically or fluorometrically, is henceforth proportional to the number of viable cells in the well[319]. The measurements here were carried out using fluorescence due to the overlap of the absorbance spectra for the oxidised and reduced forms of the dye, thus representing a more sensitive approach. As the chemical reduction does not adversely impact cell viability, the same population of cells can be measured longitudinally.

The PrestoBlue™ assay is reported to be more sensitive with a quicker incubation time than the original AlamarBlue™ assay, which works using the same resazurin dye reduction. There are no reports on how the two assays differ with regards to the mechanism or chemical reaction[320]. Henceforth, the PrestoBlue™ assay was selected over the AlamarBlue™ assay due to its increased sensitivity; as little as 10 cells per well in a 384 well plate can be seeded, and its rapid incubation time (as short as 10 minutes)[321], both favourable aspects for a high throughput screening approach.

3.3.5.1 Optimising Cell Seeding Densities for the Primary Cell Lines

An initial assay was carried out in order to determine the most appropriate cell culture period and cell seeding density for each primary cell line for the cell viability assays. GIN-8 and GIN-28 cells were seeded at 3 x 10^3, 5 x 10^3, 7 x 10^3 and 9 x 10^3 cells per well in 96 well plates. GIN-31 cells were seeded at 1 x 10^3, 2 x 10^3, 3 x 10^3, 4 x 10^3, 5 x 10^3, 7 x 10^3 and 9 x 10^3 cells per well in a 96 well plate. More seeding densities were selected

for GIN-31 as these cells were much larger than the GIN-8 and GIN-28 and thus were expected to require a smaller seeding density. After each time point (24, 48 and 72 h), the media was removed and 110 µL 10 % (v/v) PrestoBlue™ reagent diluted in HBSS was applied per well for 45 minutes. The resulting fluorescence was measured at 544/590 nm (λex./λem.) on a BMG Labtech FLUOstar Omega microplate reader. Fluorescence values between 2000 and 3000 were aimed for, to alleviate the possibility of self-quenching.

3.3.5.2 Metabolic activity assay

The PrestoBlue™ Cell Viability assay was performed to assess the metabolic activity of a model glioma cell line (U87) when exposed to the NPs (control and DOX-loaded). Prior to cell exposure, the NPs were dialysed overnight in a 3.5 kDa molecular weight cut-off pleated snakeskin tubing against PBS. The cells were seeded at a density of $5x10^3$ cells per well in 96 well plates[322–326] and cultured for 24 hours prior to treatment with NPs. Cells were exposed to NPs for 72 hours and applied in 100 µL DMEM containing 10 % (v/v) FBS. DMSO (100%) was used for a cell death (positive) control and a vehicle control containing no NPs (100% DMEM) used as a negative control. Following exposure, the NP suspensions were removed, and the cells were subsequently washed twice with warm Hank's Balanced Salt Solution (HBSS). 110 µL 10 % (v/v) PrestoBlue™ reagent diluted in HBSS was applied per well for 45 minutes. The resulting fluorescence was measured at 544/590 nm (λex./λem.) on a BMG Labtech FLUOstar Omega microplate reader.

Relative metabolic activity was calculated by setting normalised values from the negative control as 100 % and positive control as 0 % metabolic activity.

For the metabolic cell viability studies carried out on the primary cell lines (GIN-8, GIN-28 and GIN-31), the same method as above was carried out. GIN-8 and GIN-28 cells were seeded at a density of $5x10^3$ cells per well, while GIN-31 cells were seeded at a density of $3x10^3$ cells per well, in 96 well plates and cultured for 24 hours prior to exposure to the NPs.

For the metabolic cell viability studies carried out on the 9L cell line, the same method as above was carried out. The cells were seeded in 96 well plates at a seeding density of 3 x 10^3 cells per well and cultured for 24 hours prior to exposure to the NPs.

For the metabolic cell viability studies carried out on the primary human astrocyte cell line, the PrestoBlue™ reagent was diluted in DPBS and applied per well for 60 minutes. The cells were seeded at a density of $5x10^3$ cells per well in 96 well plates and cultured for 24 hours prior to exposure to the NPs.

3.3.5.3 DOX IC_{50}

Cells were seeded as stated above for each cell line and cultured for 24 hours prior to assaying. A stock solution of DOX in DMSO (10 mg/mL) was prepared. Serial dilutions of the stock (10^{-4}, 10^{-5}, 10^{-6}, 10^{-7}, 10^{-8}, 10^{-}

^{9}, 10^{-10}, 10^{-11} and 10^{-12} M) were prepared in DMEM and applied to the cells (100 µL). Following 72 h exposure, the PrestoBlue™ assay was carried out as previously described. The metabolic activity of the cells was calculated for each DOX concentration and GraphPad Prism (v8.1.2) was subsequently used to calculate the IC_{50} value by fitting the data via the least squares method to a four-parameter dose-response curve with a variable slope.

3.3.6 Cellular uptake of NPs

NPs for uptake experiments were prepared as previously described but were formulated as 10% wt/wt of $mPEG_{5000}$_LA_tBSC-Cy5 (P2-Cy5) and 90% wt/wt $mPEG_{5000}$_LA_tBSC (P2) at a final concentration of 50 µg/mL. U87 GBM cells were seeded at a density of $1x10^{4}$ cells per well in 96 well plates and cultured for 48 hours. The medium was subsequently removed, and cells washed with PBS. 100 µL of Cy5 NPs (50 µg/mL; diluted in phenol red free DMEM containing 10% (v/v) FBS) were incubated with cells for varying time points (0.5, 1h, 2h and 4h) at 37°C with 5% CO_2. Following the appropriate incubation time, the NP solution was removed, and cells were washed three times with ice cold PBS. Nuclei staining was then carried out whereby Hoechst 33342 (100 µL; 10 µg/mL) was applied in PBS onto the cells for 15 minutes at 37°C. Following removal of the staining solution, the cells were washed twice with PBS. FluoroBrite DMEM was added to wells and cells were imaged on an inverted Nikon Eclipse TE 300 fluorescent microscope on DAPI and Cy5 filters. Images were processed using ImageJ software and used

qualitatively to assess uptake of the NPs into the cells. The Cy5 and DAPI filters were overlaid to determine if the NPs were located in the nucleus.

3.3.7 Preparation of PLGA/PEG matrix

The PLGA/PEG paste was prepared as described previously[78,79]. In brief, thermosensitive microparticles were fabricated from blends of 53 kDa P_{DL}LGA (85:15 DLG 4CA) and PEG. A mixture of 93.5 : 6.5% PLGA : PEG (*w/v*) was blended at 80–90°C on a hotplate. The melted PLGA and PEG were mixed by hand using a polytetrafluoroethylene (PTFE)-coated spatula and the mixture cooled to room temperature. Polymer blend sheets were then ground into particles in a bench-top mill (Krups Mill F203) and the particles were sieved to obtain the 100–200 µm particle size fraction.

3.3.8 Release studies

3.3.8.1 DOX release from DOX-NPs

Polymer-DOX conjugates were formulated by nanoprecipitation to form DOX-NPs of size 67 nm, as previously described, at a concentration of 2 mg/mL (Chapter 2) and DOX release from DOX-NPs was measured. Following dialysis against PBS, the resultant NPs (500 µL) were pipetted into a Slide-A-Lyser® MINI Dialysis device with a 3.5kDa molecular weight cut off, with 14 mL PBS in the Eppendorf below. At set time points (t = 0.02, 0.04, 0.08, 0.17, 0.25, 1, 2, 3, 6, 7, 28 and 44 days), the entire 14 mL PBS sample was removed and replaced with fresh PBS. The

removed PBS sample was freeze-dried and resuspended in DMSO (5 mL), sonicated for 10 minutes and centrifuged for a further 10 minutes. The DOX present in the resultant supernatant sample (2 mL) was analysed by fluorescence on a Varian CaryEclipse Fluorescent Spectrometer. The sample was read on slow scan mode, 450/510-640 nm (λex./λem.) at 900V, with excitation split set at 5 nm and emission split set at 10 nm.

3.3.8.2 DOX-NP release from PLGA/PEG paste

DOX-NPs were formulated as previously described (5 mg/mL). When forming the PLGA/PEG paste, the DOX-NP solution replaced the PBS to form DOX-NP-loaded-PLGA/PEG paste. PLGA/PEG microparticles (636 mg; 100 – 200 µm) was mixed with 509 µL DOX-NPs (dialysed overnight against PBS; final conc. 2.65 mg/mL) and split evenly six ways (106 mg PLGA/PEG; 84.83 µL DOX-NP), approximately maintaining the previously optimised 1 : 0.8 (polymer : saline) ratio[79]. Three formulations were packed tightly into cylindrical moulds (6 x 6 x 2 mm; l x w x d) and the remaining three were pasted lightly into a weighing boat, producing a thin layer to mimic more closely how the polymer would be applied to a resection cavity *in vivo*. The PLGA/PEG matrices were sintered overnight at 37°C. Release was assessed through placing the sintered PLGA/PEG matrices into a scintillation vial containing 5 mL PBS. At set time points (t = 0.02, 0.04, 0.08, 0.17, 1, 2, 5, 6, 7, 28, 43 and 63 days), the entire 5 mL PBS sample was removed and replaced with fresh PBS. The PBS sample was freeze dried, resuspended in DMSO (5 mL), sonicated for 10

minutes before centrifuging for a further 10 minutes. The DOX present in the resultant supernatant sample (2 mL) was analysed by fluorescence on a Varian CaryEclipse Fluorescent Spectrometer and was, by proxy, attributed to DOX-NP release from PLGA/PEG paste. The sample was read on slow scan mode, 450/510-640 nm (λex./λem.) at 900V, with excitation split set at 5 nm and emission split set at 10 nm.

3.4 Results and Discussion

3.4.1 Nanoparticle stability studies

Stability studies were carried out whereby the control NPs were kept at 4°C to replicate storage of NPs in fridge conditions and the experimental NPs were kept at 37°C in DMEM, replicating the physiological conditions for future *in vitro* work. A one-week timeframe was chosen for this stability study to capture the cell exposure time to the NPs in the *in vitro* work carried out. A DLS-based assay was chosen as the screening technique due to the fast response time and ease of detection of aggregation within each sample. It was expected that all the formulations would be stable at 4°C, indicating that the NPs would be stable upon storage.

As can be observed in Figure 3-2., no substantial changes or aggregation was observed for the NPs kept at 4°C, confirming stability in these conditions, except the P4 formulation whereby a slight shift to a larger size was observed over time, indicating aggregation of the NPs. When incubated at 37°C in DMEM, changes in the DLS traces began at 24

hours for each of the formulations, whereby a broadening of the peaks is observed and a shift to the larger size range, suggesting the particles were aggregating before collapsing. For particles P1, P2, P3 and P5, the DLS peaks continue to broaden until the one-week time point where a complete shift of the peak to the right can be observed, indicating an increased particle size. Upon introduction of a drug to the NP system, this implies we would expect complete release of the drug within a one week timeframe. However, P4 proved to be much less stable than the other formulations as observed by the broadening and shift of the peaks to the right, indicating that aggregation of the NPs occurred within a one hour timeframe.

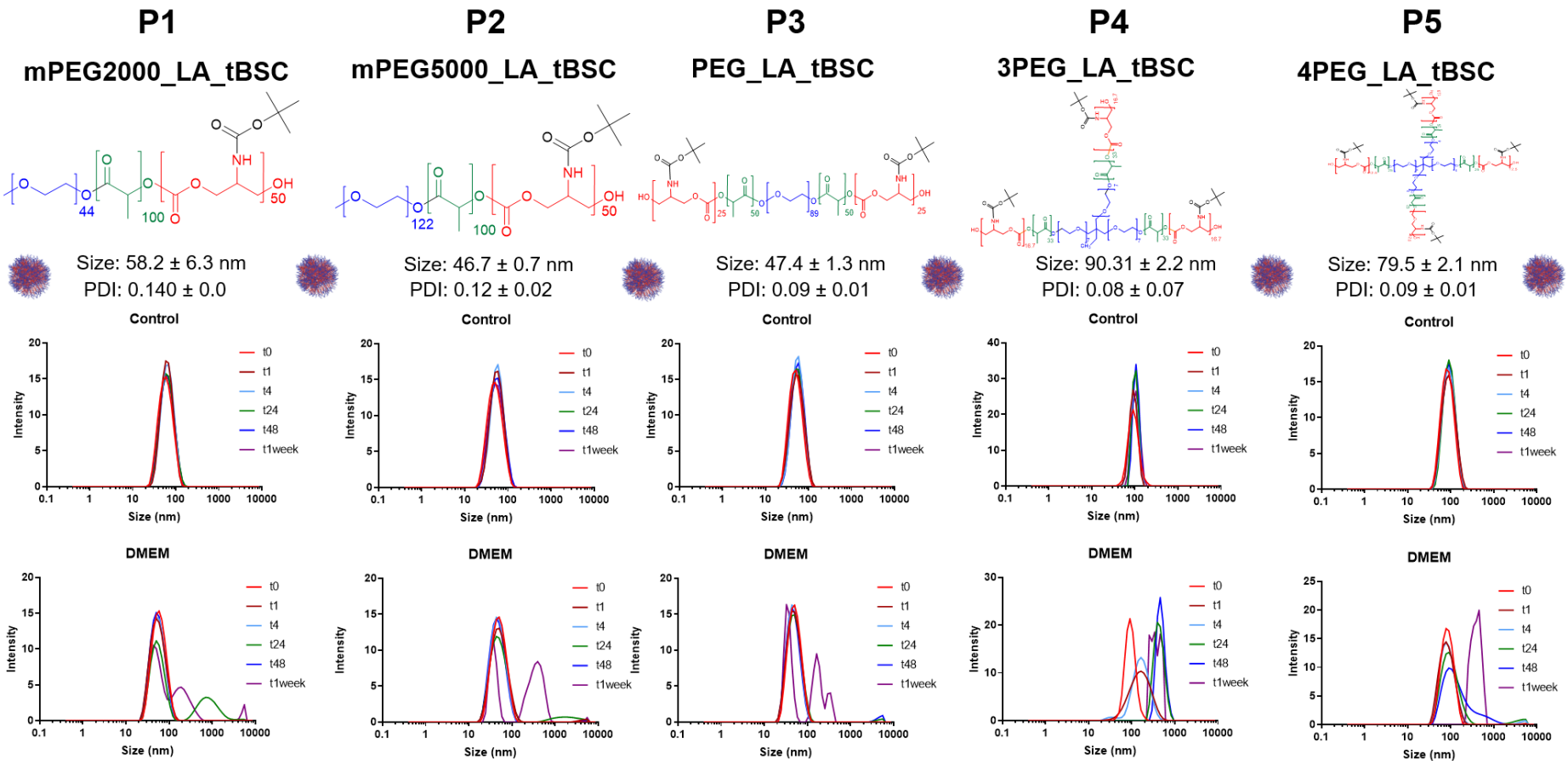


Figure 3-2 *DLS traces of formulations P1 – P5 in control conditions (PBS at 4°C; top row) and stimulated conditions (DMEM at 37°C; bottom row) after 0, 1, 24, 48 hrs and 1 week of incubation. No significant changes were observed for the NPs in control conditions. Breakdown of each of the NPs was observed within 1 week of incubation in stimulated conditions.*

It should be noted that there are differences in the size of the NPs when compared to the size profiles obtained in Chapter 2, Table 2-2. The differences between the two sets of NPs investigated were that those in Chapter 2 were formulated in PBS at a concentration of 1 mg/mL whilst those used in this study were formulated at a concentration of 500 µg/mL in DMEM. The NPs formulated at 1 mg/mL were larger than those at 500 µg/mL, and this was particularly prevalent for the branched polymers (P4 and P5). It has been previously shown by our group that varying the concentration does not significantly affect the size of NPs constituting a PEG initiator and LA polymer backbone[327]**,** implying that the size differences here could be caused by the tBSC monomer, or that there could be batch to batch variation. The tBSC monomer contains a large BOC protecting group, which could influence the packing constitution of the polymer as it forms NPs, affecting the final size of the NPs obtained. As the differences in size was more pronounced for the branched architectures, it hints at the different packing processes for each of the architectures explored[328], and shows greater influences on these parameters for branched architectures. TEM imaging should be carried out to investigate this concept further.

3.4.2 *In vitro* 2D cell viability

3.4.2.1 U87 GBM Cell Line

The PrestoBlue™ assay was used to determine the cytotoxicity of the polymers in 2D cell culture over 72h. As can be seen from Figure 3-3, increasing concentrations of each of the polymeric NP formulations tested did not alter metabolic activity compared to the negative control on the glioma cell line tested. The size and polydispersity index (PDI) of each of the formulations was consistent across batches, indicating that this method of producing NPs was highly reproducible. No observed reduction in cellular metabolic activity was observed after this time, indicating that the polymer 'platform' of PEG-poly(lactide)-co-poly(carbonate) was well-tolerated by the brain tumour cells.

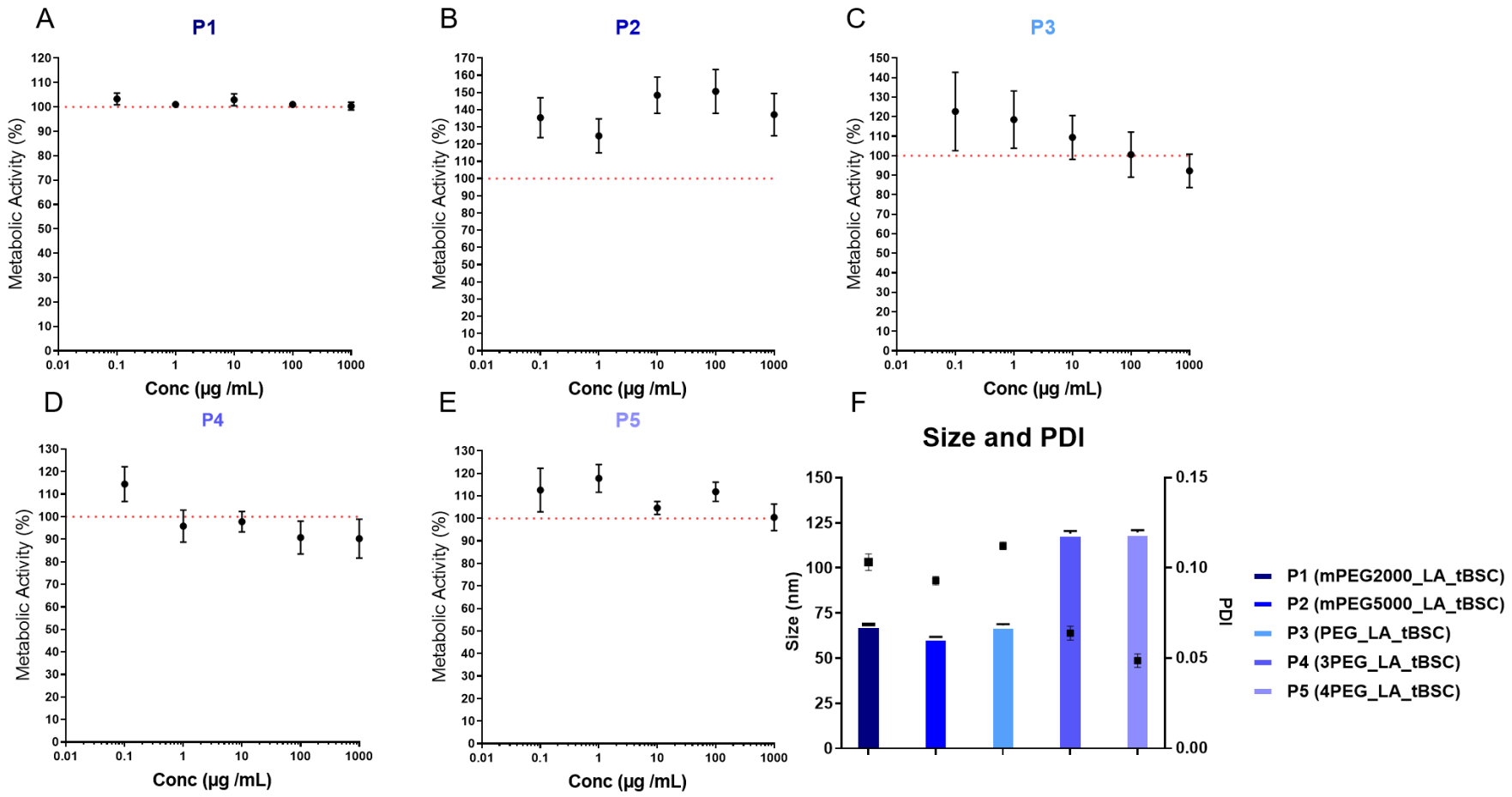


Figure 3-3 *In vitro U87 cell viability assay at 72h post treatment with different concentrations of the five NP formulations using PrestoBlue™ assay. Three independent repeats were carried out (n=4), across three different passages. Error bars show mean ± S.E.M. (A – E). The average size and PDI of each NP formulation tested in each repeat. Error bars show mean ± S.E.M (F).*

The polymeric NP formulation, P2, was selected as the lead formulation to carry forward for future *in vitro* work due to several reasons. Firstly, the formulation was of optimal size (i.e. below 100 nm), enabling the hypothesised rapid penetration of the NPs through brain tissue[329]. Secondly, the zeta potential of the selected formulation was -23.5 ± 4.5 mV (Table 2-2), indicating that this formulation was highly stable and able to avoid aggregation of particles *in vitro/in vivo*[330]. Thirdly, the critical aggregation concentration (CAC) was low (8.5 µg/mL), again signifying the ability of the NPs to avoid agglomeration. Furthermore, the P4 formulation was omitted due to its lack of stability in storage conditions, P5 was ruled out as it was the next least stable formulation. Additionally, the P4 and P5 formulations showed signs of batch to batch variation, as discussed earlier, a further consideration for not taking them further in these studies. P3 was discounted as it showed a trend of decreasing metabolic activity with increasing NP concentration. P2 was selected over P1 due to its increased PEG chain length and predicted steric stabilisation (M_n = 5000 compared to 2000, respectively). It has been well reported in literature that an increased PEGylated system has the ability to penetrate further through brain tissue[329,331] and thus P2 was selected as the lead formulation with regard to the future application.

3.4.2.2 Human Astrocyte cell line

Cell viability was next assessed using a primary human astrocyte cell line to investigate the toxicity of the NPs on healthy glial cells, as opposed to a tumour cell line.

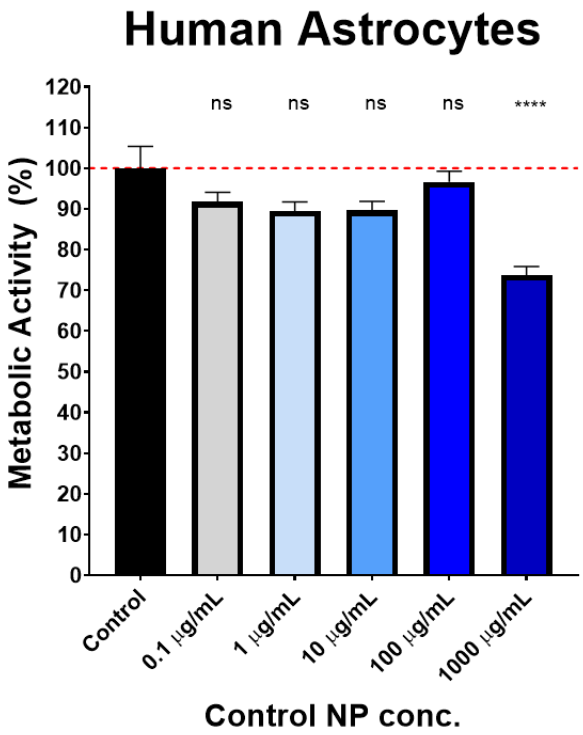


Figure 3-4 *In vitro cell viability assay at 72h post treatment with different concentrations of the P2 NP formulation on a human astrocyte cell line using the PrestoBlue™ assay. Four independent repeats (n = 4) were carried out. Error bars show mean ± S.E.M. [ns: p ≥ 0.05; ****: p < 0.0001, unpaired t-test with Welch's correction, comparing each data set to the control (negative control; medium) data set]*

As can be observed from Figure 3-4, the human astrocyte cell line was much more sensitive to the polymeric NPs than the U87 model glioma cell line; however, the NPs were still found to be cytocompatible up to a concentration of 100 µg/mL. The highest concentration, 1000 µg/mL, significantly reduced astrocyte viability; a factor to be considered when taking the formulation forward for *in vivo* work.

3.4.2.3 Primary GBM Lines

3.4.2.3.1 Cell seeding optimisation

Cell seeding optimisation experiments were carried out to decipher the ideal seeding density and cell culture period for the cell viability assays.

72 hours was selected as the culture time for the cell viability assay. These cell lines had an approximate population doubling time of 24 hours and hence 72 hours allowed for approximately two rounds of cell division. Henceforth, when a chemotherapeutic was applied to the cells, enough time would pass to ensure the chemotherapeutic may exert an acute antiproliferative effect on the cells. Specifically, the mode of action of DOX is the inhibition of topoisomerase II, which cells require to divide effectively[183].

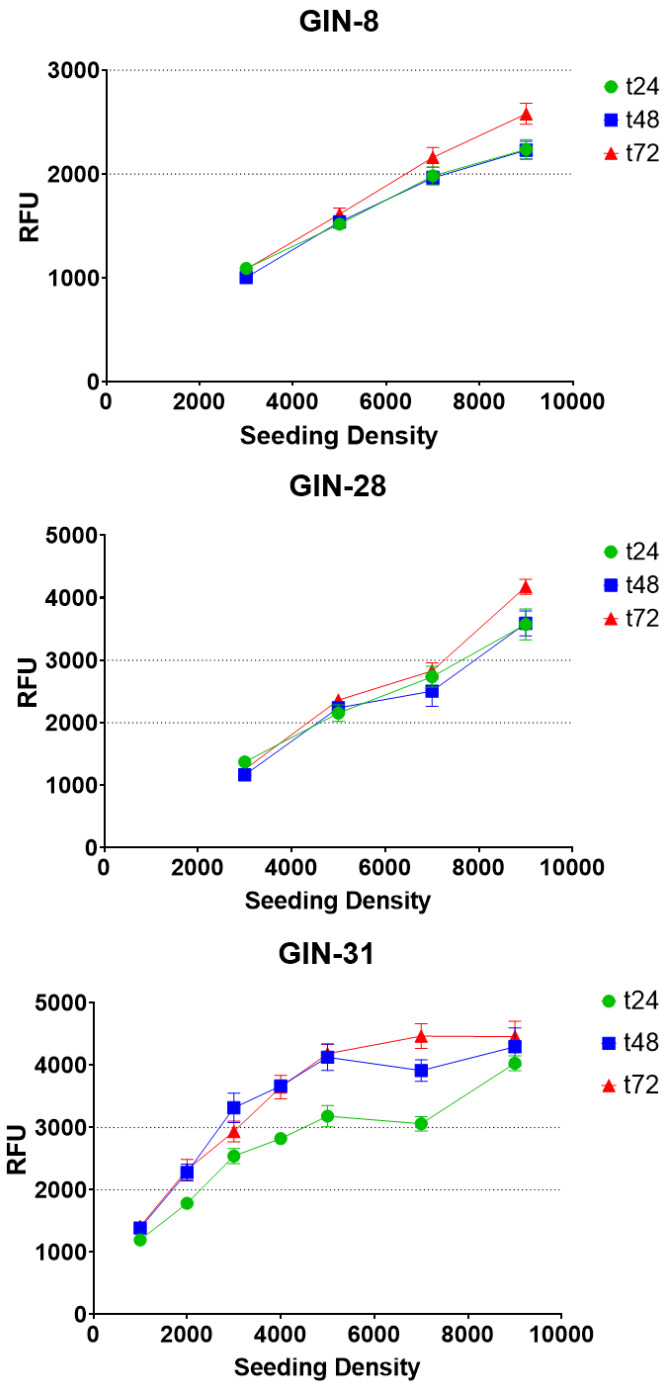


Figure 3-5 *Effect of Culture Time and Seeding Density on PrestoBlue Fluorescence. Cell seeding density experiment for the PrestoBlue™ assay at 24, 48 and 72h. Four independent repeats were carried out (n=4) for the GIN-8 line and two independent repeats (n = 4) were carried out for the GIN-28 and GIN-31 cell lines. Error bars show mean ± S.E.M.*

It has been extensively reported that the pink resorufin can be subsequently reduced to the colourless and non-fluorescent hydroresorufin[318,332] and as such, this over-reduction must be avoided through optimising the cell seeding density. A seeding density of 5 x 10^3 cells per well was selected for the GIN-8 and GIN-28 cell lines and 3 x 10^3 cells per well was selected for the GIN-31 cell line. For the GIN-28 and GIN-31 cell lines, it can be seen from the respective graphs in Figure 3-5 that at 72 hours, these cell seeding densities displayed fluorescence readings between 2000 and 3000 RFU as required. For the GIN-31 cell line, the tailing off of the fluorescence can be observed for each of the time points at a seeding density above 5 x 10^3 cells per well, indicating that over-reduction of the resazurin is taking place, resulting in a lower fluorescence readout and hence a misleadingly low metabolic activity. The GIN-8 cell line was the slowest growing of the primary cell lines, and this can be supported by the reduced fluorescence values. A seeding density of 5 x 10^3 was selected. On reflection, a seeding density of 7 x 10^3 may have been more suitable for this cell line. However, as the metabolic activity results were normalised against their control counterpart, the seeding density was considered of low significance as it was consistent throughout all experiments completed.

It should be noted that only the GIN-31 cell line acted as would be expected for a cell seeding study. There were clear differences between each of the time points, whereby the fluorescence increased as the assay time increased. Furthermore, a linear growth curve can be observed

before reaching a plateau, as expected as the fluorescence becomes quenched at the higher seeding densities. The GIN-8 and GIN-28 cell lines, however, did not behave in this way; showing only minor differences for each of the assay time periods. A linear increase of fluorescence is observed as the seeding density increases, but the linear trend continues to increase, not reaching a plateau. Thus, it could be implied the GIN-8 and GIN-28 cells are not actively proliferating. Ultimately, this could have significant impact on the viability studies carried out as if the cells are under proliferating, results of the metabolic activity of the cells could be over-estimated, showing the DOX-NPs to be more efficacious then they potentially are. However, one could argue that each of the metabolic activities were compared to a control, and so any proliferating effects would have been observed with the control, and therefore counteracted any negative effects on the experiment. Any change in metabolic activity is attributable only to DOX-NPs.

3.4.2.3.2 Cell viability

Cell viability was tested on a panel of primary cell lines, derived from the invasive margin of GBM patients. Activity of the P2 NP formulations against these cell lines would give a clinically relevant insight to the proposed application of these formulations, as these cell lines better represent the cancerous cells remaining in the brain following maximal safe surgical resection, compared to classical cell lines derived from the tumour core.

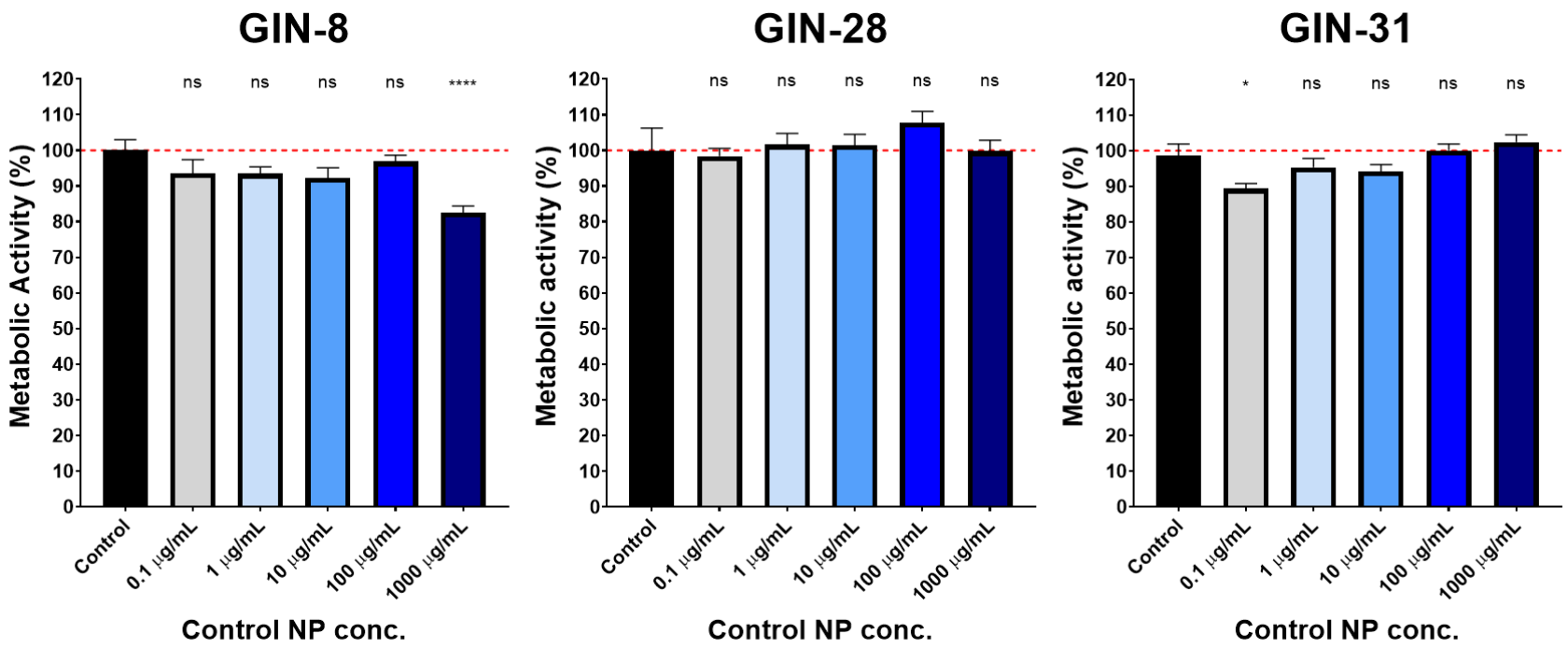


Figure 3-6 *In vitro cell viability assay at 72h post treatment with different concentrations of the P2 NP formulation on primary glioma cell lines using the PrestoBlue™ assay. Three independent repeats were carried out (n=4) for the GIN-8 cell line whilst four independent repeats (n = 4) were carried out for the GIN-28 and GIN-31 cell lines. Error bars show mean ± S.E.M. [ns: p ≥ 0.05; *: p = 0.01-0.05; ****: p < 0.0001, unpaired t-test with Welch's correction, comparing each data set to the control (negative control; medium) data set]*

The P2 control NPs did not induce a decrease in the metabolic activity of the primary cell lines, except for the 1000 µg/mL NPs on the GIN-8 cell line. Thus, it can be concluded that the P2 control NPs were well-tolerated by the primary cell lines up to 100 µg/mL, consistent with data presented for the U87 cell line and the human astrocyte cell line.

3.4.2.4 DOX-loaded nanoparticles

The cytotoxicity of DOX-loaded NPs was tested on both the commercial glioma cell line (U87) and three primary GBM cell lines, derived from the invasive region of the tumour (GIN-8, GIN-28 and GIN-31). The IC_{50} represents the concentration of a drug that is required for 50% growth inhibition *in vitro*. The IC_{50} of a drug can be calculated through constructing a dose-response curve and testing different concentrations of the drug on the biological activity of the cells. Firstly, the IC_{50} of free DOX was determined for each cell line through a 72 h PrestoBlue™ assay.

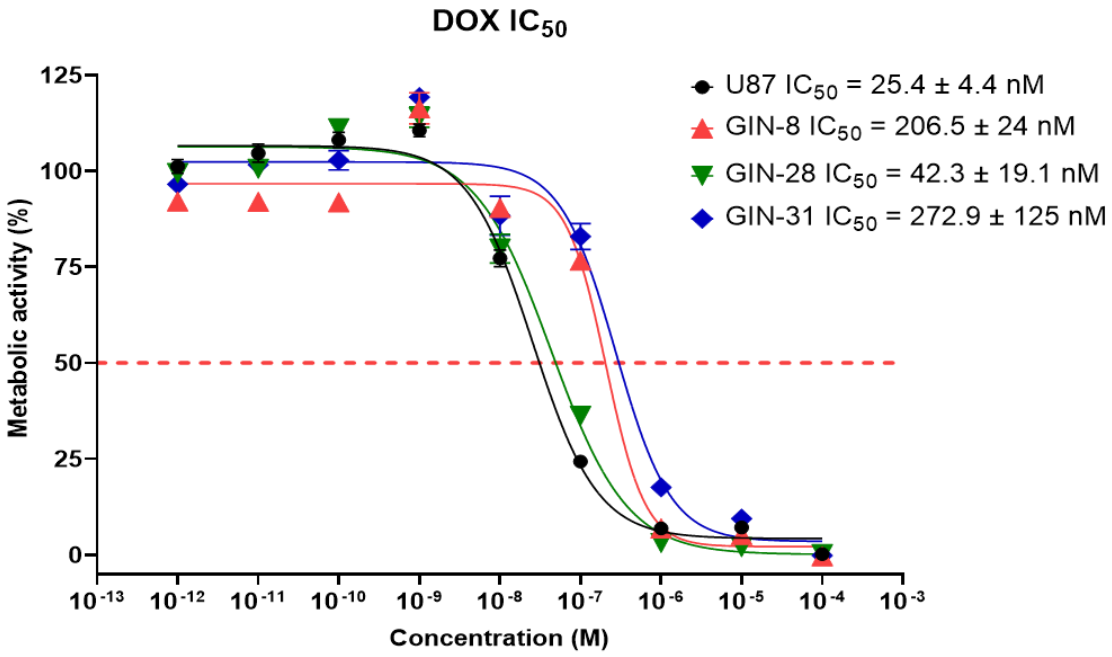


Figure 3-7 *Potency determination was achieved via measurement of cellular metabolic activity (PrestoBlue™ assay). DOX was diluted in DMEM containing 10% FBS and applied for 72 hours. U87, GIN-8 and GIN-28 cells were seeded at a density of 5x10^3 cell/well and GIN-31 cells were seeded at a density of 3x10^3 cell/well in 96 well plates. All cells were cultured for 24h prior to assaying. Data represent mean ± S.E.M and are quadruplets from four independent experiments. IC$_{50}$ values are displayed in the key and are mean ± S.D and determined via GraphPad Prism.*

It can be seen from the IC$_{50}$ curves (Figure 3-7) that the U87 cell line has the lowest IC$_{50}$ value and hence is the most sensitive to DOX. The three primary cell lines all have varying IC$_{50}$ values, all within a range for a candidate therapeutic to be considered for preclinical validation. The IC$_{50}$ data for the U87 cell line is in line with published data[333–336]. Moreover, the data give an indication of the (expected) variability between patients and thus the expected variation in response to treatment for a heterogeneous disease. As GBM cell lines derived from the infiltrative

margin are sensitive to DOX, the data supports the administration of DOX immediately post-surgical resection of the bulk GBM mass.

The DOX-loaded NPs (Figure 3-8) were next screened against the tumour cell lines to investigate their effects on the metabolic activity of the cells. Comparisons were made against a negative control.

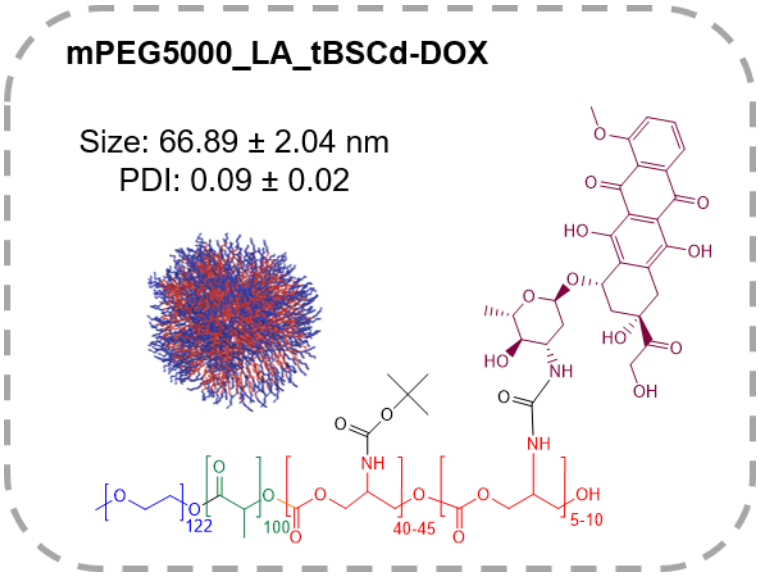


Figure 3-8 *P2-DOX formulation, showing average size obtained for each of the in vitro experiments carried out in this body of work.*

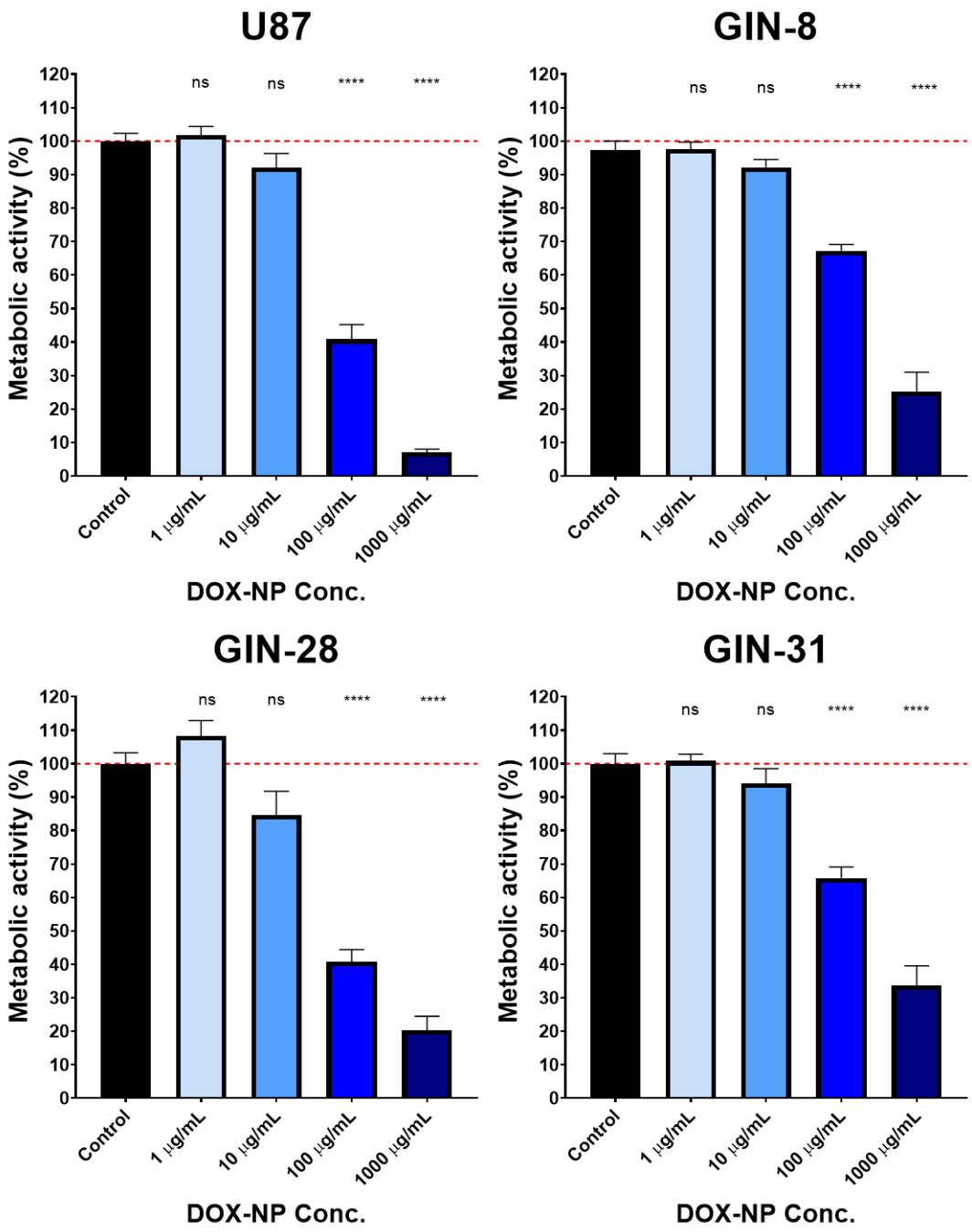


Figure 3-9 *In vitro cell viability assay at 72h post treatment with different concentrations of the P2-DOX NP formulation on glioma cell lines using the PrestoBlue™ assay. Five independent repeats were carried out (n=4) for the U87, GIN-28 and GIN-31 cell lines whilst four independent repeats (n = 4) were carried out for the GIN-8 cell line. Error bars show mean ± SEM. [ns: p ≥ 0.05; *: p = 0.01-0.05; **: p = 0.001-0.01; ***: p = 0.0001-0.001; ****: p < 0.0001, unpaired t-test with Welch's correction, comparing each data set to the control (negative control; medium) data set]*

The metabolic activity is significantly reduced for all cell lines when the DOX-NP concentration reaches 100 µg/mL and beyond. Interestingly, when assessing the highest concentration of DOX-NPs, the metabolic activity of the U87 line is reduced the most, followed by the GIN-28 line, GIN-8 line and GIN-31 line. This pattern is the same as the potency of DOX alone, when applied to these cell lines. Future work should include comparing DOX-NP and free DOX activity for each of the cell lines. In a 2D model, it is likely that the DOX would still be more potent than the DOX-NP at a comparative concentration, as has been observed in work carried out with these NP formulations in breast cancer models[337]. However, as seen in this study, significant differences in efficacy could be observed in a 3D or *in vivo* model as the NP may have an increased penetration capacity over free DOX, and thus increase its efficacious activity.

The metabolic activity of the DOX-NPs was compared to the control (drug-free) NPs at respective doses for each cell line tested (Figure 3-10). As expected from the results above, the DOX-NPs were found to have significant impact on the metabolic activity of the cells compared to their control-NP counterpart at the concentrations of 100 µg/mL and 1000 µg/mL.

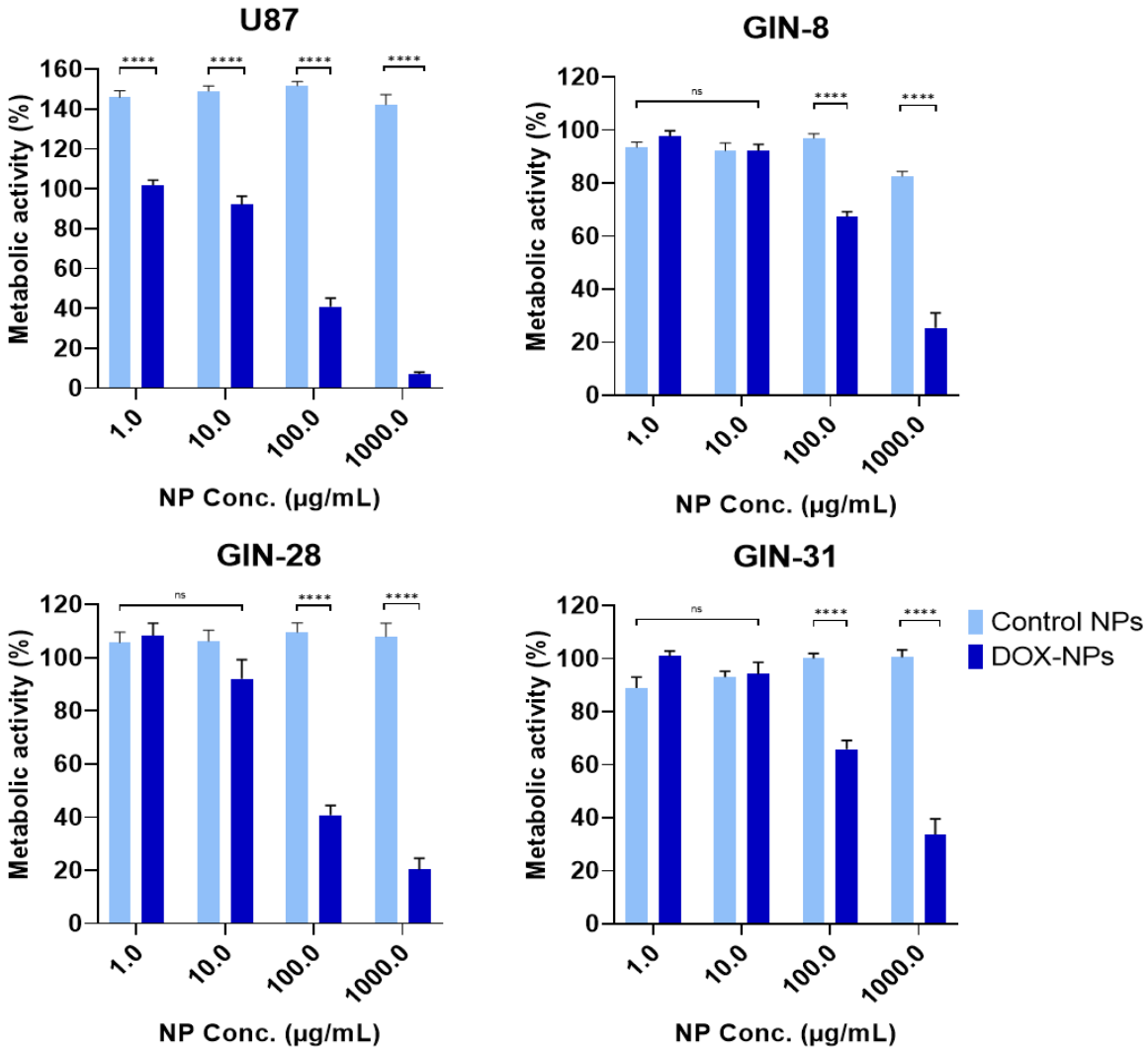


Figure 3-10 *In vitro cell viability assay at 72h post treatment with different concentrations of the P2 NP and P2-DOX NP formulations on U87, GIN-8, GIN-28 and GIN-31 cell lines using PrestoBlue™ assay. Four independent repeats were carried out (n=4). Error bars show mean ± S.E.M. (ns: p ≥ 0.05; ****p ≤ 0.0001; two-way ANOVA with Sidak's multiple comparisons test)*

Considering the Control NPs reduced the metabolic activity of the astrocyte cell line at 1000 µg/mL, it is promising to observe that the DOX-NPs significantly reduced the metabolic activity of each cell line at the concentration of 100 µg/mL.

The Presto blue assay, utilised in this body of work, measures the reductive environment of the cell over a shorter time frame where the cells may only undergo a few cell cycles. Therefore, a main advantage of performing a longer-term assay, such as the clonogenic assay, is that it is more sensitive at measuring reproductive death over several proliferation cycles. This would be of particular relevance to treatment with DOX, as it is an anti-proliferative drug. A summary of various short- and long-term cell viability assays and the advantages and disadvantages of each is detailed in Table 3-1 below[338–341].

Table 3-1 *Various Short and Long Term Cell Viability Assays*

Assay Type	Example(s)	*Long/Short term*	*Advantages*	*Disadvantages*
Fluorometric	***Presto Blue***	Short	- High throughput - More sensitive than colorimetric assays - Continuous assay	- Measures metabolic activity (reductive environment of the cell) as opposed to cell proliferation
Colorimetric	***MTT*** MTS XTT LDH	Short	- High throughput - Reproducible	- End point assay – formation of formazan crystals - Measures metabolic activity opposed to cell proliferation
Luminometric	***ATP*** Real-time viability assay	Short	- High throughput - Most sensitive and fastest cell viability method - Few plate handling steps	- Sensitivity is usually limited by pipetting reproducibility - Expensive
Dye exclusion	***Trypan blue*** Eosin Congo red Erythrosine B	Short	- Good indicator or membrane integrity - Simple - Inexpensive	- End point assay - Cell counting errors
Clonogenic	***Clonogenic cell survival assay***	Long	- Clear indication of cell ability to reproduce - Very sensitive	- Time consuming - Relies on linear relationship between cells seeded and number of colonies formed: plating efficiency

The DOX-NPs were not screened against the astrocyte cell line. This was in consideration of the future clinical application of the drug delivery system; the target of the therapy is tumour cells and hereby NPs were screened against both a commercial glioma cell line (U87), whereby the cells were derived from the core of the tumour, and primary derived cell lines (GIN-8, GIN-28 and GIN-31), whereby the cells were derived from the invasive margin of the tumour. GBM is commonly located in the

supratentorial region of the brain, consisting of the frontal, temporal, parietal and occipital lobes[342,343] which are mainly composed of terminally differentiated, non-proliferating astrocytes. As previously discussed, DOX is an antiproliferative drug, whereby it interacts with DNA by intercalation which subsequently prevents topoisomerase activity and DNA synthesis. The astrocyte cell line used in this body of work was a proliferating, progenitor cell line. Therefore, DOX would be expected to impair the growth of any proliferating cell, including the astrocyte cell line used in this section of work, henceforth leading to false negative results. We would not expect to see a toxic effect *in vivo* on non-proliferating, terminally-differentiated astrocytes[344].

For this section of work, the human astrocyte cell line used was suitable in proving the hypothesis that the control-NPs would not have a toxic affect against a representative healthy brain cell line as well as tumour cell lines. *In vivo* studies would need to be completed to answer the question as to whether the DOX-NPs had any toxic affects against healthy brain tissue, as evidenced by neuroinflammation and neurological deficits, thereby establishing whether there is a viable therapeutic window.

3.4.3 Cellular Uptake of NPs

With knowledge that the DOX-NPs were inhibiting proliferation of a variety of GBM cell lines, the nature of this interaction and the timeframe in which it occurred was investigated. The fluorescent dye, Cy5, was

used as a label and conjugated to the P2 formulation (described in Chapter 2) to yield fluorescent NPs. A simple assay could then be carried out whereby the Cy5-NPs were applied to U87 cells, and subsequently imaged using fluorescence microscopy to detect the fluorescent NPs within an intracellular cellular environment.

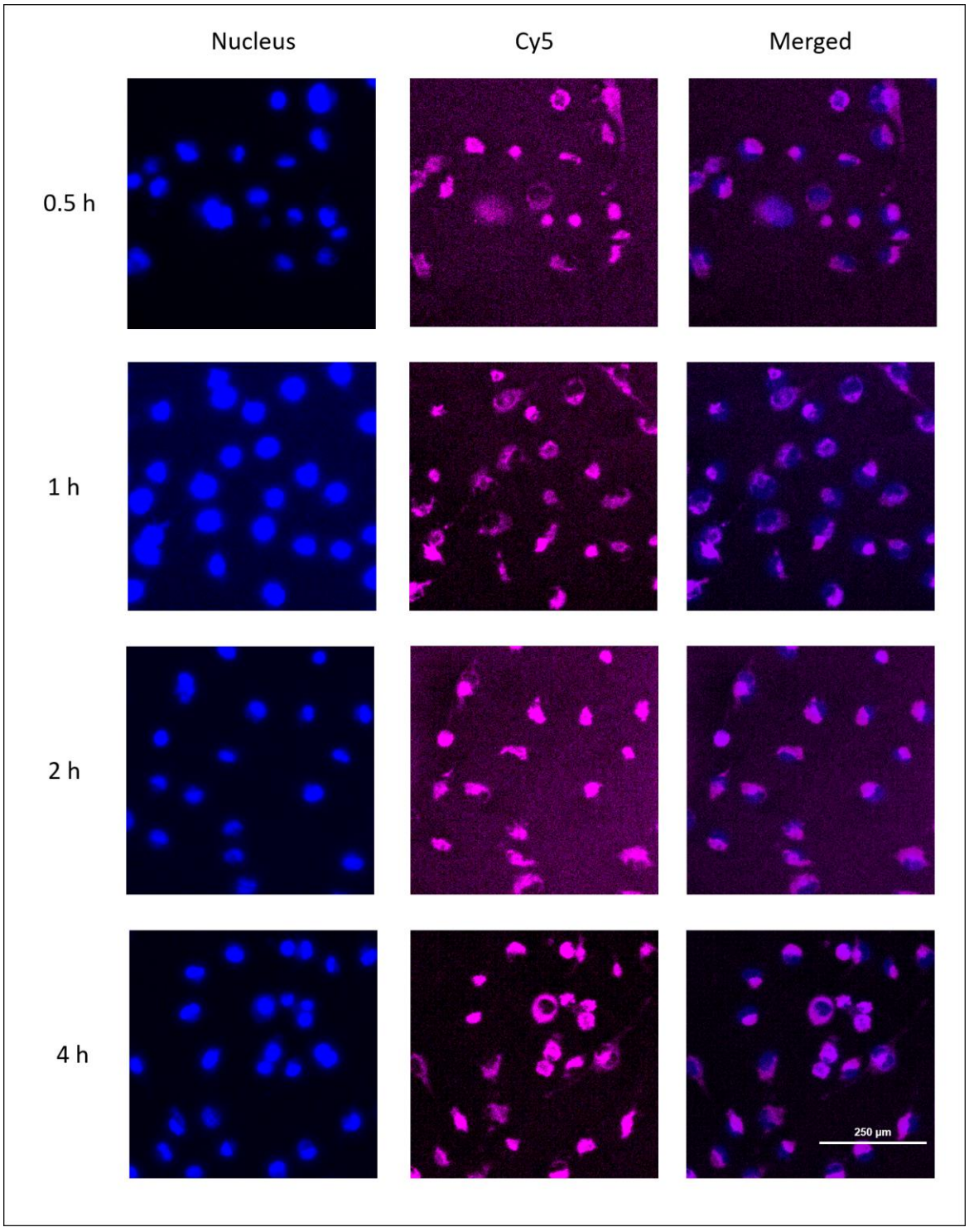


Figure 3-11 *U87 cells imaged on an inverted Nikon Eclipse TE 300 fluorescent microscope on DAPI (blue; nuclei) and Cy5 (magenta) filters. Images were merged using ImageJ software. Uptake of NPs at t = 0.5, 1, 2 and 4 hours.*

The Images in Figure 3-11 show interaction with the cells within 30 minutes. Since any NPs that had not been taken up by the cells, or which remained adhered to the surface, would have been washed away during media replacement steps, it can be assumed that intracellular uptake of the NPs had occurred. It appears that the NPs do not enter the nucleus but rather appear localised to the cytoplasm, however, confocal microscopy would need to be carried out to further support this statement and determine whether NPs are sequestered within lysosomes. Whilst the data suggests retention of the NPs over the experimental period, direct evidence would require replacement with fresh media at each time point to exclude the possibility of exocytosis. Furthermore, through confocal microscopy and/or co-immunofluorescence of Cy5 with a lysosomal marker, evidence of sequestering intracellularly would further confirm retention of the NPs within the cells.

3.4.4 Release studies

Release studies of the DOX from the DOX-NP and the DOX-NP from the PLGA/PEG microparticulate matrix were carried out to assess the nature of the release profiles and potential impact on later *in vivo* studies.

3.4.4.1 Dox release from DOX-NP

Experiments were carried out to investigate the nature of the release of the DOX from the NPs, and the timeframe in which this occurred.

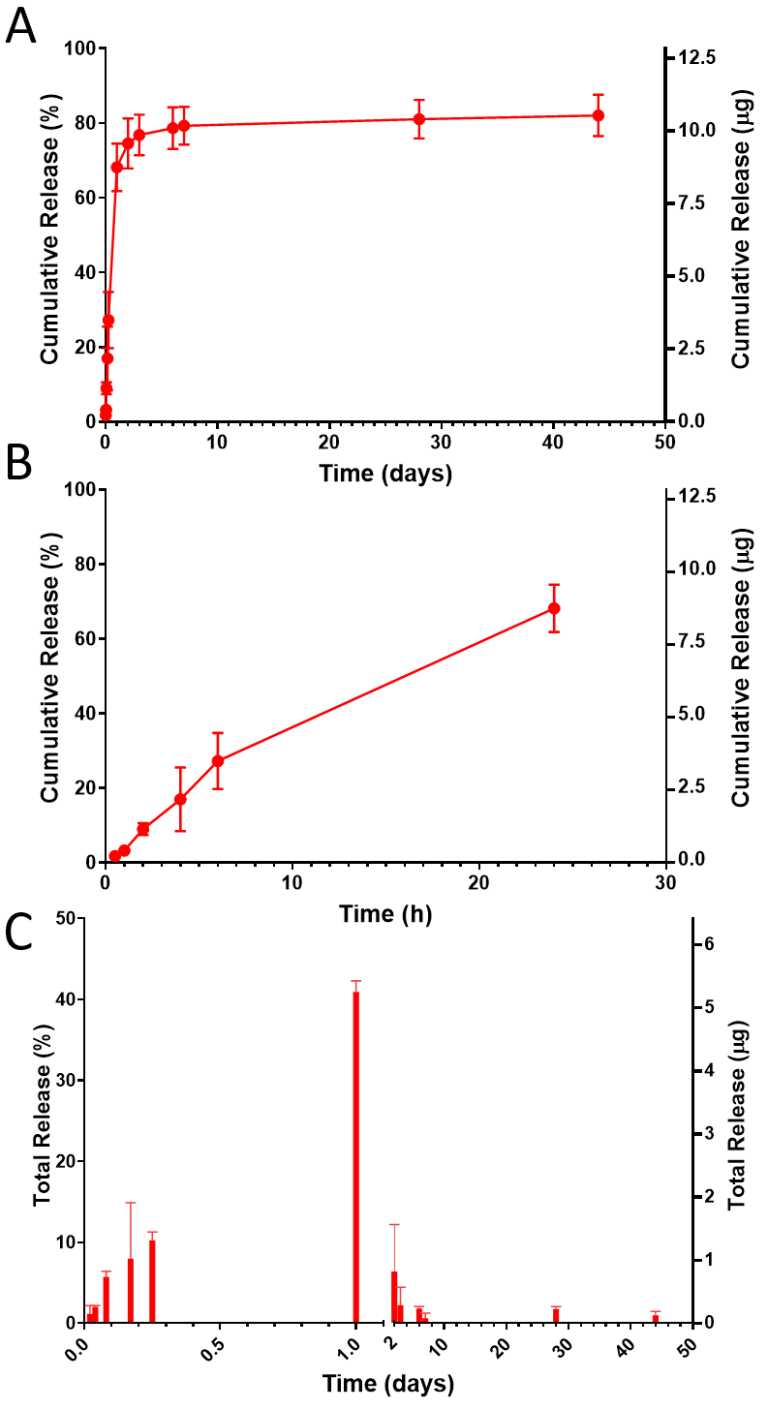


Figure 3-12 *Cumulative % and µg of DOX release from the DOX-loaded NPs over 44 days (A) and 24 hours (B) and absolute release at each time point (C). Release was carried out in PBS. Timepoints represent one independent repeat (n = 3) with error bars showing mean ± one SD.*

As can be observed in Figure 3-12, a burst release of DOX from the NPs occurred over the first 6 hours (Figure 3-12 B) with over 60% of DOX released within the first 24 hours. However, after 24 hours, a steady state of release was observed, with just over 80% of the drug released following 44 days. This large burst release was surprising, considering the high stability of the urea bond conjugating the DOX to the polymer backbone[345]. However, it has been reported that the urea bond can be weakened when a large, sterically hindered substituent group makes up the secondary amine[346–348], and this could be the case here, with the polymeric backbone acting as the "large, sterically hindered" substituent group. Furthermore, the kinetically trapped NPs formed will influence the release rate of DOX, as the access of any ureases, and also ingress of aqueous fluids to hydrolyse the polymer-DOX link, will be reduced. Therefore, polymer chains near the surface of the NP could have their urea links rapidly broken, whilst DOX-conjugates trapped near the centre of the particle would be less hydrated and slower to react and thus release the DOX more slowly. This release profile indicates the likelihood that enough of the DOX would be released from the NPs within the first 24 hours (8.746 ± 0.816 µg) to achieve potency levels above the IC_{50} of each of the GBM lines tested (Figure 3-7).

3.4.4.2 DOX-NP release from PLGA/PEG

It was of paramount importance to test that the NPs could be released from the PLGA/PEG matrix, as this was the premise of the drug delivery system. Originally, the PLGA/PEG matrix was designed as a scaffold for

bone regeneration[78–80,349] and was thus packed tightly into a cylindrical mould for the sintering process. On reflection, it was believed that this would not be representative of the PLGA/PEG matrix as a local drug delivery device in the brain. It was hypothesised that allowing the PLGA/PEG to sinter in “paste” form, as if pasted onto the cavity walls of the brain, would lead to an increased release rate which would be a more representative release profile as would be observed *in vivo.* Hence, two sets of studies were carried out in parallel to assess the release of DOX-NPs from the PLGA/PEG matrix; one set whereby the PLGA/PEG was packed tightly into a mould (red in Figure 3-13) and the second as a free “paste” (blue in Figure 3-13).

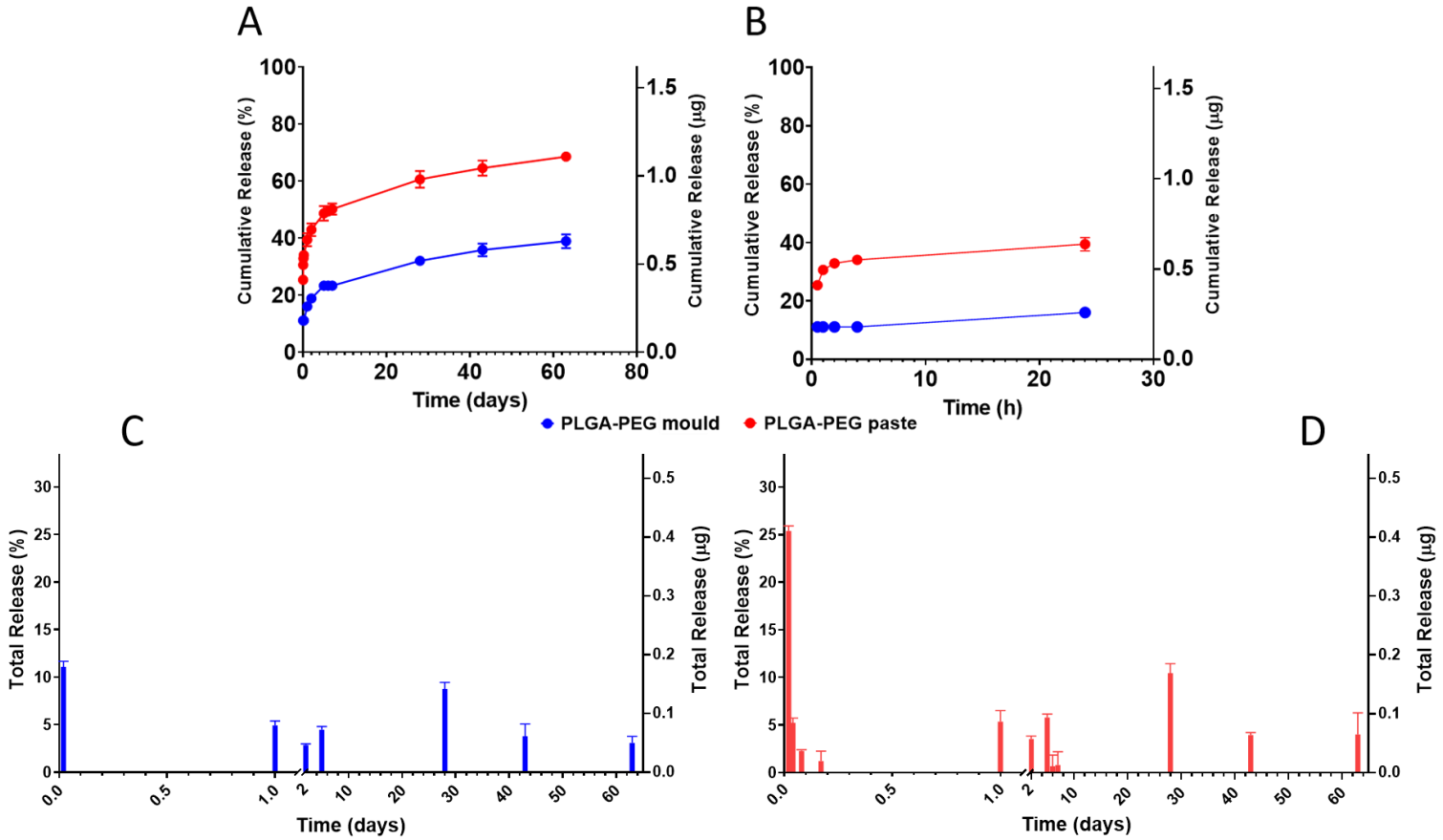


Figure 3-13 *Cumulative % and µg of DOX-NP release from the PLGA/PEG microparticulate matrix over 63 days (A) and 24 hours (B) and absolute release at each time point from the mould (C) and the paste (D). Release was carried out in PBS. Timepoints represent one independent repeat (n = 3) with error bars showing mean ± one SD.*

As predicted, the release from the “paste-like” PLGA/PEG matrix had a much faster release than that from the tightly packed mould. A burst release of the drug-conjugated NPs from the microparticulate matrix paste was observed during the first 8 hours. It is assumed that during the mixing process of the DOX-NPs with the PLGA/PEG particles, NPs remained on the surface of the matrix, thus releasing rapidly. The burst release was followed by a sustained release whereby ~70% of the DOX-NPs were released after two months, thus leading to a promising drug delivery system for the treatment of GBM.

Despite the release being much more rapid from the paste, the release profile for the mould and the paste is very similar when considering the cumulative release profiles. However, when evaluating the absolute total release in graphs C and D, it can be observed that despite the large burst release from the mould at the first time point, further release isn’t observed until day 1, whilst further release from the paste is observed at each time point between time 0 and day 1. This highlights the dependence of the release on the “packing” procedure, whereby the more tightly packed the PLGA/PEG microparticles, the smaller the initial burst release of DOX-NPs, and should be considered for future *in vivo* work. Following the 30 day timepoint, the absolute release at each time point for both release from the mould and the paste is very similar, indicating that the differences in quantity of DOX release is entirely down to the packing procedure of the microparticles and would be observed

within the first month of treatment, filling the clinical gap currently encountered in GBM treatment.

3.4.5 Systematic review of DOX-NPs

A systematic review of similar DOX-NPs was conducted and summarised in Table 3-2 below. The size, PDI and zeta-potential, alongside the method of DOX incorporation, the subsequent drug loading content and release rate were explored and compared to the system developed in this body of work. Further complexities of the systems were explored including the use of targeting moieties, responsive linkers or response to external stimulus, highlighting areas where further improvements could be made to the system developed here.

Table 3-2 Examples of DOX-NPs in oncology.

Nanoparticle material	Particle size	PDI	ζ-potential	Conjugated or encapsulated	DOX loading content (DLC)	Stability	DOX-release rate	IC_{50}	Targeting cancer type	Targeting Moiety	Responsive linker/ external stimuli	Internalisation Pathways	Ref.
Polymeric	**66.89 ± 2.04 nm**	**0.09 ± 0.02**	**-23.5 ± 4.5 mV**	**Conjugated**	**~12%**	**Stable for 1 week**	**60% in 24 h**	**---**	**GBM**	**---**	**---**	**---**	
Low MW heparin	39.87 ± 7.23 nm	0.201 ± 0.064	-32.8 ± 1.81	Encapsulated	28.03 ± 4.49% (w/w)	Stable in aq. medium 24 h	24 h = 42% DOX released	2.159 ± 0.179 μM	Prostate	Low Molecular Weight Heparin (LMHP)	---	Time – dependent H1 increased uptake	350
Chimeric polypeptides	40 nm	---	---	Conjugated	---	pH 7.4 over a 24 h period	pH 7.4 = stable pH 5.0 = first order half life of 4.9 ±0.5h	2.0 μM	4T1 carcinoma Lewis lung carcinoma	---	pH sensitive	Cellular uptake of CP-DOX, intracellular drug release and subsequent trafficking of drug to nucleus	351,352
Polymeric	125 ± 4.8 nm (TEM) 142 ± 6.1 (DLS)	---	---	Encapsulated, alongside navitoclax	DLC (loading content) = 12% DLE (efficiency) = 59%	---	pH 7.4 = 23.5% after 24 h pH 5.0 86.8% after 8 h	---	Endometrial carcinoma	---	pH sensitive	Endocytosis	353
Polymeric	127.47 ± 4.24 nm	---	−19.59 mV	Encapsulated Da = acid sensitive Sa = insensitive	DLC = 3.3% (wt/wt)	---	~40% released 24h	---	Breast cancer	R9 peptide (CPP)	pH sensitive	---	354
Polymeric	(ND6) 82 nm	0.243	---	Encapsulated	DLC = 4.2% DLE = 28%	---	>50% released after 12 h at pH 5.8 15% at pH 7.4	---	HeLa-tumour bearing mice	---	pH sensitive	Endocytosis, DOX released once in the cell	355
Gold nanostar	90.5 ± 9.9 nm	---	-32.7 ± 6.4	Conjugated to a DNA duplex	Conjugation efficiency	---	---	---	Breast Cancer	Aptamer-conjugated NPs	Acid labile linkers; photothermal	---	356

					= 55.1 ± 8%								
Hyaluronic acid polymeric	50 nm	<0.2	---	Conjugated	DLC = 10.3%	---	<10% at pH 7.4 ~60% at pH 5.5 @24 h	1.3 µg/mL	Colorectal cancer	HA	pH responsive imine bond	Endocytosis and captured by lysosomes, DOX then released and enters nucleus	357
Fe_3O_4 polymeric NPs	337 nm	0.219	-16.9 mV	Encapsulated	DLC = 7.13%	Stable in PBS for 3 days	24 h no stimuli = 3.6% pH 5.5 +GSH = 19.96% triple stimulation (+ NIR) = 32.7%	---	HeLa (generic cancer)	HA	pH responsive (Disulfide bridge); light irradiation	HA increased cell uptake	358
Hyperbranched polymer	79 nm	---	-36 mV	Encapsulated	EE = 82%	Stable at physiological conditions	---	Cell viability at 24 h = 55%	Prostate cancer	Folic acid	---	Folate receptor increased internalisation within 24 h	359
Iron oxide (Fe3O4) with polymeric brushes as the cloak	69 nm	---	−17.4 mV	Encapsulated	DLC = 8.95 ± 0.26%	---	---	Cell viability at 24 h = 32.71%	Breast cancer	---	Magneto-thermal	Increased cell uptake over DOX alone	360
Polymeric	42.0 ± 7.0 nm	---	---	Encapsulated	DLC = 12.8% ± 0.3%	---	pH 7.4 = 38.7% pH 5.0 = 60.5% over 48 h	2.252 ± 0.006 µg/mL	Primary CNS Lymphoma	Angiopep-2	---	Uptake mediated by the ANG peptide	361
galactose-based glycopolymers	30 nm	---	-25 mV at pH 7.4 but -9 at pH 5.5	Encapsulated	DLC = 8.63%	---	72 h pH 7.4 = 20% ph 5.0 – 45.0%	---	Hepatocellular carcinoma	---	Sensitive to acidic conditions	---	362
Polymeric pro-drug DEX_{1000}	37.56 nm	---	Neutral	Conjugated	DLC = 42.7%	Stable for 9 days	pH 7.4 = 30% at 24 h pH 5.0 = 70% at 24 h	HeLa ~0.2 µg/mL MCF-7 ~1.2 µg/mL	Cervical and breast cancer	---	Acid activatable hydrazine bond	Endocytosis	363

DEX_{5000}	49.26 nm				DLC = 48.1%			HeLa ~2.5 µg/mL MCF-7 ~1 µg/mL					
Polymeric micelles	82.1 ± 3.9 nm	0.196 ± 0.008	−9.1 ± 1.3 mV	Encapsulated	DLE = 87.1 ± 1.4	---	72 h pH 5.0 = 80% pH 7.4 = 32.5%	14.2 µg/mL after 24 h	Breast cancer	Y1R ligands to target overexpression	pH responsive	Endocytosis	[364]
Polymeric	23.3 ± 9.3 nm	---	---	Encapsulated	DLC = 18.4 wt%	---	12 h pH 5.0 = 95% release	0.263 and 0.110 µgmL−1 at 48 and 72 h, respectively	General	---	ROS responsive through phenylboronic	Endocytosis	[365]
Polymeric cross-linked micelle	85 nm	---	−1.7 ± 0.3 mV at pH 7.4 7.0 ± 0.7 mV at pH 6.0	Encapsulated	DLC = 6.1%	---	GSH 10 mM, 37% cargos of DOX-ICM 2 h 86% in 72 h	---	General, tested in C6 glioma cells	---	pH responsive (Disulfide bridge)	---	[366]
PEGylated liposomal	105 nm	---	−50.8 mA	---	---	Stable under storage and serum conditions for 7 days		0.07 µgmL−1 at 96 h	Breast cancer	HER 2	---	Endocytosis	[367]
Polymeric	228.6 ± 12.6	0.262	-1.02 mV	---	DLC = 13.8%	---	pH 7.4 ~20%pH 5.0+GSH ~70%	---	Breast Cancer	---	pH responsive (Disulfide bridge)	Clathrin-mediated endocytosis and mainly trapped in the endosome/ lysosome.	[368]

The overall aim of this body of work was to demonstrate a proof-of-concept; that the incorporation of drug-loaded NPs into a microparticulate drug delivery system could be achieved, and the NPs could also be released at a rate that would produce a high enough drug concentration to exert a cytotoxic effect. This has indeed been realised but does not necessarily imply that the DOX-loaded NPs are the most advanced they could be, with regards to preclinical translation.

Following screening of the recent literature for examples of DOX-loaded NPs, the majority of the NPs differed significantly from those designed in this body of work. The differences mainly occurred in the incorporation of DOX into the NP; most studies used an encapsulation method, as opposed to conjugating DOX to the polymeric chain as presented here. Furthermore, most systems introduced further complexities into the formulation, through utilising targeting moieties, responsive linkers or designing the NPs to be sensitive to external stimulus, such as near infrared light or heat. However, similarities could be drawn between the system developed in this body of work and a few others, whereby DOX was conjugated onto the polymeric backbone[357,363].

The first system explored, HA–mPEG$_{2k}$–DOX[357], is also PEGylated, but differs in the use of a targeting moiety, hyaluronic acid (HA), and also the pH-responsive imine bond used to graft the DOX to the aldehyde HA. The subsequent NP was of smaller size, 50 nm, than the P2-DOX NP investigated here. The drug loading was, however, ever so slightly greater for the P2-DOX system than the HA–mPEG$_{2k}$–DOX system (12%

vs 10.3% respectively). However, the rate of release was much more controlled in this system, whereby only 10% of DOX was released at pH 7.4 but 60% was released at the acidic pH 5.0, after 24 h. Conversely, 60% of the DOX was released from P2-DOX within 24 h at pH 7.4.

The second system utilises the OH functional groups on Dextran (DEX), to conjugate DOX via a pH-responsive hydrazone bond. The poly(ethylene glycol) methyl ether methacrylate (OEGMA) monomer was conjugated to the backbone of the co-polymer as the hydrophilic block, resulting in a DEX prodrug with bottlebrush-architecture (DOM@DOX^{363}). This system had a particularly high DOX loading of 42.7% or 48.1%, depending on the molecular weight of the DEX (1000 and 5000 Da, respectively). Similar to the HA–mPEG$_{2k}$–DOX system, the DOM@DOX system was pH sensitive and the DOX release rate was ~30% for the micelles at pH 7.4 but ~70% at pH 5.0 after 24 h.

These two systems indicate the successful targeting of DOX-loaded NPs to a cancerous environment through utilising pH responsive bonds, and is a factor which could potentially be incorporated into the P2-DOX formulation. The free amine group on the deprotected P2 polymeric backbone offers scope to incorporate either the hydrazone or imine bond described in these two studies and could offer a solution to minimise the large burst release of DOX observed from the P2-DOX system.

Some of the systems previously investigated incorporate the use of a targeting agent to further increase the uptake selectivity of NPs into the

targeted cancer cell. Examples of targeting moieties explored here include low molecular weight heparin (LMHP) which has the potential to form a strong complex with histone, which is overexpressed on the cell membrane of some cancerous cells[350], hyaluronic acid (HA), a natural polysaccharide, which can bind to the CD44 receptor overexpressed on tumour cells[357,358], folic acid which targets the folate receptor which is overexpressed on cancer cells[359], Y1R ligands to target overexpression of the Y1 receptor on tumour cells[364] and HER 2 which is overexpressed on cancer cell surfaces[367]. Each of these examples show an increase of NP uptake in the targeted cancer cell when the targeting moiety is utilised. Again, these data highlight the relevance of the use of targeting moieties, a factor that could enhance and improve the P2-DOX formulation investigated here.

However, increasing the complexity of such formulations also increases the complexity of synthesis, design and formulation procedures which may incur higher costs in production and an extended timeline to approval. A fine balance must be struck between a highly specific, targeted system with improved clinical outcome and reduced side effects, whilst maintaining GMP-compliance and gaining regulatory approval to market the formulation.

3.4.6 Representative Animal Glioma Cell Line

Finally, the NPs were screened against a representative animal glioma cell line to investigate the translational capability of the NPs from human

glioma cell lines to animal glioma cell lines for future *in vivo* work. The model selected was the 9L rat glioma cell line, on which the *in vivo* orthotopic allograft model would be based[76].

Firstly, the free DOX IC_{50} was calculated using the same method described for the other cell lines. The resultant IC_{50} of 61.94 ± 0.34 nM (Figure 3-14) indicated that the 9L cell line sensitivity to DOX fell within the IC_{50} range of the U87 and primary cell lines tested previously (Figure 3-7). This led to the hypothesis that similar reductions in metabolic activity, caused by the DOX-NPs, would be observed for the 9L cell line as it had for the human GBM cell lines.

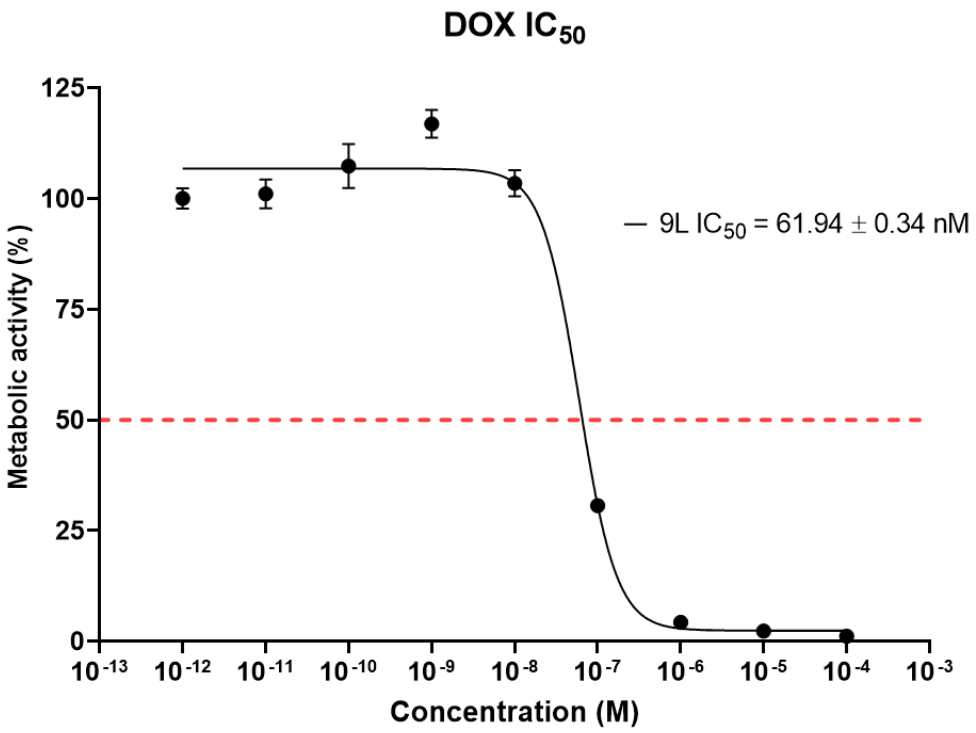


Figure 3-14 *Potency determination from DOX applied to the 9L rat glioma line was achieved via measurement of cellular metabolic activity (PrestoBlue™ assay). DOX was diluted in DMEM containing 10% FBS and applied for 72 hours. 9L cells were plated at 3 x 10^3 cells per well in 96 well plates. All were cultured for 24h prior to assaying. Data represent mean ± S.E.M and are quadruplets from three independent experiments. IC_{50} value is displayed in the key and are mean ± S.D and determined via GraphPad Prism.*

The control NPs and DOX-NPs, based on the P2 polymeric formulation, were screened against the 9L cell line. As can be observed in Figure 3-15, the control NPs did not have any negative impact on the metabolic activity of the 9L cells, whereas the DOX-NPs significantly reduced the metabolic activity of the 9L cells at a concentration of 1000 µg/mL. From these results, it was clear that the 9L cell line was more resistant to the DOX-NPs than the human cell lines tested, as no reduction in metabolic activity was observed at the concentration of 100 µg/mL.

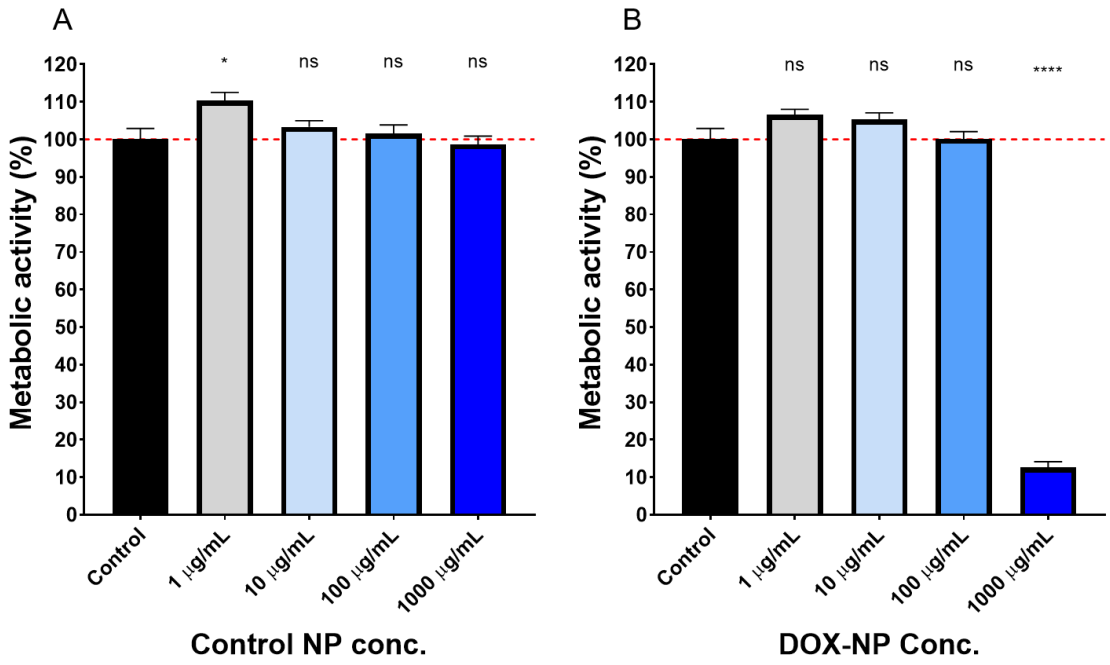


Figure 3-15 *In vitro cell viability assay at 72h post treatment with different concentrations of the P2 NP formulation (A) and P2-DOX NP formulation (B) on the 9L rat glioma cell line using the PrestoBlue™ assay. Three independent repeats were carried out (n=4). Error bars show mean ± SEM. [ns: p ≥ 0.05; *: p = 0.01-0.05; ****: p < 0.0001, unpaired t-test with Welch's correction, comparing each data set to the control (negative control; medium) data set]*

When the DOX-NPs were compared against their relative control NP counterpart (Figure 3-16), as expected, there was only a significant reduction in the metabolic activities of the cell line at a concentration of 1000 µg/mL, again implying that the 9L rat glioma cell line was more resistant to the DOX-NPs than the human glioma cell lines tested. This demonstrates the importance of testing the formulation against the cell line used to generate the orthotopic tumour for future *in vivo* studies, as the dosing will be extrapolated from this data.

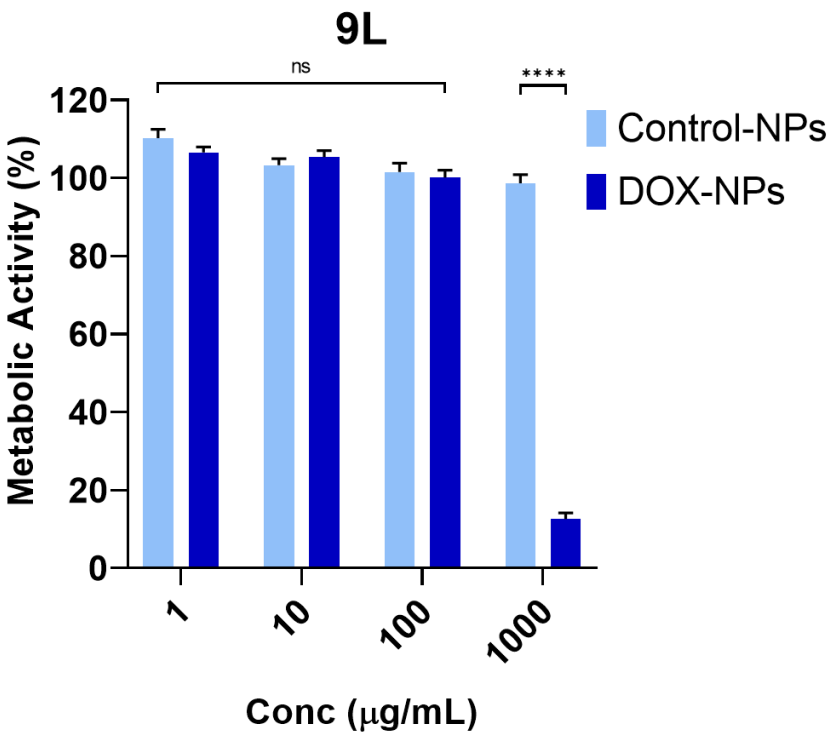


*Figure 3-16 In vitro cell viability assay at 72h post treatment with different concentrations of the P2 NP and P2-DOX NP formulations on the 9L glioma rat cell line using PrestoBlue™ assay. Three independent repeats were carried out (n=4). Error bars show mean ± SEM. (ns: $p \geq 0.05$; ****$p \leq 0.0001$; two-way ANOVA with Sidak's multiple comparisons test)*

The control NPs were found to exhibit no significant effects against the 9L rat glioma cell line. The potency of the DOX-NPs transitioned to the 9L cell line but was found to only have a significant effect on the metabolic activity of the cell line when at the highest concentration of 1000 µg/mL. This indicated that when considering an *in vivo* model using the 9L cell line, higher concentrations of DOX-NPs may be needed to induce a potent affect. However, overall these results confirmed that the synthesised NPs could be potentially applied to an *in vivo* model to asses tolerability and efficacy.

3.5 Conclusion

This body of work has investigated the effect of the NPs on the metabolic activity of a commercial GBM cell line. Each NP from the library of five polymeric formulations were found to be cytocompatible. Subsequent *in vitro* studies were carried out with the selected P2 formulation. These studies included investigating the metabolic activity of the control NPs on a primary human astrocyte cell line and both the control NPs and DOX-loaded NPs on a panel of primary GBM cell lines. It was concluded that the control NPs were cytocompatible at concentrations up to 100 µg/mL, when assessing the astrocyte line and with each of the primary GBM cell lines. Significant differences in cell metabolic activity could be observed for the DOX-NPs at 100 µg/mL and 1000 µg/mL, compared to both a negative control and their control NP counterpart on all cell lines tested, and thus deemed as potent at these concentrations. This cytotoxic nature of the drug-conjugated NPs in primary cell lines, derived from the tumour invasive margin of GBM patients, gives a clinically-relevant insight into the activity of the formulations.

The NPs were also screened against the 9L rat glioma cell line to give insight of these formulations on a potential *in vivo* model cell line. The 9L cell line was found to be more resistant to the drug-loaded NPs, but they were still found to significantly reduce the metabolic activity of the 9L cell line at the highest concentration of 1000 µg/mL, thus indicating the formulation's promise for future preclinical validation.

Finally, release studies were carried out whereby both the release of DOX from the NPs and DOX-NPs from the PLGA/PEG paste were investigated. The results indicated that a sufficient amount of DOX could be incorporated into the NPs to achieve a cytotoxic response upon release *in vitro*. A burst release of the drug-conjugated NPs from the microparticulate matrix was observed during the first 8 hours followed by a sustained release whereby 70% of the drug was released after one month, leading to a potential bridge for the treatment gap currently observed with GBM patients post-surgery.

Chapter 4 Future Outlook and Summary

4.1 Future Outlook

4.1.1 Release Studies

Release studies of the P2-DOX formulation from the PLGA/PEG paste were carried out and showed a burst release followed by a steady state release up until two months when approximately 70% of the DOX had been released. It would be interesting to compare this release profile to that of the DOX alone from the PLGA/PEG paste.

The PLGA/PEG system sinters at body temperature because PEG acts as a plasticiser, thus reducing the T_g of the PLGA which it is mixed with. While the microparticles are in their soft state (i.e. in paste form), the hydrophilic PEG component begins to leach out of the particles as it is drawn towards the liquid carrier solution, causing the T_g to increase and the microparticles to stick together and sinter. Since the NPs used here are PEGylated, it would be interesting to investigate whether they are also drawn to the liquid carrier solution and leach out, which may have led to the very high burst release of the NPs. Comparing the DOX-NP release rate to that of DOX alone may give an indication as to whether this theory is correct.

4.1.2 Penetration studies

As previously discussed, the $mPEG_{5000}$ system was selected over the $mPEG_{2000}$ system as the formulation to take forward for more in depth *in vitro* work due to the proposal that it would penetrate brain tissue more effectively because of the increased PEGylation. This was based on a review of the literature, particularly studies carried out by Elizabeth Nance and colleagues, discussed in the introduction[329,331]. It would be interesting to explore this idea here, to accept or reject the hypothesis that "NPs with an increased PEGylation would lead to increased penetration through brain tissue". An experimental plan to test this hypothesis would include measuring DOX-NPs penetration through brain tissue using an *ex vivo* model.

Members of our group are exploring the idea of using Time-of-Flight Secondary Ion Mass Spectrometry (ToF-SIMS) and 3D Orbi-SIMS to detect drugs on the surface of brain tissue *(unpublished data).* ToF-SIMS and 3D Orbi-SIMS are highly sensitive surface analysis techniques which have been utilised to analyse various tissues, including the brain[369–374]. Henceforth, it is proposed that ToF-SIMS/3D Orbi-SIMS imaging could be utilised to decipher the spatial distribution of DOX, and subsequently provide information regarding the penetration of DOX-NPs within brain tissue *ex vivo*. The DOX-NPs could be incorporated into the PLGA/PEG paste, as for the release experiments, and applied to the resection cavity lining of a pig brain which would form the *ex vivo* model. The brain could include a resection site in each hemisphere in order to compare two

different NP formulations within the same model. Once a suitable time has passed to allow for penetration, slices of the brain could be taken and subsequently analysed by TOF-SIMS/3D Orbi-SIMS to investigate the extent of penetration through the brain.

Alternatively, this method could be applied to an *in vivo* model and following culling the mice, the brains could be snap frozen, sliced and analysed by ToF-SIMS/3D Orbi-SIMS. This method would give a more realistic idea of penetration given that the brain would be in a native environment and therefore effects of flow from cerebral spinal and interstitial fluid, for example, could be considered.

4.1.3 Further enhancement of polymeric formulation

One of the exciting prospects of the PEGylated poly(lactide)-poly(carbonate) co-polymers developed in this body of work is the capability to conjugate different chemotherapeutics to the deprotected functionalisable monomer. DOX was used as a model drug for this piece of work but there is potential to conjugate other chemotherapeutics which have a free amine group, theoretically using the same chemistry and methods. For example, gemcitabine, a deoxycytidine analogue which inhibits DNA synthesis[375], has a free amine group as outline in Figure 4-1.

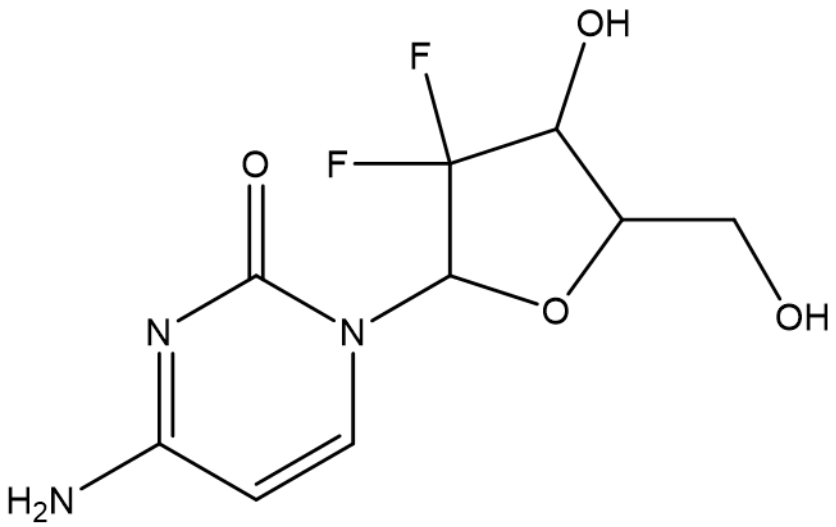


Figure 4-1 The chemical structure of Gemcitabine, indicating the free amine group on the chemotherapeutic.

Following optimisation of the conjugation procedure of DOX to the polymeric backbone, this method could be theoretically transferred to conjugate different therapeutics, such as gemcitabine. Despite this polymeric formulation being optimised for localised delivery in the treatment of GBM via the PLGA/PEG matrix, it has the potential to be used to treat other cancers whereby surgery is first-line treatment and localised recurrence rates are high, for example breast[376], ovarian[377] and colorectal cancers[378]. The P2-DOX has been screened against breast cancer cell lines and showed potency greater than that of free DOX[304], again highlighting its successful translation to other cancers. Furthermore, biodistribution experiments of the Cy5-labelled P1, P2 and P3 formulations to assess their distribution, organ accumulation and clearance have been carried out in mice[337]. No adverse effects were

noted over the 24 h period following systemic injection, highlighting the potential use of these polymeric NPs as both systemic and localised drug delivery vehicles.

Based on an increasing understanding of GBM intra-tumour heterogeneity, the capability to deliver multiple therapeutic moieties from single formulations or device is clinically relevant. Vincristine and temozolomide have been combined into solid lipid NPs (SLNs) and nanostructured lipid carriers (NLCs) to investigate dual drug delivery methods on the U87 GBM cell line. Significantly greater glioma inhibition was observed when using NLC formulations relative to SLNs[379]. Furthermore, paclitaxel and temozolomide were co-loaded in mPEG-PLGA NPs where the dual drug NPs showed greater inhibition against both U87 and C6 rat glioma cells relative to single drug NPs and significantly inhibited tumour growth in a subcutaneous U87 mouse xenograft model[380].

One of the original aims of this project was to develop a library of polymers, based on linear and star structures, leading to polymers with varying macromolecular architectures. An aspect that wasn't studied in this thesis, but would be of great interest, is the prospective capability of these DOX-conjugated polymeric systems to also encapsulate a second drug into the system, and act as a dual-drug delivery nanocarrier. It is hypothesised that the greater degree of branching will lead to an increased encapsulation efficiency[304], and thus may make the P4 and P5

systems more desirable than the P2 system, which was the most extensively investigated in this body of work.

4.1.4 Further enhancement of the PLGA/PEG drug delivery system

Successful studies carried out with the PLGA/PEG drug delivery system have shown the effective incorporation of various chemotherapeutics directly into the paste and the subsequent long term survival of rats using an orthotopic allograft model of high-grade glioma[87,88]. These studies provide evidence that mixing a chemotherapeutic directly into the paste leads to efficacy in the treatment of GBM *in vivo*. Therefore, it would be interesting to explore the concept of a dual-drug delivery system, using the P2-DOX NPs and a naked chemotherapeutic, mixed directly into the paste. Studies could then be carried out to demonstrate potential synergism, using the median-effect algorithm established by Chou and Talalay (Figure 4-2)[381–383].

$$CI = \frac{IC_{50}(A+B)}{IC_{50}(A)} + \frac{IC_{50}(A+B)}{IC_{50}(B)}$$

Figure 4-2 The median-effect algorithm, used to determine the Combination Index (CI) where IC_{50} (A) and IC_{50} (B) are the IC_{50} values obtained from each drug separately. IC_{50} (A + B) is the IC_{50} value of both drugs in combination.

The determined combination index (CI) values would either indicate strong synergism (<0.7), synergism (0.7 – 0.9), additive effect (0.9 - 1.1), antagonism (1.1 - 3.3) or strong antagonism (>3.3)[381,382].

4.1.5 *In vivo* tolerability and efficacy study using a high-grade glioma rat allograft model

An *in vivo* study was planned, using a high-grade glioma rat allograft model to establish the efficacy of the localised delivery of DOX-loaded NPs via the PLGA/PEG microparticulate paste to test the following hypotheses.

Hypothesis 1 – DOX-NPs released from PLGA/PEG is well tolerated in orthotopic glioma models *in vivo.*

Hypothesis 2 – DOX-NPs released from PLGA/PEG confers a significant survival benefit in orthotopic glioma models, relative to standard-of-care.

Aims:

1. Conduct a dose-escalation tolerability study using a high-grade glioma rat allograft model, to determine if DOX-NP delivered from PLGA/PEG paste is safe to use and to establish a maximum tolerated dose.

2. Conduct a therapy study, to determine if DOX-NP delivered from PLGA/PEG paste confers a survival benefit over standard-of-care treated animals.
3. Carry out post-sacrificial histology and immunohistochemistry (for markers of proliferation) for each treatment arm to directly assess DOX-NP-related cytotoxicity *in vivo*.

A localised *in vivo* model whereby the tumour is debulked, without complete resection, was planned to mimic the clinical scenario. The aim of this drug delivery system was to treat the infiltrative disease left behind following surgical resection.

Previous *in vivo* studies applying the intracranial delivery of PLGA/PEG have utilised 9L allografts to establish long term survival[88], which was also the model used in the pre-clinical development of Gliadel™. These studies confirmed the aggressiveness of the 9L allograft orthotopic model, evidenced by the extensive infiltration in the brain parenchyma adjacent to the original tumour site[88]. Furthermore, the 9L cell line is syngeneic, meaning the *in vivo* study would be completed on animals with an intact immune system. A limitation of using a rodent GBM allograft is that the model may not be phenotypically similar to human GBM[384]. However, transplanting a human GBM cell line would require immunocompromised rats, again not giving a true representation of the human disease. For the purpose of this *in vivo* study planned, the 9L model was ideal for investigating the effect of the drug-loaded NP formulations on a highly infiltrative, aggressive model of GBM.

A wide number of hydrophobic chemotherapeutic drugs, including DOX, are actively pumped out of cancer cells via ATP-binding cassette (ABC) transporters, leading to multi-drug resistance (MDR)[385]. MDR is a common trait of GBM, a factor contributing to its dismal prognosis[386]. Studies have been carried out whereby MDR has been successfully overcome through the encapsulation of DOX into various nanocarriers[387,388], leading to a promising strategy to overcoming MDR in GBM. When taking the P2-DOX formulation forward for *in vivo* studies, resistance should be taken into consideration and the affect this may have on subsequent survival. It could be hypothesised that the release of P2-DOX NPs from the PLGA/PEG paste would be more efficacious than the release of DOX alone, due to the increased MDR found with DOX in the treatment of GBM. This hypothesis could be tested through directly measuring the intracellular quantity of DOX comparing cells exposed to DOX alone and DOX-NPs. However, a major caveat of *in vivo* GBM models is the inability to recapitulate the heterogenic nature of the tumour, thus proposed resistance may not be as close to that observed in the clinic.

4.1.5.1 Primary derived cells for in vivo studies

Due to the increased understanding that GBM biology, therapy and therapy resistance are highly influenced by interactions between cancer cells and their microenvironment, the use of patient derived orthotopic xenografts (PDXs) has increased dramatically. They have been developed through the direct implantation of freshly isolated tumour cells,

without intervening cell culture steps. This has the advantage of capturing genetic diversity without any *in vitro* selection[389]. Despite the use of human GBM cell lines being more clinically relevant than rodent GBM cell lines, murine stroma inevitably takes over the implanted cells resulting in a genetic drift[389]. It has also been observed that developing human xenografts for rodent *in vivo* studies leads to problems concerning the lack of infiltrative disease, and does not truly recapitulate the tumour microenvironment with regards to cancer cell-host cell interactions and signalling[384]. It has therefore been suggested that for long term *in vivo* culture, direct patient xenografts may not perform any better than GSC cultures expanded *in vitro* prior to transplantation[390].

4.1.5.2 Organoid models of GBM

Despite the shift from mouse/rat genetic GBM models to potentially more representative PDX GBM models, there remain major drawbacks and lack of translation and prediction from *in vivo* studies to clinical trials. In particular, models are needed which have the capability to recapitulate the tumour microenvironment, ideally providing a better understanding of disease biology, including cell-cell and cell-environment interaction and crosstalk. A factor that is poorly translated in a rodent model is the infiltrative nature of the human disease, a component which is highly regarded as the translation failing point from *in vivo* success to clinical failure.

Organoids offer potential in overcoming some of the issues observed in 2D *in vitro* models and *in vivo* models. Alongside the successful development of organoids to model various cancer types including pancreatic[391], prostate[392], liver[393], breast[394], bladder[395], ovarian[396] and gastrointestinal[397], the development of organoids to model GBM has also taken place. The subsequent organoid models have the potential to simulate tumour complexity and heterogeneity, not only in tumour growth but also in response to treatment. The first GBM organoid was developed in 2016 whereby GBM cells and GBM biopsies were embedded in Matrigel[398]. The organoid was able to grow to 3 – 4 mm in two months and could be maintained in culture for over a year. Incredibly, these organoids retained the stem cell density in relation to hypoxia levels, closely simulating that found *in vivo*. However, one of the drawbacks to this system was the long period of time necessary to establish cultures (1 – 2 months) and the minimal throughput capacity. More recently, a faster protocol (1 – 2 weeks) has been reported and the organoids produced, termed GBOs, were developed in serum free conditions in order to avoid selection of specific cell populations, thus maintaining the inter and intra-tumoural heterogeneity[399].

Another method to establish 3D GBM organoid models is to genetically engineer brain organoids to develop tumours[400,401] or through co-culturing brain organoids with GBM cells[402,403]. The first method is advantageous in effectively modelling the initiation of GBM but lacks the ability to recapitulate the genomic complexity and heterogeneity of GBM.

The latter overcomes this shortcoming through co-culturing patient-derived glioma stem cells (GSCs) with brain organoids, demonstrating the ability of the GSCs to integrate into the organoids, termed ‘Glioma Cerebral Organoids’ (GLICO). The GLICO model offers a truer representation of the heterogeneity and infiltrative nature of GBM, as it was observed that co-cultured GSCs which exhibited a higher degree of invasiveness in the GLICO model, equated to a shorter life-span when transplanted in mice[401]. Furthermore, the formation of a network of microtubules in the GLICO model was observed, connecting bulk tumour with satellite tumour colonies, indicating the successful translation of the infiltrative nature of GBM[402].

One of the major benefits to these systems is the rapid development of a primary tumour derived organoid, which could be co-cultured with primary derived GSCs, resulting in a patient-derived “mini brain”[404], allowing the unprecedented opportunity to explore personalised medicine for the treatment of GBM. Each patient could have drugs screened against their “mini-brain” to afford them the best treatment method based on their own, specific tumour biology. This will lead to the continuous revision of clinical trial designs, whereby a combination of drugs can be screened against stratified patient cohorts, introducing flexibility to continue treatment for patients responding and similarly discontinue treatment for those patients who are not responding.

The models discussed offer an important opportunity to screen drugs against a library of GBM-organoids in a high throughput manner to gain

a more clinically-relevant insight to drug activity and resistance than is currently available in traditional 2D or *in vivo* models. However, the appropriate selection of which model to use would highly depend on the research question being asked. In this body of work, the enhanced penetration and efficacy of drug-loaded NPs was investigated and similar drawbacks observed with *in vivo* models, such as size difference between rat and human brain, would not necessarily be overcome with organoid models, even if the tumour microenvironment may be more closely related to that of a human GBM.

4.2 Summary

The work presented in this thesis highlights the application of polymeric nanotherapeutics for the localised treatment of GBM via a pre-existing microparticulate paste. A panel of cytocompatible polymeric formulations were designed and shown to form self-assembling NPs. The ROP method was optimised to advance further the use of organobasic catalysts, decreasing the reaction time, temperature and alleviating laborious column separation steps. In this way a quick, easy and user-friendly ROP method generated polymers with highly predictable final molecular weights and narrow molar mass dispersities (Đ). Furthermore, a functionalisable monomer, tBSC, was synthesised and the optimised ROP method was successfully able to include this BOC-protected monomer, resulting in co-polymers with functional “handles” scattered throughout the backbone. Following the successful deprotection of the

BOC group on the tBSC monomer, DOX was conjugated to the polymeric backbone, generating drug-loaded polymers, which were formulated into kinetically-trapped NPs as a proof-of-concept drug delivery system.

The subsequent DOX-NPs were screened against a panel of GBM cell lines, both commercially available and primary-derived cell lines from the infiltrative margin of patients' tumours, providing a more clinically-relevant insight to the activity of the formulations. Whilst the drug-free NPs were cytocompatible with the cell lines tested, the DOX-NPs were efficacious against each GBM cell line tested.

The predominant aim of the designed DOX-NPs was incorporation of the formulation into a previously developed PLGA/PEG microparticulate matrix for the localised treatment of GBM. Henceforth, *in vitro* release studies of the DOX-NPs from the PLGA/PEG matrix were set up to ensure successful release of the drug from the depot. A burst release of DOX was observed after the first 30 minutes, most likely due to the adherence of some of the DOX-NPs to the surface of the PLGA/PEG microparticles at the edge of the matrix prompting their initial release via high local acidity at the matrix surface. This observed burst release lasted 4 days and was followed by a steady-state release up until day 63 when approximately 70% of the drug had been released from the matrix. This steady state release was expected, as it had been previously observed when drug alone had been incorporated into the PLGA/PEG matrix[86,88], and was attributed to the drugs becoming trapped within microparticulate pores. It is hypothesised that the release of the remaining 30% of drug

would be PLGA degradation-dependent, and thus the remaining DOX would be released following degradation, which could be tested through longer *in vitro* release studies.

Based on the amount of DOX conjugated to the polymeric platform forming the DOX-loaded NPs, the cumulative release concentration during the initial burst release over the 4 days is expected to have a cytotoxic effect against residual tumour cells most proximal to the invasive margin. The remaining DOX-NPs released over the following 60 days may potentially penetrate further into the brain parenchyma and target more infiltrative tumour cells, thus potentially filling the current oncological treatment gap between surgery and adjuvant chemotherapy and radiation treatment.

Overall, this project has emphasised the potential of incorporating nanotherapeutics into a microparticulate localised delivery system for the first time in neuro-oncology, an exciting prospect for the future treatment of GBM.

Chapter 5 References

1. Wesseling, P. & Capper, D. WHO 2016 Classification of gliomas. *Neuropathol. Appl. Neurobiol.* **44**, 139–150 (2018).

2. Louis, D. N. *et al.* The 2007 WHO Classification of Tumours of the Central Nervous System. *Acta Neuropathol.* **114**, 97–109 (2007).

3. Ohgaki, H. & Kleihues, P. Population-Based Studies on Incidence, Survival Rates, and Genetic Alterations in Astrocytic and Oligodendroglial Gliomas. *J. Neuropathol. Exp. Neurol.* **64**, 479–489 (2005).

4. Thakkar, J. P. *et al.* Epidemiologic and molecular prognostic review of glioblastoma. *Cancer Epidemiology Biomarkers and Prevention* **23**, 1985–1996 (2014).

5. Scherer, H. J. Cerebral astrocytomas and their derivatives. *Am. J. Cancer* **40**, 159–198 (1940).

6. Peiffer, J. & Kleihues, P. Hans-Joachim Scherer (1906-1945), Pioneer in Glioma Research. *Brain Pathol.* **9**, 241–245 (2006).

7. Stoyanov, G. S., Petkova, L. & Dzhenkov, D. L. Hans Joachim Scherer and His Impact on the Diagnostic, Clinical, and Modern Research Aspects of Glial Tumors. *Cureus* **11**, (2019).

8. Ohgaki, H. & Kleihues, P. The Definition of Primary and Secondary Glioblastoma. (2013). doi:10.1158/1078-0432.CCR-12-3002

9. Louis, D. N., Wiestler, O. D., International Agency for Research on Cancer & World Health Organization. *WHO classification of tumours of the central nervous system*. (World Health Organization, 2007).

10. Stupp, R. *et al.* Radiotherapy plus concomitant and adjuvant temozolomide for glioblastoma. *N. Engl. J. Med.* **352**, 987–996 (2005).

11. Young, R. M., Jamshidi, A., Davis, G. & Sherman, J. H. Current

trends in the surgical management and treatment of adult glioblastoma. *Annals of Translational Medicine* **3**, (2015).

12. Perry, J. *et al.* The use of prophylactic anticonvulsants in patients with brain tumours-a systematic review. *Curr. Oncol.* **13**, 222–9 (2006).

13. Schiff, D. *et al.* Medical management of brain tumors and the sequelae of treatment. *Neuro. Oncol.* **17**, 488–504 (2015).

14. Louis, D. N. Molecular pathway of malignant gliomas. *Annu. Rev. Pathol. Mech. Dis.* **1**, 97–117 (2006).

15. Davis, M. E. Glioblastoma: Overview of disease and treatment. *Clin. J. Oncol. Nurs.* **20**, 1–8 (2016).

16. Stummer, W. *et al.* Intraoperative Detection of Malignant Gliomas by 5-Aminolevulinic Acid-induced Porphyrin Fluorescence. *Neurosurgery* **42**, 518–523 (1998).

17. Stummer, W. *et al.* Fluorescence-guided resection of glioblastoma multiforme by using 5-aminolevulinic acid-induced porphyrins: A prospective study in 52 consecutive patients. *J. Neurosurg.* **93**, 1003–1013 (2000).

18. Ennis, S. R. *et al.* Transport of 5-aminolevulinic acid between blood and brain. *Brain Res.* **959**, 226–234 (2003).

19. Roberts, D. Glioblastoma Multiforme Treatment with Clinical Trials for Neurosurg Surgical Resection (Aminolevulinic Acid). *Neurosurg Clin N Am* **23**, 371–377 (2013).

20. Ehrhardt, A. *et al.* Technical Principles for Protoporphyrin-IX-Fluorescence Guided Microsurgical Resection of Malignant Glioma Tissue. *Acta Neurochir. (Wien).* **140**, 995–1000 (1998).

21. Duffner, F. *et al.* Specific intensity imaging for glioblastoma and neural cell cultures with 5-aminolevulinic acid-derived protoporphyrin IX. *J. Neurooncol.* **71**, 107–111 (2005).

22. Zhao, S. *et al.* Intraoperative Fluorescence-Guided Resection of High-Grade Malignant Gliomas Using 5-Aminolevulinic Acid-

Induced Porphyrins: A Systematic Review and Meta-Analysis of Prospective Studies. *PLoS ONE* **8**, (2013).

23. Stupp, R. *et al.* Radiotherapy plus Concomitant and Adjuvant Temozolomide for Glioblastoma. *N. Engl. J. Med.* **352**, 987–996 (2005).

24. Stupp, R. *et al.* Effects of radiotherapy with concomitant and adjuvant temozolomide versus radiotherapy alone on survival in glioblastoma in a randomised phase III study: 5-year analysis of the EORTC-NCIC trial. *Lancet Oncol.* **10**, 459–466 (2009).

25. Barani, I. J. & Larson, D. A. Radiation therapy of glioblastoma. *Cancer Treat. Res.* **163**, 49–73 (2015).

26. Brindley, C. J., Antoniw, P. & Newlands, E. S. Plasma and tissue disposition of mitozolomide in mice. *Br. J. Cancer* **53**, 91–97 (1986).

27. Tisdale, M. J. Antitumour imidazotetrazines-XV. Role of guanine O6 alkylation in the mechanism of cytotoxicity of imidazotetrazinones. *Biochem. Pharmacol.* **36**, 457–462 (1987).

28. Baer, J. C. *et al.* Depletion of O6-alkylguanine-DNA alkyltransferase correlates with potentiation of temozolomide and CCNU toxicity in human tumour cells. *Br. J. Cancer* **67**, 1299–1302 (1993).

29. Lee, S. M., Thatcher, N., Crowther, D. & Margison, G. P. Inactivation of O6-alkylguanine-DNA alkyltransferase in human peripheral blood mononuclear cells by temozolomide. *Br. J. Cancer* **69**, 452–456 (1994).

30. Wedge, S. R., Porteous, J. K. & Newlands, E. S. 3-Aminobenzamide and/or O6-benzylguanine evaluated as an adjuvant to temozolomide or BCNU treatment in cell lines of variable mismatch repair status and O6-alkylguanine-DNA alkyltransferase activity. *Br. J. Cancer* **74**, 1030–1036 (1996).

31. Plummer, E. R. *et al.* Temozolomide pharmacodynamics in patients with metastatic melanoma: DNA damage and activity of repair enzymes O6-alkylguanine alkyltransferase and poly(ADP-ribose) polymerase-1. *Clin. Cancer Res.* **11**, 3402–3409 (2005).

32. Hegi, M. E. *et al.* Clinical Trial Substantiates the Predictive Value of O-6-Methylguanine-DNA Methyltransferase Promoter Methylation in Glioblastoma Patients Treated with Temozolomide. *Clin. Cancer Res.* **10**, 1871–1874 (2004).

33. Hegi, M. E. *et al.* MGMT gene silencing and benefit from temozolomide in glioblastoma. *N. Engl. J. Med.* **352**, 997–1003 (2005).

34. Goth, R. & Rajewsky, M. F. Persistence of 06 ethylguanine in rat brain DNA: correlation with nervous system specific carcinogenesis by ethylnitrosourea. *Proc. Natl. Acad. Sci. U. S. A.* **71**, 639–643 (1974).

35. Margison, G. P. & Kleihues, P. Chemical carcinogenesis in the nervous system. Preferential accumulation of O6 methylguanine in rat brain deoxyribonucleic acid during repetitive administration of N methyl N nitrosourea. *Biochem. J.* **148**, 521–525 (1975).

36. Bello, M. J. *et al.* Hypermethylation of the DNA repair gene MGMT: association with TP53 G:C to A:T transitions in a series of 469 nervous system tumors. *Mutat. Res.* **554**, 23–32 (2004).

37. Kamiryo, T. *et al.* Correlation between Promoter Hypermethylation of the O6-Methylguanine-Deoxyribonucleic Acid Methyltransferase Gene and Prognosis in Patients with High-grade Astrocytic Tumors Treated with Surgery, Radiotherapy, and 1-(4-Amino-2-methyl-5-pyrimidinyl)methyl-3-(2-chloroethyl)-3-nitrosourea-based Chemotherapy. *Neurosurgery* **54**, 349–357 (2004).

38. Nakamura, M., Watanabe, T., Yonekawa, Y., Kleihues, P. & Ohgaki, H. *Promoter methylation of the DNA repair gene MGMT in astrocytomas is frequently associated with G:C → A:T mutations of the TP53 tumor suppressor gene*. *Carcinogenesis* **22**, (2001).

39. WHO | WHO Definition of Palliative Care. Available at: https://www.who.int/cancer/palliative/definition/en/. (Accessed: 22nd April 2020)

40. Giammalva, G. R. *et al.* End-of-life care in high-grade glioma patients. The palliative and supportive perspective. *Brain Sciences* **8**, (2018).

41. Catt, S., Chalmers, A. & Fallowfield, L. Psychosocial and

supportive-care needs in high-grade glioma. *Lancet Oncol.* **9**, 884–891 (2008).

42. Koekkoek, J. A. F. *et al.* Symptoms and medication management in the end of life phase of high-grade glioma patients. *J. Neurooncol.* **120**, 589–595 (2014).

43. Stupp, R. *et al.* NovoTTF-100A versus physician's choice chemotherapy in recurrent glioblastoma: A randomised phase III trial of a novel treatment modality. *Eur. J. Cancer* **48**, 2192–2202 (2012).

44. Kirson, E. D. *et al.* Alternating electric fields arrest cell proliferation in animal tumor models and human brain tumors. *Proc. Natl. Acad. Sci. U. S. A.* **104**, 10152–10157 (2007).

45. Stupp, R. *et al.* Maintenance therapy with tumor-Treating fields plus temozolomide vs temozolomide alone for glioblastoma a randomized clinical trial. *JAMA - J. Am. Med. Assoc.* **314**, 2535–2543 (2015).

46. Stupp, R. *et al.* Effect of tumor-treating fields plus maintenance temozolomide vs maintenance temozolomide alone on survival in patients with glioblastoma a randomized clinical trial. *JAMA - J. Am. Med. Assoc.* **318**, 2306–2316 (2017).

47. Novocure's Tumor Treating Fields: Innovative brain cancer therapy with survival and safety benefits. Available at: https://www.nature.com/articles/d42473-018-00156-3. (Accessed: 29th April 2020)

48. Taphoorn, M. J. B. *et al.* Influence of treatment with tumor-treating fields on health-related quality of life of patients with newly diagnosed glioblastoma a secondary analysis of a randomized clinical trial. *JAMA Oncol.* **4**, 495–504 (2018).

49. Therapies - Brainstrust, brain tumour charity. Available at: https://brainstrust.org.uk/brain-tumour-support/navigating-your-pathway/treatment-information/therapies/. (Accessed: 29th April 2020)

50. Hottinger, A. F., Pacheco, P. & Stupp, R. Tumor treating fields: A novel treatment modality and its use in brain tumors. *Neuro. Oncol.* **18**, 1338–1349 (2016).

51. Galanis, E. & Buckner, J. Chemotherapy for high-grade gliomas. *British Journal of Cancer* **82**, 1371–1380 (2000).

52. Juratli, T. A., Schackert, G. & Krex, D. Current status of local therapy in malignant gliomas — A clinical review of three selected approaches. *Pharmacol. Ther.* **139**, 341–358 (2013).

53. Bock, H. C. *et al.* First-line treatment of malignant glioma with carmustine implants followed by concomitant radiochemotherapy: a multicenter experience. *Neurosurg Rev* **33**, 441–449 (2010).

54. Perry, J., Chambers, A., Spithoff, K. & Laperriere, N. Gliadel wafers in the treatment of malignant glioma: a systematic review. *Curr. Oncol.* **14**, 189–94 (2007).

55. Bregy, A. *et al.* The role of Gliadel wafers in the treatment of high-grade gliomas. *Expert Rev. Anticancer Ther.* **13**, 1453–1461 (2013).

56. Lesniak, M. S. & Brem, H. Targeted therapy for brain tumours. *Nat. Rev. Drug Discov.* **3**, 499–508 (2004).

57. Rainov, N. G. & Heidecke, V. Clinical development of experimental therapies for malignant glioma. *Sultan Qaboos Univ. Med. J.* **11**, 5–28 (2011).

58. Bobo, R. H. *et al.* Convection-enhanced delivery of macromolecules in the brain. *Proc. Natl. Acad. Sci. USA* **91**, 2076–80 (1994).

59. Allard, E., Passirani, C. & Benoit, J.-P. Convection-enhanced delivery of nanocarriers for the treatment of brain tumors. *Biomaterials* **30**, 2302–2318 (2009).

60. Arshad, A. *et al.* Convection-Enhanced Delivery of Carboplatin PLGA Nanoparticles for the Treatment of Glioblastoma. *PLoS One* **10**, e0132266 (2015).

61. Zhou, J. *et al.* Highly penetrative, drug-loaded nanocarriers improve treatment of glioblastoma. *Proc. Natl. Acad. Sci. U. S. A.* **110**, 11751–6 (2013).

62. Sawyer, A. J. *et al.* Convection-enhanced delivery of camptothecin-loaded polymer nanoparticles for treatment of intracranial tumors. *Drug Deliv. Transl. Res.* **1**, 34–42 (2011).

63. Bernal, G. M. *et al.* Convection-enhanced delivery and in vivo imaging of polymeric nanoparticles for the treatment of malignant glioma. *Nanomedicine Nanotechnology, Biol. Med.* **10**, 149–157 (2014).

64. Hadjipanayis, C. G. *et al.* EGFRvIII Antibody-Conjugated Iron Oxide Nanoparticles for Magnetic Resonance Imaging-Guided Convection-Enhanced Delivery and Targeted Therapy of Glioblastoma. *Cancer Res.* **70**, 6303–6312 (2010).

65. Vogelbaum, M. A. & Aghi, M. K. Convection-enhanced delivery for the treatment of glioblastoma. *Neuro. Oncol.* **17**, ii3–ii8 (2015).

66. Sonabend, A. M. *et al.* Prolonged intracerebral convection-enhanced delivery of topotecan with a subcutaneously implantable infusion pump. *Neuro. Oncol.* **13**, 886–93 (2011).

67. neuroinfuse™ drug delivery system. Available at: https://www.renishaw.com/en/neuroinfuse-drug-delivery-system--42358. (Accessed: 28th July 2020)

68. Lewis, O. *et al.* Chronic, intermittent convection-enhanced delivery devices. *Journal of Neuroscience Methods* **259**, 47–56 (2016).

69. Lewis, O. *et al.* Chronic, intermittent convection-enhanced delivery devices. *Journal of Neuroscience Methods* **259**, 47–56 (2016).

70. Barua, N. U. *et al.* A novel implantable catheter system with transcutaneous port for intermittent convection-enhanced delivery of carboplatin for recurrent glioblastoma. *Drug Deliv.* **23**, 167–173 (2016).

71. Barua, N. U. *et al.* Robot-guided convection-enhanced delivery of carboplatin for advanced brainstem glioma. *Acta Neurochir. (Wien).* **155**, 1459–1465 (2013).

72. Zentner, G. M. *et al.* Biodegradable block copolymers for delivery of proteins and water-insoluble drugs. *J. Control. Release* **72**, 203–215 (2001).

73. Elstad, N. L. & Fowers, K. D. OncoGel (ReGel/paclitaxel)-Clinical applications for a novel paclitaxel delivery system. *Adv. Drug Deliv. Rev.* **61**, 785–794 (2009).

74. Tyler, B. *et al.* A thermal gel depot for local delivery of paclitaxel to treat experimental brain tumors in rats. *J. Neurosurg.* **113**, 210–217 (2010).

75. Bastiancich, C. *et al.* Lauroyl-gemcitabine-loaded lipid nanocapsule hydrogel for the treatment of glioblastoma. *J. Control. Release* **225**, 283–293 (2016).

76. Bastiancich, C. *et al.* Evaluation of lauroyl-gemcitabine-loaded hydrogel efficacy in glioblastoma rat models. *Nanomedicine* **13**, 1999–2013 (2018).

77. Bastiancich, C. *et al.* Drug combination using an injectable nanomedicine hydrogel for glioblastoma treatment. (2019). doi:10.1016/j.ijpharm.2019.01.042

78. Rahman, C. V. *et al.* PLGA/PEG-hydrogel composite scaffolds with controllable mechanical properties. *J. Biomed. Mater. Res. Part B Appl. Biomater.* **101B**, 648–655 (2013).

79. Dhillon, A. *et al.* Analysis of sintered polymer scaffolds using concomitant synchrotron computed tomography and in situ mechanical testing. *J. Mater. Sci. Mater. Med.* **22**, 2599–2605 (2011).

80. Qutachi, O. *et al.* Injectable and porous PLGA microspheres that form highly porous scaffolds at body temperature. *Acta Biomater.* **10**, 5090–5098 (2014).

81. Park, K. *et al.* Injectable, long-acting PLGA formulations: Analyzing PLGA and understanding microparticle formation. *J. Control. Release* **304**, 125–134 (2019).

82. Suk, J. S., Xu, Q., Kim, N., Hanes, J. & Ensign, L. M. PEGylation as a strategy for improving nanoparticle-based drug and gene delivery. *Advanced Drug Delivery Reviews* **99**, 28–51 (2016).

83. Veronese, F. M. & Pasut, G. PEGylation, successful approach to drug delivery. *Drug Discovery Today* **10**, 1451–1458 (2005).

84. Rezwan, K., Chen, Q. Z., Blaker, J. J. & Boccaccini, A. R. Biodegradable and bioactive porous polymer/inorganic composite scaffolds for bone tissue engineering. *Biomaterials* **27**, 3413–3431 (2006).

85. Scammell, B. E. A biodegradable antibiotic-impregnated scaffold to prevent osteomyelitis in a contaminated in vivo bone defect model. *Eur. Cells Mater.* **27**, 332–349 (2014).

86. Rahman, C. V. *et al.* Adjuvant Chemotherapy for Brain Tumors Delivered via a Novel Intra-Cavity Moldable Polymer Matrix. *PLoS One* **8**, e77435 (2013).

87. Smith, S. J. *et al.* Surgical delivery of drug releasing poly(lactic-co-glycolic acid)/poly(ethylene glycol) paste with in vivo effects against glioblastoma. *Ann. R. Coll. Surg. Engl.* **96**, 495–501 (2014).

88. Smith, S. J. *et al.* Overall survival in malignant glioma is significantly prolonged by neurosurgical delivery of etoposide and temozolomide from a thermo-responsive biodegradable paste. *Clin. Cancer Res.* clincanres.3850.2018 (2019). doi:10.1158/1078-0432.CCR-18-3850

89. Rosenblum, D., Joshi, N., Tao, W., Karp, J. M. & Peer, D. Progress and challenges towards targeted delivery of cancer therapeutics. *Nature Communications* **9**, 1–12 (2018).

90. Gudbergsson, J. M., Jønsson, K., Simonsen, J. B. & Johnsen, K. B. Systematic review of targeted extracellular vesicles for drug delivery – Considerations on methodological and biological heterogeneity. *Journal of Controlled Release* **306**, 108–120 (2019).

91. Zhang, S., Gao, H. & Bao, G. Physical Principles of Nanoparticle Cellular Endocytosis. *ACS Nano* **9**, 8655–8671 (2015).

92. Xu, S., Olenyuk, B. Z., Okamoto, C. T. & Hamm-Alvarez, S. F. Targeting receptor-mediated endocytotic pathways with nanoparticles: Rationale and advances. *Advanced Drug Delivery Reviews* **65**, 121–138 (2013).

93. Sasso, L., Purdie, L., Grabowska, A., Jones, A. T. & Alexander, C. Time and cell-dependent effects of endocytosis inhibitors on the internalization of biomolecule markers and nanomaterials. *J. Interdiscip. Nanomedicine* **3**, 67–81 (2018).

94. Freitas Jr, R. A. *Nanomedicine, Volume I: Basic Capabilities*. (Landes Bioscience, 1999).

95. Seigneuric, R. *et al.* From Nanotechnology to Nanomedicine: Applications to Cancer Research. *Curr. Mol. Med.* **10**, 640–652 (2010).

96. Zhao, M. *et al.* Codelivery of paclitaxel and temozolomide through a photopolymerizable hydrogel prevents glioblastoma recurrence after surgical resection. *J. Control. Release* **309**, 72–81 (2019).

97. Sousa, F., Dhaliwal, H. K., Gattacceca, F., Sarmento, B. & Amiji, M. M. Enhanced anti-angiogenic effects of bevacizumab in glioblastoma treatment upon intranasal administration in polymeric nanoparticles. *J. Control. Release* **309**, 37–47 (2019).

98. Jhaveri, A., Deshpande, P., Pattni, B. & Torchilin, V. Transferrin-targeted, resveratrol-loaded liposomes for the treatment of glioblastoma. *J. Control. Release* **277**, 89–101 (2018).

99. Zhou, Y., Peng, Z., Seven, E. S. & Leblanc, R. M. Crossing the blood-brain barrier with nanoparticles. *J. Control. Release* **270**, 290–303 (2018).

100. Kim, J. S., Shin, D. H. & Kim, J. S. Dual-targeting immunoliposomes using angiopep-2 and CD133 antibody for glioblastoma stem cells. *J. Control. Release* **269**, 245–257 (2018).

101. Zhou, M. *et al.* H7K(R2)2-modified pH-sensitive self-assembled nanoparticles delivering small interfering RNA targeting hepatoma-derived growth factor for malignant glioma treatment. *J. Control. Release* **310**, 24–35 (2019).

102. Säälik, P. *et al.* Peptide-guided nanoparticles for glioblastoma targeting. *J. Control. Release* **308**, 109–118 (2019).

103. Schwendeman, S. P. A local combination therapy to inhibit GBM recurrence. *J. Control. Release* **309**, 339–340 (2019).

104. Lakkadwala, S., dos Santos Rodrigues, B., Sun, C. & Singh, J. Dual functionalized liposomes for efficient co-delivery of anti-cancer chemotherapeutics for the treatment of glioblastoma. *J. Control. Release* **307**, 247–260 (2019).

105. Papachristodoulou, A. *et al.* Chemotherapy sensitization of glioblastoma by focused ultrasound-mediated delivery of therapeutic liposomes. *J. Control. Release* **295**, 130–139 (2019).

106. Khan, A. R., Yang, X., Fu, M. & Zhai, G. Recent progress of drug nanoformulations targeting to brain. *Journal of Controlled Release* **291**, 37–64 (2018).

107. Zhang, Y. *et al.* Cell-permeable NF-κB inhibitor-conjugated liposomes for treatment of glioma. *J. Control. Release* **289**, 102–113 (2018).

108. Ganipineni, L. P., Danhier, F. & Préat, V. Drug delivery challenges and future of chemotherapeutic nanomedicine for glioblastoma treatment. *Journal of Controlled Release* **281**, 42–57 (2018).

109. Lee Ventola, C. The Nanomedicine Revolution, Part 1: Emerging Concepts. **37**, (2012).

110. Bertrand, N., Wu, J., Xu, X., Kamaly, N. & Farokhzad, O. C. Cancer nanotechnology: The impact of passive and active targeting in the era of modern cancer biology. *Adv. Drug Deliv. Rev.* **66**, 2–25 (2014).

111. Wilhelm, S. *et al.* Analysis of nanoparticle delivery to tumours. *Nature Reviews Materials* **1**, (2016).

112. Hansch, C., Rockwell, S. D., Jow, P. Y. C., Leo, A. & Steller, E. E. Substituent Constants for Correlation Analysis. *Journal of Medicinal Chemistry* **20**, 304–306 (1977).

113. Tamargo, R. J. & Brem, H. Drug delivery to the central nervous system: A review. *Neurosurgery Quarterly* **2**, 259–279 (1992).

114. Pardridge, W. M. Blood-brain barrier delivery. *Drug Discov. Today* **12**, (2007).

115. Shen, D. D., Artru, A. A. & Adkison, K. K. Principles and applicability of CSF sampling for the assessment of CNS drug delivery and pharmacodynamics. *Adv. Drug Deliv. Rev.* **56**, 1825–1857 (2004).

116. Klibanov, A. L., Maruyama, K., Torchilin, V. P. & Huang, L. Amphipathic polyethyleneglycols effectively prolong the circulation time of liposomes. *FEBS Lett.* **268**, 235–7 (1990).

117. Meng, Y. *et al.* Safety and efficacy of focused ultrasound induced blood-brain barrier opening, an integrative review of animal and human studies. *Journal of Controlled Release* **309**, 25–36 (2019).

118. Cohen-Inbar, O., Xu, Z. & Sheehan, J. P. Focused ultrasound-aided immunomodulation in glioblastoma multiforme: A therapeutic concept. *Journal of Therapeutic Ultrasound* **4**, (2016).

119. Lin, Y.-J., Chen, K.-T., Huang, C.-Y. & Wei, K.-C. Non-invasive focused ultrasound-based synergistic treatment of brain tumors. *J. Cancer Res. Pract.* **3**, 63–68 (2016).

120. Mross, K. *et al.* A phase I clinical and pharmacokinetic study of the camptothecin glycoconjugate, BAY 38-3441, as a daily infusion in patients with advanced solid tumors. *Ann. Oncol.* **15**, 1284–1294 (2004).

121. Householder, K. T. *et al.* Intravenous delivery of camptothecin-loaded PLGA nanoparticles for the treatment of intracranial glioma. *Pharm. Nanotechnol.* (2015). doi:10.1016/j.ijpharm.2015.01.002

122. Wohlfart, S. *et al.* Efficient Chemotherapy of Rat Glioblastoma Using Doxorubicin-Loaded PLGA Nanoparticles with Different Stabilizers. *PLoS One* **6**, e19121 (2011).

123. Jiang, X. *et al.* PEGylated poly(trimethylene carbonate) nanoparticles loaded with paclitaxel for the treatment of advanced glioma: In vitro and in vivo evaluation. *Int. J. Pharm.* **420**, 385–394 (2011).

124. Weksler, B., Romero, I. A. & Couraud, P.-O. The hCMEC/D3 cell line as a model of the human blood brain barrier. *Fluids Barriers CNS* **10**, 16 (2013).

125. Battaglia, L. *et al.* Bevacizumab loaded solid lipid nanoparticles prepared by the coacervation technique: preliminary *in vitro* studies. *Nanotechnology* **26**, 255102 (2015).

126. Battaglia, L. *et al.* Solid Lipid Nanoparticles for Potential

Doxorubicin Delivery in Glioblastoma Treatment: Preliminary In Vitro Studies. *J. Pharm. Sci.* **103**, 2157–2165 (2014).

127. Kuo, Y.-C. & Chao, I.-W. Conjugation of melanotransferrin antibody on solid lipid nanoparticles for mediating brain cancer malignancy. *Biotechnol. Prog.* **32**, 480–490 (2016).

128. Kim, K. J. *et al.* Inhibition of vascular endothelial growth factor-induced angiogenesis suppresses tumour growth in vivo. *Nature* **362**, 841–844 (1993).

129. Knizetova, P. *et al.* Autocrine regulation of glioblastoma cell-cycle progression, viability and radioresistance through the VEGF-VEGFR2 (KDR) interplay. *Cell Cycle* **7**, 2553–2561 (2008).

130. Oehring, R. D. *et al.* Vascular endothelial growth factor (VEGF) in astrocytic gliomas - A prognostic factor? *J. Neurooncol.* **45**, 117–125 (1999).

131. Elkstrand, A.J., James, C.D., Cavanee W.K., Seliger, B., Pettersson, R.F. and Collins, V. P. Genes for Epidermal Growth Factor Receptor, Transforming Growth Factor a, and Epidermal Growth Factor and Their Expression in Human Gliomas in Vivo. *Cancer Res.* **51**, 2164–2172 (1991).

132. Nilewski, L. G., Singh, M., Baskin, D. S., Tour, J. M. & Sharpe, M. A. Transfer of Dyes and Drugs into Cells Using EGFR-Targeted Nanosyringes. (2017). doi:10.1021/acschemneuro.7b00138

133. Macdiarmid, J. A. *et al.* Targeted Doxorubicin Delivery to Brain Tumors via Minicells: Proof of Principle Using Dogs with Spontaneously Occurring Tumors as a Model. (2016). doi:10.1371/journal.pone.0151832

134. Mortensen, J. H. *et al.* Targeted antiepidermal growth factor receptor (cetuximab) immunoliposomes enhance cellular uptake in vitro and exhibit increased accumulation in an intracranial model of glioblastoma multiforme. *J. Drug Deliv.* **2013**, 209205 (2013).

135. A Study to Evaluate the Safety, Tolerability and Immunogenicity of EGFR(V)-EDV-Dox in Subjects With Recurrent Glioblastoma Multiforme (GBM). Available at: https://clinicaltrials.gov/ct2/show/NCT02766699. (Accessed: 17th June 2019)

136. Ramalho, M. J. *et al.* Receptor-mediated PLGA nanoparticles for glioblastoma multiforme treatment. *Int. J. Pharm.* **545**, 84–92 (2018).

137. Bu, G., Maksymovitch, E. A., Geuze, H. & Schwartz, A. L. Subcellular localization and endocytic function of low density lipoprotein receptor-related protein in human glioblastoma cells. *J. Biol. Chem.* **269**, 29874–82 (1994).

138. Yamamoto, M. *et al.* Increased expression of low density lipoprotein receptor-related protein/alpha2-macroglobulin receptor in human malignant astrocytomas. *Cancer Res.* **57**, 2799–805 (1997).

139. Maletínská, L. *et al.* Human glioblastoma cell lines: levels of low-density lipoprotein receptor and low-density lipoprotein receptor-related protein. *Cancer Res.* **60**, 2300–3 (2000).

140. Jefferies, W. A. *et al.* Transferrin receptor on endothelium of brain capillaries. *Nature* **312**, 162–3 (1984).

141. Ahmed, S., Vepuri, S. B., Kalhapure, R. S. & Govender, T. Interactions of dendrimers with biological drug targets: reality or mystery-a gap in drug delivery and development research. *Biomater. Sci* **4**, 1032 (2016).

142. Kageyama, T. *et al.* The 4F2hc/LAT1 complex transports L-DOPA across the blood-brain barrier. *Brain Res.* **879**, 115–121 (2000).

143. Duelli, R., Enerson, B. E., Gerhart, D. Z. & Drewes, L. R. Expression of large amino acid transporter LAT1 in rat brain endothelium. *J. Cereb. Blood Flow Metab.* **20**, 1557–1562 (2000).

144. Kharya, P. *et al.* Phenylalanine-coupled solid lipid nanoparticles for brain tumor targeting. *J Nanopart Res* **15**, 2022–2026 (2013).

145. Hare, J. I. *et al.* Challenges and strategies in anti-cancer nanomedicine development: An industry perspective. *Advanced Drug Delivery Reviews* **108**, 25–38 (2017).

146. Xin, H. *et al.* Anti-glioblastoma efficacy and safety of paclitaxel-loading Angiopep-conjugated dual targeting PEG-PCL nanoparticles. *Biomaterials* **33**, 8167–8176 (2012).

147. Kang, T. *et al.* Enhancing Glioblastoma-Specific Penetration by Functionalization of Nanoparticles with an Iron-Mimic Peptide Targeting Transferrin/Transferrin Receptor Complex. *Mol. Pharm.* **12**, 2947–2961 (2015).

148. Kim, S.-S. *et al.* Encapsulation of temozolomide in a tumor-targeting nanocomplex enhances anti-cancer efficacy and reduces toxicity in a mouse model of glioblastoma. (2015). doi:10.1016/j.canlet.2015.08.022

149. Bhunia, S. *et al.* Large Amino Acid Transporter 1 Selective Liposomes of L-DOPA Functionalized Amphiphile for Combating Glioblastoma. *Mol. Pharm.* **14**, 3834–3847 (2017).

150. Kuo, Y.-C. & Lee, C.-H. Dual targeting of solid lipid nanoparticles grafted with 83-14 MAb and anti-EGF receptor for malignant brain tumor therapy. (2016). doi:10.1016/j.lfs.2016.01.025

151. Kuo, Y. C. & Chen, Y. C. Targeting delivery of etoposide to inhibit the growth of human glioblastoma multiforme using lactoferrin- and folic acid-grafted poly(lactide-co-glycolide) nanoparticles. *Int. J. Pharm.* **479**, 138–149 (2015).

152. Kuo, Y.-C. & Cheng, S.-J. Brain targeted delivery of carmustine using solid lipid nanoparticles modified with tamoxifen and lactoferrin for antitumor proliferation. *Int. J. Pharm.* **499**, 10–19 (2016).

153. Prabhu, S. *et al.* A polymeric temozolomide nanocomposite against orthotopic glioblastoma xenograft: tumor-specific homing directed by nestin. *Nanoscale* **9**, 10919 (2017).

154. Kim, J. S., Shin, H. & Kim, J.-S. Dual-targeting immunoliposomes using angiopep-2 and CD133 antibody for glioblastoma stem cells. *J. Control. Release* **269**, 245–257 (2018).

155. Gao, J.-Q. *et al.* Glioma targeting and blood-brain barrier penetration by dual-targeting doxorubincin liposomes. *Biomaterials* **34**, 5628–5639 (2013).

156. Porru, M. *et al.* Medical treatment of orthotopic glioblastoma with transferrin-conjugated nanoparticles encapsulating zoledronic acid. *Oncotarget* **5**, 10446–59 (2014).

157. Nance, E. *et al.* Brain-Penetrating Nanoparticles Improve Paclitaxel Efficacy in Malignant Glioma Following Local Administration. (2014). doi:10.1021/nn504210g

158. Nance, E. A. *et al.* A Dense Poly(ethylene glycol) Coating Improves Penetration of Large Polymeric Nanoparticles within Brain Tissue. doi:10.1126/scitranslmed.3003594

159. Thorne, R. G. & Nicholson, C. In vivo diffusion analysis with quantum dots and dextrans predicts the width of brain extracellular space. *Proc. Natl. Acad. Sci. USA* **103**, 5567–5572 (2006).

160. Suk, J. S., Xu, Q., Kim, N., Hanes, J. & Ensign, L. M. PEGylation as a strategy for improving nanoparticle-based drug and gene delivery. *Advanced Drug Delivery Reviews* **99**, 28–51 (2016).

161. Fourniols, T. *et al.* Temozolomide-loaded photopolymerizable PEG-DMA-based hydrogel for the treatment of glioblastoma. *J. Control. Release* **210**, (2015).

162. Zhao, M. *et al.* Post-resection treatment of glioblastoma with an injectable nanomedicine-loaded photopolymerizable hydrogel induces long-term survival. *Int. J. Pharm.* **548**, 522–529 (2018).

163. Danhier, F. *et al.* Novel self-assembling PEG-p-(CL-co-TMC) polymeric micelles as safe and effective delivery system for Paclitaxel. *Eur. J. Pharm. Biopharm.* **73**, 230–238 (2009).

164. Danhier, F. *et al.* Paclitaxel-loaded micelles enhance transvascular permeability and retention of nanomedicines in tumors. *Int. J. Pharm.* **479**, 399–407 (2015).

165. Nuyken, O. & Pask, S. D. Ring-opening polymerization-An introductory review. *Polymers (Basel).* **5**, 361–403 (2013).

166. Fontaine, L. Handbook of Ring-Opening Polymerization. Edited by Philippe Dubois, Olivier Coulembier and Jean-Marie Raquez. *Angew. Chemie Int. Ed.* **48**, 9780–9780 (2009).

167. Cameron, D. J. A. & Shaver, M. P. Aliphatic polyester polymer stars: Synthesis, properties and applications in biomedicine and nanotechnology. *Chemical Society Reviews* **40**, 1761–1776 (2011).

168. Jérôme, C. & Lecomte, P. Recent advances in the synthesis of aliphatic polyesters by ring-opening polymerization. *Adv. Drug Deliv. Rev.* **60**, 1056–1076 (2008).

169. Kamber, N. E. *et al.* Organocatalytic Ring-Opening Polymerization. *Chem. Rev.* **107**, 5813–5840 (2007).

170. Tempelaar, S., Mespouille, L., Coulembier, O., Dubois, P. & Dove, A. P. Synthesis and post-polymerisation modifications of aliphatic poly(carbonate)s prepared by ring-opening polymerisation. *Chem. Soc. Rev* **42**, 1312 (2013).

171. Pounder, R. J. & Dove, A. P. Synthesis and organocatalytic ring-opening polymerization of cyclic esters derived from l-malic acid. *Biomacromolecules* **11**, 1930–1939 (2010).

172. Nederberg, F. *et al.* New ground for organic catalysis: A ring-opening polymerization approach to hydrogels. *Biomacromolecules* **8**, 3294–3297 (2007).

173. Du Boullay, O. T., Saffon, N., Diehl, J. P., Martin-Vaca, B. & Bourissou, D. Organo-catalyzed ring opening polymerization of a 1,4-dioxane-2,5-dione deriving from glutamic acid. *Biomacromolecules* **11**, 1921–1929 (2010).

174. Pounder, R. J. & Dove, A. P. Towards poly(ester) nanoparticles: Recent advances in the synthesis of functional poly(ester)s by ring-opening polymerization. *Polymer Chemistry* **1**, 260–271 (2010).

175. Dove, A. P., Gibson, V. C., Marshall, E. L., White, A. J. P. & Williams, D. J. A well defined tin(II) initiator for the living polymerisation of lactide. *Chem. Commun.* 283–284 (2001). doi:10.1039/b008770j

176. Degée, P., Dubois, P., Jérŏme, R., Jacobsen, S. & Fritz, H.-G. New catalysis for fast bulk ring-opening polymerization of lactide monomers. *Macromol. Symp.* **144**, 289–302 (1999).

177. Naumann, S. & Dove, A. P. N-Heterocyclic carbenes for metal-free polymerization catalysis: an update. *Polym. Int.* **65**, 16–27 (2016).

178. Connor, E. F., Nyce, G. W., Myers, M., Ck, A. M. & Hedrick, J. L. First Example of N-Heterocyclic Carbenes as Catalysts for Living

Polymerization: Organocatalytic Ring-Opening Polymerization of Cyclic Esters. *J Am Chem Soc* **124**, (2002).

179. Russell C. Pratt, †, Bas G. G. Lohmeijer, †, David A. Long, ‡, Robert M. Waymouth, *,§ and & James L. Hedrick*, †. Triazabicyclodecene: A Simple Bifunctional Organocatalyst for Acyl Transfer and Ring-Opening Polymerization of Cyclic Esters. (2006). doi:10.1021/JA060662+

180. Simón, L. & Goodman, J. M. The Mechanism of TBD-Catalyzed Ring-Opening Polymerization of Cyclic Esters. *J Org Chem* **72**, 9656–9662 (2007).

181. Naumann, S., Scholten, P. B. V, Wilson, J. A. & Dove, A. P. Dual Catalysis for Selective Ring-Opening Polymerization of Lactones: Evolution toward Simplicity. *J Am Chem Soc* **137**, 14439–14445 (2015).

182. Hortobdgyi, G. N. *Anthracyclines in the Treatment of Cancer An Overview*. *Drugs* **54**, (1997).

183. Froelich-Ammon, S. J. & Osheroff, N. Topoisomerase poisons: Harnessing the dark side of enzyme mechanism. *Journal of Biological Chemistry* **270**, 21429–21432 (1995).

184. Gewirtz, D. A. A critical evaluation of the mechanisms of action proposed for the antitumor effects of the anthracycline antibiotics adriamycin and daunorubicin. *Biochem. Pharmacol.* **57**, 727–741 (1999).

185. Tewey, K., Rowe, T., Yang, L., Halligan, B. & Liu, L. Adriamycin-Induced DNA Damage Mediated by Mammalian DNA Topoisomerase II. *Science (80-.).* **226**, 466–468 (1983).

186. Liu, L. F., Rowe, T. C., Yang, L., Tewey, K. M. & Chen, G. L. Cleavage of DNA by mammalian DNA topoisomerase II. *J. Biol. Chem.* **258**, 15365–15370 (1983).

187. Munger, C. *et al.* Evidence for Inhibition of Growth Related to Compromised DNA Synthesis in the Interaction of Daunorubicin with H-35 Rat Hepatoma. *Cancer Res.* **48**, 2404–2411 (1988).

188. Di Marco, A., Silvestrini, R., Di Marco, S. & Dasdia, T. Inhibiting

effect of the new cytotoxic antibiotic daunomycin on nucleic acids and mitotic activity of HeLa cells. *J. Cell Biol.* **27**, 545–550 (1965).

189. Feinstein, E., Canaani, E. & Weiner, L. M. Dependence of Nucleic Acid Degradation on in Situ Free-Radical Production by Adriamycin. *Biochemistry* **32**, 13156–13161 (1993).

190. Cutts, S., Nudelman, A., Rephaeli, A. & Phillips, D. The Power and Potential of Doxorubicin-DNA Adducts. *IUBMB Life (International Union Biochem. Mol. Biol. Life)* **57**, 73–81 (2005).

191. Cutts, S. M., Swift, L. P., Rephaeli, A., Nudelman, A. & Phillips, D. R. Recent advances in understanding and exploiting the activation of anthracyclines by formaldehyde. *Current Medicinal Chemistry - Anti-Cancer Agents* **5**, 431–447 (2005).

192. Hasegawa, S. *et al.* Possible involvement of multidrug-resistance-associated protein (MRP) gene expression in spontaneous drug resistance to vincristine, etoposide and adriamycin in human glioma cells. *Int. J. Cancer* **58**, 860–864 (1994).

193. Darling, J. L. & Thomas, D. G. T. Response of short-term cultures derived from human malignant glioma to aziridinylbenzoquinone, etoposide and doxorubicin: An in vitro phase II trial. *Anticancer. Drugs* **12**, 753–760 (2001).

194. Stan, A. C., Casares, S., Radu, D., Walter, G. F. & Brumeanu, T. D. Doxorubicin-induced cell death in highly invasive human gliomas. *Anticancer Res.* **19**, 941–950 (1999).

195. Wolff, J. E. A., Trilling, T., Mölenkamp, G., Egeler, R. M. & Jürgens, H. Chemosensitivity of glioma cells in vitro: A meta analysis. *Journal of Cancer Research and Clinical Oncology* **125**, 481–486 (1999).

196. Lin, R., Ng, L. S. & Wang, C. H. In vitro study of anticancer drug doxorubicin in PLGA-based microparticles. *Biomaterials* **26**, 4476–4485 (2005).

197. Pang, Z. *et al.* Enhanced intracellular delivery and chemotherapy for glioma rats by transferrin-conjugated biodegradable polymersomes loaded with doxorubicin. *Bioconjug. Chem.* **22**, 1171–1180 (2011).

198. Pang, Z. *et al.* Lactoferrin-conjugated biodegradable polymersome holding doxorubicin and tetrandrine for chemotherapy of glioma rats. *Mol. Pharm.* **7**, 1995–2005 (2010).

199. Arai, T. *et al.* Novel local drug delivery system using thermoreversible gel in combination with polymeric microspheres or liposomes. *Anticancer Res.* **30**, 1057–1064 (2010).

200. Manome, Y. *et al.* Local delivery of doxorubicin for malignant glioma by a biodegradable PLGA polymer sheet. *Anticancer Res.* **26**, 3317–3326 (2006).

201. Vinchon-Petit, S. *et al.* Local implantation of doxorubicin drug eluting beads in rat glioma. *Int. J. Pharm.* **402**, 184–189 (2010).

202. Sewing, A. C. P. *et al.* Preclinical evaluation of convection-enhanced delivery of liposomal doxorubicin to treat Pediatric diffuse intrinsic pontine glioma and thalamic high-grade glioma. *J. Neurosurg. Pediatr.* **19**, 518–530 (2017).

203. Mamot, C. *et al.* Epidermal growth factor receptor (EGFR)-targeted immunoliposomes mediate specific and efficient drug delivery to EGFR- and EGFRvIII-overexpressing tumor cells. *Women's Oncol. Rev.* **4**, 101–103 (2004).

204. Muldoon, L. L. & Neuwelt, E. A. BR96-DOX immunoconjugate targeting of chemotherapy in brain tumor models. *J. Neurooncol.* **65**, 49–62 (2003).

205. Pavillard, V., Kherfellah, D., Richard, S., Robert, J. & Montaudon, D. Effects of the combination of camptothecin and doxorubicin or etoposide on rat glioma cells and camptothecin-resistant variants. *Br. J. Cancer* **85**, 1077–1083 (2001).

206. Saito, R. *et al.* Distribution of Liposomes into Brain and Rat Brain Tumor Models by Convection-Enhanced Delivery Monitored with Magnetic Resonance Imaging. *Cancer Res.* **64**, 2572–2579 (2004).

207. Saul, J. M., Annapragada, A., Natarajan, J. V. & Bellamkonda, R. V. Controlled targeting of liposomal doxorubicin via the folate receptor in vitro. *J. Control. Release* **92**, 49–67 (2003).

208. Steiniger, S. C. J. *et al.* Chemotherapy of glioblastoma in rats using doxorubicin-loaded nanoparticles. *Int. J. Cancer* **109**, 759–767 (2004).

209. Lesniak, M. S., Upadhyay, U., Goodwin, R., Tyler, B. & Brem, H. Local delivery of doxorubicin for the treatment of malignant brain tumors in rats. *Anticancer Res.* **25**, 3825–3831 (2005).

210. Guo, L. *et al.* TRAIL and doxorubicin combination enhances anti-glioblastoma effect based on passive tumor targeting of liposomes. *J. Control. Release* **154**, 93–102 (2011).

211. Voulgaris, S. *et al.* Intratumoral doxorubicin in patients with malignant brain gliomas. *Am. J. Clin. Oncol.* **25**, 60–4 (2002).

212. Hau, P. *et al.* Pegylated liposomal doxorubicin-efficacy in patients with recurrent high-grade glioma. *Cancer* **100**, 1199–1207 (2004).

213. Beier, C. P. *et al.* RNOP-09: Pegylated liposomal doxorubicine and prolonged temozolomide in addition to radiotherapy in newly diagnosed glioblastoma - a phase II study. *BMC Cancer* **9**, 308 (2009).

214. Barenholz, Y. Doxil® - The first FDA-approved nano-drug: Lessons learned. *J. Control. Release* **160**, 117–134 (2012).

215. Hanna, A. D., Lam, A., Tham, S., Dulhunty, A. F. & Beard, N. A. Adverse effects of doxorubicin and its metabolic product on cardiac RyR2 and SERCA2A. *Mol. Pharmacol.* **86**, 438–449 (2014).

216. Bigotte, L. & Olsson, Y. Cytofluorescence localization of adriamycin in the nervous system. III. Distribution of the drug in the brain of normal adult mice after intraventricular and arachnoidal injections. *Acta Neuropathol.* **58**, 193–202 (1982).

217. Tangpong, J. *et al.* Adriamycin-induced, TNF-α-mediated central nervous system toxicity. *Neurobiol. Dis.* **23**, 127–139 (2006).

218. Merker, P. C., Lewis, M. R., Walker, M. D. & Richardson, E. P. Neurotoxicity of adriamycin (Doxorubicin) perfused through the cerebrospinal fluid spaces of the rhesus monkey. *Toxicol. Appl. Pharmacol.* **44**, 191–205 (1978).

219. Neuwelt, E. A., Pagel, M., Glassberg, M. & Frenkel, E. P. Pharmacology and toxicity of intracarotid adriamycin administration following osmotic blood-brain barrier modification. *Cancer Res.* **41**, 4466–4470 (1981).

220. Almubarak, M., Newton, M. & Altaha, R. Reinduction of Bevacizumab in Combination with Pegylated Liposomal Doxorubicin in a Patient with Recurrent Glioblastoma Multiforme Who Progressed on Bevacizumab/Irinotecan. *J. Oncol.* (2008). doi:10.1155/2008/942618

221. Kikuchi, T. *et al.* Convection-enhanced delivery of polyethylene glycol-coated liposomal doxorubicin: Characterization and efficacy in rat intracranial glioma models: Laboratory investigation. *J. Neurosurg.* **109**, 867–873 (2008).

222. Cheng, Y. *et al.* Nanoparticle-programmed self-destructive neural stem cells for glioblastoma targeting and therapy. *Small* **9**, 4123–4129 (2013).

223. Chen, H. *et al.* Lactoferrin modified doxorubicin-loaded procationic liposomes for the treatment of gliomas. in *European Journal of Pharmaceutical Sciences* **44**, 164–173 (Elsevier, 2011).

224. Qin, Y. *et al.* Liposome formulated with TAT-modified cholesterol for improving brain delivery and therapeutic efficacy on brain glioma in animals. *Int. J. Pharm.* **420**, 304–312 (2011).

225. Baltes, S., Freund, I., Lewis, A. L., Nolte, I. & Brinker, T. Doxorubicin and irinotecan drug-eluting beads for treatment of glioma: A pilot study in a rat model. *J. Mater. Sci. Mater. Med.* **21**, 1393–1402 (2010).

226. Chaichana, K. L., Pinheiro, L. & Brem, H. Delivery of local therapeutics to the brain: working toward advancing treatment for malignant gliomas. *Ther. Deliv.* **6**, 353–69 (2015).

227. Ommaya, A. K. Subcutaneous reservoir and pump for sterile access to ventricular cerebrospinal fluid. *Lancet* **282**, 983–4 (1963).

228. Malinovskaya, Y. *et al.* Delivery of doxorubicin-loaded PLGA nanoparticles into U87 human glioblastoma cells. *Int. J. Pharm.* **524**, 77–90 (2017).

229. Kreuter, J. Nanoparticulate systems for brain delivery of drugs. *Adv. Drug Deliv. Rev.* **64**, 213–222 (2012).

230. Gelperina, S. *et al.* Drug delivery to the brain using surfactant-coated poly(lactide-co-glycolide) nanoparticles: Influence of the formulation parameters. *Eur. J. Pharm. Biopharm.* **74**, 157–163 (2010).

231. Wohlfart, S. *et al.* Efficient Chemotherapy of Rat Glioblastoma Using Doxorubicin-Loaded PLGA Nanoparticles with Different Stabilizers. *PLoS One* **6**, e19121 (2011).

232. Geldenhuys, W., Wehrung, D., Groshev, A., Hirani, A. & Sutariya, V. Brain-targeted delivery of doxorubicin using glutathione-coated nanoparticles for brain cancers. *Pharm. Dev. Technol.* **20**, 497–506 (2015).

233. Fabel, K. *et al.* Long-term stabilization in patients with malignant glioma after treatment with liposomal doxorubicin. *Cancer* **92**, 1936–1942 (2001).

234. Doxil - Drug Information - Chemocare. Available at: http://chemocare.com/chemotherapy/drug-info/doxil.aspx. (Accessed: 1st May 2020)

235. Harris, L. *et al.* Liposome-encapsulated doxorubicin compared with conventional doxorubicin in a randomized multicenter trial as first-line therapy of metastatic breast carcinoma. *Cancer* **94**, 25–36 (2002).

236. Ranson, M. R. *et al.* Treatment of advanced breast cancer with sterically stabilized liposomal doxorubicin: Results of a multicenter phase II trial. *J. Clin. Oncol.* **15**, 3185–3191 (1997).

237. Siegal, T., Horowitz, A. & Gabizon, A. Doxorubicin encapsulated in sterically stabilized liposomes for the treatment of a brain tumor model: Biodistribution and therapeutic efficacy. *J. Neurosurg.* **83**, 1029–1037 (1995).

238. Cabanes, A., Tzemach, D., Goren, D., Horowitz, A. T. & Gabizon, A. Comparative study of the antitumor activity of free doxorubicin and polyethylene glycol-coated liposomal doxorubicin in a mouse lymphoma model. *Clin. Cancer Res.* **4**, 499–505 (1998).

239. Gao, Y. *et al.* Predictive models of diffusive nanoparticle transport in 3-dimensional tumor cell spheroids. *AAPS J.* **15**, 816–831 (2013).

240. Pelaz, B. *et al.* Surface Functionalization of Nanoparticles with Polyethylene Glycol: Effects on Protein Adsorption and Cellular Uptake. *ACS Nano* **9**, 6996–7008 (2015).

241. Callari, M. *et al.* Drug induced self-assembly of triblock copolymers into polymersomes for the synergistic dual-drug delivery of platinum drugs and paclitaxel. *Polym. Chem.* **8**, 6289–6299 (2017).

242. Duncan, R. Polymer therapeutics at a crossroads? Finding the path for improved translation in the twenty-first century. *J. Drug Target.* **25**, 759–780 (2017).

243. Ferrari, R., Sponchioni, M., Morbidelli, M. & Moscatelli, D. Polymer nanoparticles for the intravenous delivery of anticancer drugs: the checkpoints on the road from the synthesis to clinical translation. *Nanoscale* **10**, 22701 (2018).

244. Ko, J. H. & Maynard, H. D. A guide to maximizing the therapeutic potential of protein-polymer conjugates by rational design. *Chem. Soc. Rev.* **47**, 8998–9014 (2018).

245. Duncan, R. Polymer therapeutics: Top 10 selling pharmaceuticals — What next? *J. Control. Release* **190**, 371–380 (2014).

246. Ahmed, S., Vepuri, S. B., Kalhapure, R. S. & Govender, T. Biomaterials Science REVIEW Interactions of dendrimers with biological drug targets: reality or mystery-a gap in drug delivery and development research. *Cite this Biomater. Sci* **4**, 1032 (2016).

247. Shim, G., Kim, M.-G., Kim, D., Park, J. Y. & Oh, Y.-K. Nanoformulation-based sequential combination cancer therapy. *Adv. Drug Deliv. Rev.* **115**, 57–81 (2017).

248. Wagner, H. J., Sprenger, A., Rebmann, B. & Weber, W. Upgrading biomaterials with synthetic biological modules for advanced medical applications. *Adv. Drug Deliv. Rev.* **105**, 77–95 (2016).

249. Fan, X., Li, Z. & Loh, X. J. Recent development of unimolecular micelles as functional materials and applications. *Polym. Chem.* **7**,

5898 (2016).

250. Duncan, R. & Gaspar, R. Nanomedicine(s) under the Microscope. *Mol. Pharm.* **8**, 2101–2141 (2011).

251. Gaspar, R. & Duncan, R. Polymeric carriers: Preclinical safety and the regulatory implications for design and development of polymer therapeutics. *Adv. Drug Deliv. Rev.* **61**, 1220–1231 (2009).

252. Arias, V., Olsén, P., Odelius, K., Höglund, A. & Albertsson, A.-C. Selective degradation in aliphatic block copolyesters by controlling the heterogeneity of the amorphous phase. *Polym. Chem* **6**, 3271 (2015).

253. Dailey, L. A., Wittmar, M. & Kissel, T. The role of branched polyesters and their modifications in the development of modern drug delivery vehicles. *J. Control. Release* **101**, 137–149 (2005).

254. Yu, K. *et al.* Comparison of three different conjugation strategies in the construction of herceptin-bearing paclitaxel-loaded nanoparticles. *Cite this Biomater. Sci* **4**, 1219 (2016).

255. Yin, Q., Tong, R., Yin, L., Fan, T. M. & Cheng, J. Anticancer camptothecin-N-poly(lactic acid) nanoconjugates with facile hydrolysable linker †. (2014). doi:10.1039/c3py01245j

256. Kasperczyk, J., Li, S., Jaworska, J., Dobrzyński, P. & Vert, M. Degradation of copolymers obtained by ring-opening polymerization of glycolide and ε-caprolactone: A high resolution NMR and ESI-MS study. *Polym. Degrad. Stab.* **93**, 990–999 (2008).

257. Danhier, F. *et al.* PLGA-based nanoparticles: An overview of biomedical applications. *J. Control. Release* **161**, 505–522 (2012).

258. Werner, M. E. *et al.* Preclinical evaluation of genexol-pm, a nanoparticle formulation of paclitaxel, as a novel radiosensitizer for the treatment of non-small cell lung cancer. *Int. J. Radiat. Oncol. Biol. Phys.* **86**, 463–468 (2013).

259. Gerhardt, W. W. *et al.* Functional Lactide Monomers: Methodology and Polymerization. *Biomacromolecules* **7**, 1735 (2006).

260. Alla, A., Oxelbark, J., Rodríguez-Galán, A. & Muñoz-Guerra, S. Acylated and hydroxylated polyamides derived from L-tartaric acid. *Polymer (Guildf).* **46**, 2854–2861 (2005).

261. Lewitus, D. Y., Smith, K. L., Shain, W., Bolikal, D. & Kohn, J. The fate of ultrafast degrading polymeric implants in the brain. *Biomaterials* **32**, 5543–50 (2011).

262. Wilson, J. A., Hopkins, S. A., Wright, P. M. & Dove, A. P. Synthesis and Postpolymerization Modification of One-Pot Pentadecalactone Block-like Copolymers. *Biomacromolecules* **16**, 3191–3200 (2015).

263. Qian, H., Wohl, A. R., Crow, J. T., MacOsko, C. W. & Hoye, T. R. A strategy for control of 'random' copolymerization of lactide and glycolide: Application to synthesis of PEG- b -PLGA block polymers having narrow dispersity. *Macromolecules* **44**, 7132–7140 (2011).

264. Lohmeijer, B. G. G. *et al.* Guanidine and amidine organocatalysts for ring-opening polymerization of cyclic esters. *Macromolecules* **39**, 8574–8583 (2006).

265. Chin, W. *et al.* A macromolecular approach to eradicate multidrug resistant bacterial infections while mitigating drug resistance onset. *Nat. Commun.* **9**, 917 (2018).

266. Baroni, A. *et al.* TAD Click Chemistry on Aliphatic Polycarbonates: A First Step Toward Tailor-Made Materials. *Macromol. Rapid Commun.* **40**, 1800743 (2019).

267. Venkataraman, S., Veronica, N., Voo, Z. X., Hedrick, J. L. & Yang, Y. Y. 2-Amino-1,3-propane diols: a versatile platform for the synthesis of aliphatic cyclic carbonate monomers. *Polym. Chem.* **4**, 2945 (2013).

268. Qiu, Y., Song, C.-C., Zhang, M., Du, F.-S. & Li, Z.-C. Oxidation-Promoted Degradation of Aliphatic Poly(carbonate)s via Sequential 1,6-Elimination and Intramolecular Cyclization. *ACS Macro Lett.* **4**, 1220–1224 (2015).

269. Cheng, W. *et al.* A facile synthetic approach to a biodegradable polydisulfide MRI contrast agent. *J. Mater. Chem. B* **2**, 5295–5301 (2014).

270. Zielinska, A. & Nowak, I. Solid lipid nanoparticles and nanostructured lipid carriers as novel carriers for cosmetic ingredients. in *Nanobiomaterials in Galenic Formulations and Cosmetics: Applications of Nanobiomaterials* 231–255 (Elsevier Inc., 2016). doi:10.1016/B978-0-323-42868-2.00010-3

271. Stark, N. M., Yelle, D. J. & Agarwal, U. P. Techniques for Characterizing Lignin. in *Lignin in Polymer Composites* 49–66 (Elsevier Inc., 2016). doi:10.1016/B978-0-323-35565-0.00004-7

272. Alawam, K. Application of proteomics in diagnosis of ADHD, schizophrenia, major depression, and suicidal behavior. in *Advances in Protein Chemistry and Structural Biology* **95**, 283–315 (Academic Press Inc., 2014).

273. Gaffney, J. S., Marley, N. A. & Jones, D. E. Fourier Transform Infrared (FTIR) Spectroscopy. in *Characterization of Materials* 1–33 (John Wiley & Sons, Inc., 2012). doi:10.1002/0471266965.com107.pub2

274. Agilent Technologies Inc. *An Introduction to Gel Permeation Chromatography and Size Exclusion Chromatography*. *Primer* (2015).

275. Robinson, J. W. *Undergraduate instrumental analysis*. (Marcel Dekker, 2005).

276. Jin, W. *et al.* Nanoemulsions for food: properties, production, characterization, and applications. in *Emulsions* 1–36 (Elsevier, 2016). doi:10.1016/b978-0-12-804306-6.00001-5

277. Stetefeld, J., McKenna, S. A. & Patel, T. R. Dynamic light scattering: a practical guide and applications in biomedical sciences. *Biophysical Reviews* **8**, 409–427 (2016).

278. A basic introduction to Dynamic Light Scattering (DLS) for particle size analysis | Malvern Panalytical. Available at: https://www.malvernpanalytical.com/en/learn/events-and-training/webinars/W180201BasicDynamicLightScattering. (Accessed: 26th June 2020)

279. Malvern Instruments Ltd. Size theory. *Zetasizer Nano User Man.* **MAN0485**, 250 (2013).

280. Biondi, M., Guarnieri, D., Yu, H., Belli, V. & Netti, P. A. Sub-100 nm biodegradable nanoparticles: *in vitro* release features and toxicity testing in 2D and 3D cell cultures. *Nanotechnology* **24**, 045101 (2013).

281. Luan, B., Huynh, T. & Zhou, R. Nanopore-Based Sensors for Ligand-Receptor Lead Optimization. *J. Phys. Chem. Lett.* **6**, 331–7 (2015).

282. Luo, F. *et al.* Biodegradable and Thermosensitive Monomethoxy Poly(ethylene glycol)–Poly(lactic acid) Hydrogel as a Barrier for Prevention of Post-Operative Abdominal Adhesion. *J. Biomed. Nanotechnol.* **10**, 427–435 (2013).

283. Ananda, S. *et al.* Phase 2 trial of temozolomide and pegylated liposomal doxorubicin in the treatment of patients with glioblastoma multiforme following concurrent radiotherapy and chemotherapy. *J. Clin. Neurosci.* **18**, 1444–1448 (2011).

284. Lesniak, W. G. *et al.* Biodistribution of fluorescently labeled PAMAM dendrimers in neonatal rabbits: Effect of neuroinflammation. *Mol. Pharm.* **10**, 4560–4571 (2013).

285. Zhang, Q. *et al.* Aminoglycoside-based novel probes for bacterial diagnostic and therapeutic applications. *Chem. Commun.* **53**, 1366–1369 (2017).

286. Späte, A. K., Schart, V. F., Schöllkopf, S., Niederwieser, A. & Wittmann, V. Terminal Alkenes as Versatile Chemical Reporter Groups for Metabolic Oligosaccharide Engineering. *Chem. - A Eur. J.* **20**, 16502–16508 (2014).

287. Bishop, C. J., Tzeng, S. Y. & Green, J. J. Degradable polymer-coated gold nanoparticles for co-delivery of DNA and siRNA. *Acta Biomater.* **11**, 393–403 (2015).

288. Rabanel, J. M. *et al.* Effect of the polymer architecture on the structural and biophysical properties of PEG-PLA nanoparticles. *ACS Appl. Mater. Interfaces* **7**, 10374–10385 (2015).

289. Garofalo, C. *et al.* Different insight into amphiphilic PEG-PLA copolymers: Influence of macromolecular architecture on the micelle formation and cellular uptake. *Biomacromolecules* **15**, 403–415 (2014).

290. Kakde, D. *et al.* Amphiphilic block copolymers from a renewable ϵ-decalactone monomer: Prediction and characterization of micellar core effects on drug encapsulation and release. *J. Mater. Chem. B* **4**, 7119–7129 (2016).

291. Nasrollahzadeh, M., Atarod, M., Sajjadi, M., Sajadi, S. M. & Issaabadi, Z. Plant-Mediated Green Synthesis of Nanostructures: Mechanisms, Characterization, and Applications. in *Interface Science and Technology* **28**, 199–322 (Elsevier B.V., 2019).

292. Yang, N. J. . & Hinner, M. J. Getting Across the Cell Membrane: An Overview for Small Molecules, Peptides, and Proteins. *Methods Mol Biol.* 29–53 (2015). doi:10.1007/978-1-4939-2272-7

293. Chou, L. Y. T., Ming, K. & Chan, W. C. W. Strategies for the intracellular delivery of nanoparticles. *Chem. Soc. Rev* **40**, 233–245 (2011).

294. Zhang, R., Qin, X., Kong, F., Chen, P. & Pan, G. Improving cellular uptake of therapeutic entities through interaction with components of cell membrane. *Drug Deliv.* **26**, 328–342 (2019).

295. Zhao, J. & Stenzel, M. H. Entry of nanoparticles into cells: the importance of nanoparticle properties. *Polym. Chem* **9**, 259 (2018).

296. Kim, Y., Pourgholami, M. H., Morris, D. L., Lu, H. & Stenzel, M. H. Effect of shell-crosslinking of micelles on endocytosis and exocytosis: Acceleration of exocytosis by crosslinking. *Biomater. Sci.* **1**, 265–275 (2013).

297. Marsh, M. & Mcmahon, H. T. The Structural Era of Endocytosis. *Science (80-.).* **285**, 215–220 (1999).

298. Behzadi, S. *et al.* Cellular uptake of nanoparticles: journey inside the cell. *Chem. Soc. Rev* **46**, 4218–4244 (2017).

299. Carver, L. A. & Schnitzer, J. E. Caveolae: Mining little caves for new cancer targets. *Nature Reviews Cancer* **3**, 571–581 (2003).

300. Doherty, G. J. & McMahon, H. T. Mechanisms of endocytosis. *Annual Review of Biochemistry* **78**, 857–902 (2009).

301. Lu, Y. & Low, P. S. Folate-mediated delivery of macromolecular anticancer therapeutic agents. *Advanced Drug Delivery Reviews* **54**, 675–693 (2002).

302. Litwack, G. Membrane Transport. in *Human Biochemistry* 553–589 (Elsevier, 2018). doi:10.1016/b978-0-12-383864-3.00018-1

303. Oh, N. & Park, J. H. Endocytosis and exocytosis of nanoparticles in mammalian cells. *Int. J. Nanomedicine* **9**, 51–63 (2014).

304. Vasey, C. E. *et al.* Amphiphilic tri- and tetra-block co-polymers combining versatile functionality with facile assembly into cytocompatible nanoparticles. *Biomater. Sci.* (2019). doi:10.1039/c9bm00667b

305. Sodano, F. *et al.* Enhancing doxorubicin anticancer activity with a novel polymeric platform photoreleasing nitric oxide. *Biomater. Sci.* (2020). doi:10.1039/C9BM01644A

306. von Holst, H. *et al.* Uptake of Adriamycin in tumour and surrounding brain tissue in patients with malignant gliomas. *Acta Neurochir. (Wien).* **104**, 13–16 (1990).

307. Maksimenko, O. *et al.* Doxorubicin-loaded PLGA nanoparticles for the chemotherapy of glioblastoma: Towards the pharmaceutical development. *Int. J. Pharm.* **572**, 118733 (2019).

308. Lu, H. *et al.* Enhanced transcellular penetration and drug delivery by crosslinked polymeric micelles into pancreatic multicellular tumor spheroids. *Biomater. Sci.* **3**, 1085–1095 (2015).

309. Lu, M. *et al.* Importance of Polymer Length in Fructose-Based Polymeric Micelles for an Enhanced Biological Activity. *Macromolecules* **52**, 59 (2019).

310. Lu, H., Su, J., Mamdooh, R., Li, Y. & Stenzel, M. H. Cellular Uptake of Gold Nanoparticles and Their Movement in 3D Multicellular Tumor Spheroids: Effect of Molecular Weight and Grafting Density of Poly(2-hydroxyl ethyl acrylate). *Macromol. Biosci.* **20**, 1–11 (2020).

311. Lu, H. & Stenzel, M. H. Multicellular Tumor Spheroids (MCTS) as a 3D In Vitro Evaluation Tool of Nanoparticles. *Small* **14**, 1–26

(2018).

312. Lu, M. *et al.* Sugar Concentration and Arrangement on the Surface of Glycopolymer Micelles Affect the Interaction with Cancer Cells. *Biomacromolecules* **20**, 273–284 (2018).

313. Perrin, S. L. *et al.* Glioblastoma heterogeneity and the tumour microenvironment: implications for preclinical research and development of new treatments. *Biochem. Soc. Trans.* **47**, 625–638 (2019).

314. Petrecca, K., Guiot, M.-C., Panet-Raymond, V. & Souhami, L. Failure pattern following complete resection plus radiotherapy and temozolomide is at the resection margin in patients with glioblastoma. *J. Neurooncol.* **111**, 19–23 (2013).

315. Smith, S. J. *et al.* The Invasive Region of Glioblastoma Defined by 5ALA Guided Surgery Has an Altered Cancer Stem Cell Marker Profile Compared to Central Tumour. *Int. J. Mol. Sci.* **18**, 2452 (2017).

316. Greco, C. *et al.* Development of Pyrazolo[3,4-d]pyrimidine Kinase Inhibitors as Potential Clinical Candidates for Glioblastoma Multiforme. *ACS Med. Chem. Lett.* **0**, (2020).

317. Stoddart, M. J. Chapter 1 Cell Viability Assays: Introduction. in *Methods in Molecular Biology* **740**, 1–6 (Humana Press, 2011).

318. O'Brien, J., Wilson, I., Orton, T. & Pognan, F. Investigation of the Alamar Blue (resazurin) fluorescent dye for the assessment of mammalian cell cytotoxicity. *Eur. J. Biochem.* **267**, 5421–5426 (2000).

319. Czekanska, E. M. Chapter 5 Assessment of Cell Proliferation with Resazurin-Based Fluorescent Dye. in *Methods in Molecular Biology* **740**, 27–32 (Humana Press, 2011).

320. Xu, M., McCanna, D. J. & Sivak, J. G. Use of the viability reagent PrestoBlue in comparison with alamarBlue and MTT to assess the viability of human corneal epithelial cells. *J. Pharmacol. Toxicol. Methods* **71**, 1–7 (2015).

321. ThermoFisher Scientific. PrestoBlue™ Cell Viability Reagent.

Available at: https://www.thermofisher.com/order/catalog/product/A13261#/A13261. (Accessed: 26th March 2020)

322. Xia, W. *et al.* Angiogenin promotes U87MG cell proliferation by activating NF-κB signaling pathway and downregulating its binding partner FHL3. *PLoS One* **10**, (2015).

323. Ruan, C. *et al.* Substance P-modified human serum albumin nanoparticles loaded with paclitaxel for targeted therapy of glioma. *Acta Pharm. Sin. B* **8**, 85–96 (2018).

324. Rizk, S. S. *et al.* An engineered substance P variant for receptor-mediated delivery of synthetic antibodies into tumor cells. *Proc. Natl. Acad. Sci. U. S. A.* **106**, 11011–11015 (2009).

325. Jaworski, S. *et al.* Analysis of the cytotoxicity of hierarchical nanoporous graphenic carbon against human glioblastoma grade IV cells. *Int. J. Nanomedicine* **12**, 3839–3849 (2017).

326. Jaworski, S. *et al.* In vitro evaluation of the effects of graphene platelets on glioblastoma multiforme cells. *Int. J. Nanomedicine* **8**, 413–420 (2013).

327. Phan, H. *et al.* Role of self-assembly conditions and amphiphilic balance on nanoparticle formation of PEG-PDLLA copolymers in aqueous environments. *J. Polym. Sci. Part A Polym. Chem.* (2019). doi:10.1002/pola.29451

328. Pearce, A. K. *et al.* Functional polymers for drug delivery: Prospects and challenges. *Chim. Oggi/Chemistry Today* **36**, 38–42 (2018).

329. Nance, E. *et al.* Brain-penetrating nanoparticles improve paclitaxel efficacy in malignant glioma following local administration. *ACS Nano* **8**, 10655–10664 (2014).

330. Barhoum, A., García-Betancourt, M. L., Rahier, H. & Van Assche, G. Physicochemical characterization of nanomaterials: Polymorph, composition, wettability, and thermal stability. in *Emerging Applications of Nanoparticles and Architectural Nanostructures: Current Prospects and Future Trends* 255–278 (Elsevier Inc., 2018). doi:10.1016/B978-0-323-51254-1.00009-9

331. Nance, E. A. *et al.* A dense poly(ethylene glycol) coating improves penetration of large polymeric nanoparticles within brain tissue. *Sci. Transl. Med.* **4**, 149ra119-149ra119 (2012).

332. Erb, R. E. & Ehlers, M. H. Resazurin Reducing Time as an Indicator of Bovine Semen Fertilizing Capacity. *J. Dairy Sci.* **33**, 853–864 (1950).

333. Liu, Y. S., Chen, H. Y., Yeh, J. A. & Wang, L. F. Folate-mediated and doxorubicin-conjugated poly(ε-caprolactone)-g-chondroitin sulfate copolymers for enhanced intracellular drug delivery. *RSC Adv.* **4**, 59548–59557 (2014).

334. Han, J. *et al.* Rapid emergence and mechanisms of resistance by U87 glioblastoma cells to doxorubicin in an in vitro tumor microfluidic ecology. *Proc. Natl. Acad. Sci. U. S. A.* **113**, 14283–14288 (2016).

335. Heggannavar, G. B., Hiremath, C. G., Achari, D. D., Pangarkar, V. G. & Kariduraganavar, M. Y. Development of Doxorubicin-Loaded Magnetic Silica−Pluronic F-127 Nanocarriers Conjugated with Transferrin for Treating Glioblastoma across the Blood−Brain Barrier Using an in Vitro Model. (2018). doi:10.1021/acsomega.8b00152

336. Drug: Doxorubicin - Cancerrxgene - Genomics of Drug Sensitivity in Cancer. Available at: https://www.cancerrxgene.org/compound/Doxorubicin/133/overview/ic50?tissue=GBM&screening_set=GDSC1. (Accessed: 12th December 2020)

337. Taresco, V. *et al.* Functionalized Block Co-Polymer Pro-Drug Nanoparticles with Anti-Cancer Efficacy in 3D Spheroids and in an Orthotopic Triple Negative Breast Cancer Model. *Adv. Ther.* (2020). doi:10.1002/adtp.202000103

338. Aslantürk, Ö. S. In Vitro Cytotoxicity and Cell Viability Assays: Principles, Advantages, and Disadvantages. in *Genotoxicity - A Predictable Risk to Our Actual World* (InTech, 2018). doi:10.5772/intechopen.71923

339. Riss, T. L. *et al. Cell Viability Assays*. *Assay Guidance Manual* (Eli Lilly & Company and the National Center for Advancing Translational Sciences, 2004).

340. Munshi, A., Hobbs, M. & Meyn, R. E. Clonogenic cell survival assay. *Methods Mol. Med.* **110**, 21–28 (2005).

341. Franken, N. A. P., Rodermond, H. M., Stap, J., Haveman, J. & van Bree, C. Clonogenic assay of cells in vitro. *Nat. Protoc.* **1**, 2315–2319 (2006).

342. Chakrabarti, I., Cockburn, M., Cozen, W., Wang, Y.-P. & Preston-Martin, S. A population-based description of glioblastoma multiforme in Los Angeles County, 1974-1999. *Cancer* **104**, 2798–2806 (2005).

343. Blissitt, P. A. Clinical practice guideline series update. *Journal of Neuroscience Nursing* **46**, 367–368 (2014).

344. Schneider, L., Fumagalli, M. & Di Fagagna, F. D. A. Terminally differentiated astrocytes lack DNA damage response signaling and are radioresistant but retain DNA repair proficiency. *Cell Death Differ.* **19**, 582–591 (2012).

345. Hutchby, M. *et al.* Hindered ureas as masked isocyanates: Facile carbamoylation of nucleophiles under neutral conditions. *Angew. Chemie - Int. Ed.* **48**, 8721–8724 (2009).

346. Ying, H., Zhang, Y. & Cheng, J. Dynamic urea bond for the design of reversible and self-healing polymers. *Nat. Commun.* **5**, (2014).

347. Wang, Z. *et al.* Dynamic covalent urea bonds and their potential for development of self-healing polymer materials. *J. Mater. Chem. A* **7**, 15933–15943 (2019).

348. Hutchby, M. *et al.* Switching pathways: Room-temperature neutral solvolysis and substitution of amides. *Angew. Chemie - Int. Ed.* **51**, 548–551 (2012).

349. Rahman, C. V. *et al.* Controlled release of BMP-2 from a sintered polymer scaffold enhances bone repair in a mouse calvarial defect model. *J. Tissue Eng. Regen. Med.* **8**, 59–66 (2014).

350. Zhang, S. *et al.* Anti-tumour activity of low molecular weight heparin doxorubicin nanoparticles for histone H1 high-expressive prostate cancer PC-3M cells. *J. Control. Release* **295**, 102–117 (2019).

351. Mastria, E. M. *et al.* Doxorubicin-conjugated polypeptide nanoparticles inhibit metastasis in two murine models of carcinoma. *J. Control. Release* **208**, 52–58 (2015).

352. Andrew MacKay, J. *et al.* Self-assembling chimeric polypeptide-doxorubicin conjugate nanoparticles that abolish tumours after a single injection. *Nat. Mater.* **8**, 993–999 (2009).

353. Ding, J. *et al.* Ultra pH-sensitive polymeric nanovesicles co-deliver doxorubicin and navitoclax for synergetic therapy of endometrial carcinoma. *Biomater. Sci.* **8**, 2264–2273 (2020).

354. Zhang, L. *et al.* A polymeric nanocarrier with a tumor acidity-activatable arginine-rich (R9) peptide for enhanced drug delivery. *Biomater. Sci.* **8**, 2255–2263 (2020).

355. Luo, Q. *et al.* A biodegradable CO2-based polymeric antitumor nanodrug: Via a one-pot surfactant- and solvent-free miniemulsion preparation. *Biomater. Sci.* **8**, 2234–2244 (2020).

356. Del Valle, A. C., Su, C. K., Sun, Y. C. & Huang, Y. F. NIR-cleavable drug adducts of gold nanostars for overcoming multidrug-resistant tumors. *Biomater. Sci.* **8**, 1934–1950 (2020).

357. Zhang, X. *et al.* Construction of a tumor microenvironment pH-responsive cleavable PEGylated hyaluronic acid nano-drug delivery system for colorectal cancer treatment. *Biomater. Sci.* **8**, 1885–1896 (2020).

358. Lin, X. *et al.* Multifunctional theranostic nanosystems enabling photothermal-chemo combination therapy of triple-stimuli-responsive drug release with magnetic resonance imaging. *Biomater. Sci.* **8**, 1875–1884 (2020).

359. Shaw, Z. *et al.* Pseudo-branched polyester copolymer: An efficient drug delivery system to treat cancer. *Biomater. Sci.* **8**, 1592–1603 (2020).

360. Xie, L. *et al.* Construction of small-sized superparamagnetic Janus nanoparticles and their application in cancer combined chemotherapy and magnetic hyperthermia. *Biomater. Sci.* **8**, 1431–1441 (2020).

361. Shi, X. X. *et al.* Angiopep-2 conjugated nanoparticles loaded with doxorubicin for the treatment of primary central nervous system lymphoma. *Biomater. Sci.* **8**, 1290–1297 (2020).

362. Li, J. *et al.* Collaborative assembly of doxorubicin and galactosyl diblock glycopolymers for targeted drug delivery of hepatocellular carcinoma. *Biomater. Sci.* **8**, 189–200 (2020).

363. Zhang, T. *et al.* A bottlebrush-architectured dextran polyprodrug as an acidity-responsive vector for enhanced chemotherapy efficiency. *Biomater. Sci.* **8**, 473–484 (2020).

364. Wang, Y. *et al.* A Y1 receptor ligand synergized with a P-glycoprotein inhibitor improves the therapeutic efficacy of multidrug resistant breast cancer. *Biomater. Sci.* **7**, 4748–4757 (2019).

365. Zhang, Y. *et al.* A PEGylated alternating copolymer with oxidation-sensitive phenylboronic ester pendants for anticancer drug delivery. *Biomater. Sci.* **7**, 3898–3905 (2019).

366. Su, Z. *et al.* A pH and reduction dual-sensitive polymeric nanomicelle for tumor microenvironment triggered cellular uptake and controlled intracellular drug release. *Biomater. Sci.* **7**, 3821–3831 (2019).

367. Cheng, Y. A. *et al.* Enhanced drug internalization and therapeutic efficacy of PEGylated nanoparticles by one-step formulation with anti-mPEG bispecific antibody in intrinsic drug-resistant breast cancer. *Biomater. Sci.* **7**, 3404–3417 (2019).

368. Wu, Z. *et al.* PH/redox dual-responsive amphiphilic zwitterionic polymers with a precisely controlled structure as anti-cancer drug carriers. *Biomater. Sci.* **7**, 3190–3203 (2019).

369. Yoon, S. & Lee, T. G. Biological tissue sample preparation for time-of-flight secondary ion mass spectrometry (ToF–SIMS) imaging. *Nano Convergence* **5**, 24 (2018).

370. Bich, C. *et al.* Argon cluster ion source evaluation on lipid standards and rat brain tissue samples. *Anal. Chem.* **85**, 7745–7752 (2013).

371. Sjövall, P., Lausmaa, J. & Johansson, B. Mass spectrometric imaging of lipids in brain tissue. *Anal. Chem.* **76**, 4271–4278

(2004).

372. Nygren, H., Börner, K., Hagenhoff, B., Malmberg, P. & Månsson, J. E. Localization of cholesterol, phosphocholine and galactosylceramide in rat cerebellar cortex with imaging TOF-SIMS equipped with a bismuth cluster ion source. *Biochim. Biophys. Acta - Mol. Cell Biol. Lipids* **1737**, 102–110 (2005).

373. Touboul, D., Brunelle, A. & Laprévote, O. Mass spectrometry imaging: Towards a lipid microscope? *Biochimie* **93**, 113–119 (2011).

374. Lazar, A. N. *et al.* Time-of-flight secondary ion mass spectrometry (TOF-SIMS) imaging reveals cholesterol overload in the cerebral cortex of Alzheimer disease patients. *Acta Neuropathol.* **125**, 133–144 (2013).

375. De Sousa Cavalcante, L. & Monteiro, G. Gemcitabine: Metabolism and molecular mechanisms of action, sensitivity and chemoresistance in pancreatic cancer. *European Journal of Pharmacology* **741**, 8–16 (2014).

376. Eccles, S. A. *et al.* Critical research gaps and translational priorities for the successful prevention and treatment of breast cancer. *Breast Cancer Res.* **15**, 1–37 (2013).

377. Ushijima, K. Treatment for recurrent ovarian cancer - At first relapse. *J. Oncol.* **2010**, (2010).

378. Hellinger, M. D. & Santiago, C. A. Reoperation for recurrent colorectal cancer. *Clinics in Colon and Rectal Surgery* **19**, 228–236 (2006).

379. Wu, M. *et al.* Vincristine and temozolomide combined chemotherapy for the treatment of glioma: a comparison of solid lipid nanoparticles and nanostructured lipid carriers for dual drugs delivery. *Drug Deliv.* **23**, 2720–2725 (2016).

380. Xu, Y. *et al.* The synergic antitumor effects of paclitaxel and temozolomide co-loaded in mPEG-PLGA nanoparticles on glioblastoma cells. *Oncotarget* **7**, 20890–901 (2016).

381. Chou, T. C. Drug combination studies and their synergy

quantification using the chou-talalay method. *Cancer Research* **70**, 440–446 (2010).

382. Chou, T. C. Theoretical basis, experimental design, and computerized simulation of synergism and antagonism in drug combination studies. *Pharmacol. Rev.* **58**, 621–681 (2006).

383. Chou, T. C. & Talalay, P. Quantitative analysis of dose-effect relationships: the combined effects of multiple drugs or enzyme inhibitors. *Adv. Enzyme Regul.* **22**, 27–55 (1984).

384. Lenting, K., Verhaak, R., ter Laan, M., Wesseling, P. & Leenders, W. Glioma: experimental models and reality. *Acta Neuropathologica* **133**, 263–282 (2017).

385. Szakács, G., Paterson, J. K., Ludwig, J. A., Booth-Genthe, C. & Gottesman, M. M. Targeting multidrug resistance in cancer. *Nat. Rev. Drug Discov.* **5**, 219–234 (2006).

386. Decleves, X., Amiel, A., Delattre, J.-Y. & Scherrmann, J.-M. Role of ABC Transporters in the Chemoresistance of Human Gliomas. *Curr. Cancer Drug Targets* **6**, 433–445 (2006).

387. Jabr-Milane, L. S., van Vlerken, L. E., Yadav, S. & Amiji, M. M. Multi-functional nanocarriers to overcome tumor drug resistance. *Cancer Treatment Reviews* **34**, 592–602 (2008).

388. Dong, X. & Mumper, R. J. Nanomedicinal strategies to treat multidrug-resistant tumors: Current progress. *Nanomedicine* **5**, 597–615 (2010).

389. Robertson, F. L., Marqués-Torrejón, M. A., Morrison, G. M. & Pollard, S. M. Experimental models and tools to tackle glioblastoma. *DMM Disease Models and Mechanisms* **12**, (2019).

390. Decarvalho, A. C. *et al.* Discordant inheritance of chromosomal and extrachromosomal DNA elements contributes to dynamic disease evolution in glioblastoma. *Nat. Genet.* **50**, 708–717 (2018).

391. Boj, S. F. *et al.* Organoid models of human and mouse ductal pancreatic cancer. *Cell* **160**, 324–338 (2015).

392. Gao, D. *et al.* Organoid cultures derived from patients with advanced prostate cancer. *Cell* **159**, 176–187 (2014).

393. Broutier, L. *et al.* Human primary liver cancer-derived organoid cultures for disease modeling and drug screening. *Nat. Med.* **23**, 1424–1435 (2017).

394. Sachs, N. *et al.* A Living Biobank of Breast Cancer Organoids Captures Disease Heterogeneity. *Cell* **172**, 373-386.e10 (2018).

395. Lee, S. H. *et al.* Tumor Evolution and Drug Response in Patient-Derived Organoid Models of Bladder Cancer. *Cell* **173**, 515-528.e17 (2018).

396. Kopper, O. *et al.* An organoid platform for ovarian cancer captures intra- and interpatient heterogeneity. *Nat. Med.* **25**, 838–849 (2019).

397. Yan, H. H. N. *et al.* A Comprehensive Human Gastric Cancer Organoid Biobank Captures Tumor Subtype Heterogeneity and Enables Therapeutic Screening. *Cell Stem Cell* **23**, 882-897.e11 (2018).

398. Hubert, C. G. *et al.* A three-dimensional organoid culture system derived from human glioblastomas recapitulates the hypoxic gradients and cancer stem cell heterogeneity of tumors found in vivo. *Cancer Res.* **76**, 2465–2477 (2016).

399. Jacob, F. *et al.* A Patient-Derived Glioblastoma Organoid Model and Biobank Recapitulates Inter- and Intra-tumoral Heterogeneity. *Cell* **180**, 188-204.e22 (2020).

400. Bian, S. *et al.* Genetically engineered cerebral organoids model brain tumor formation. *Nat. Methods* **15**, 631–639 (2018).

401. Ogawa, J., Pao, G. M., Shokhirev, M. N. & Verma, I. M. Glioblastoma Model Using Human Cerebral Organoids. *Cell Rep.* **23**, 1220–1229 (2018).

402. Linkous, A. *et al.* Modeling Patient-Derived Glioblastoma with Cerebral Organoids. *Cell Rep.* **26**, 3203-3211.e5 (2019).

403. Linkous, A. & Fine, H. A. Generating Patient-Derived Gliomas within Cerebral Organoids. *STAR Protoc.* **1**, 100008 (2020).

404. Camp, J. G. & Treutlein, B. Human development: Advances in mini-brain technology. *Nature* **545**, 39–40 (2017).

Chapter 6 Appendices

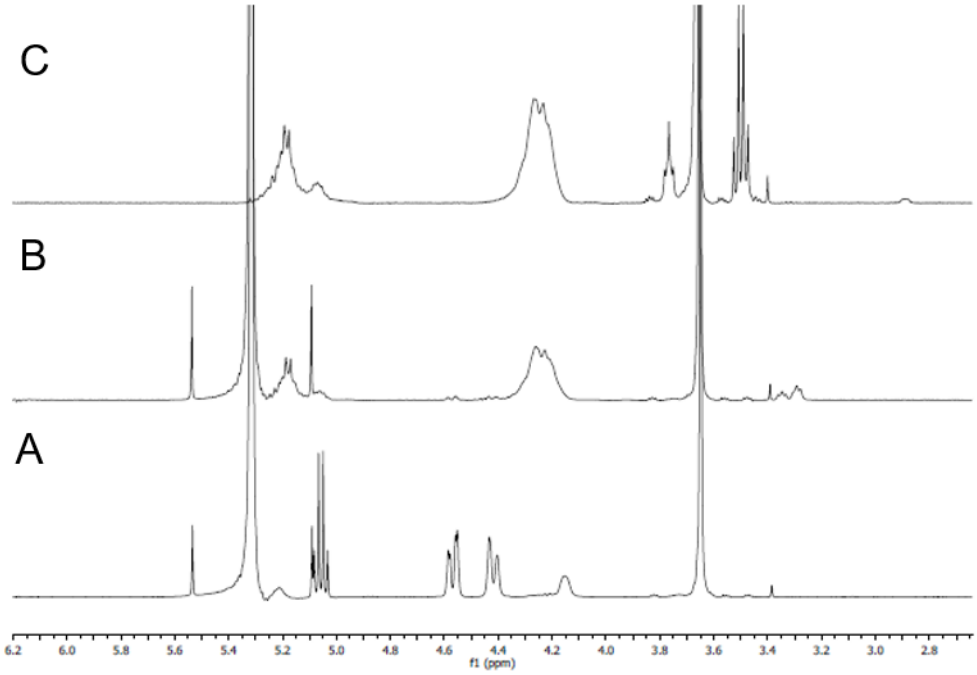


Figure A 1 Representative ^{1}H NMR graph (400 MHz, $CDCl_3$) for the ROP of lactide and tBSC initiated by $mPEG_{5000}$ (P2), showing quantitative polymerisation of both lactide and tBSC after 15 minutes. (A) time = 0 minutes, (B) time = 15 minutes, and (C) post purification.

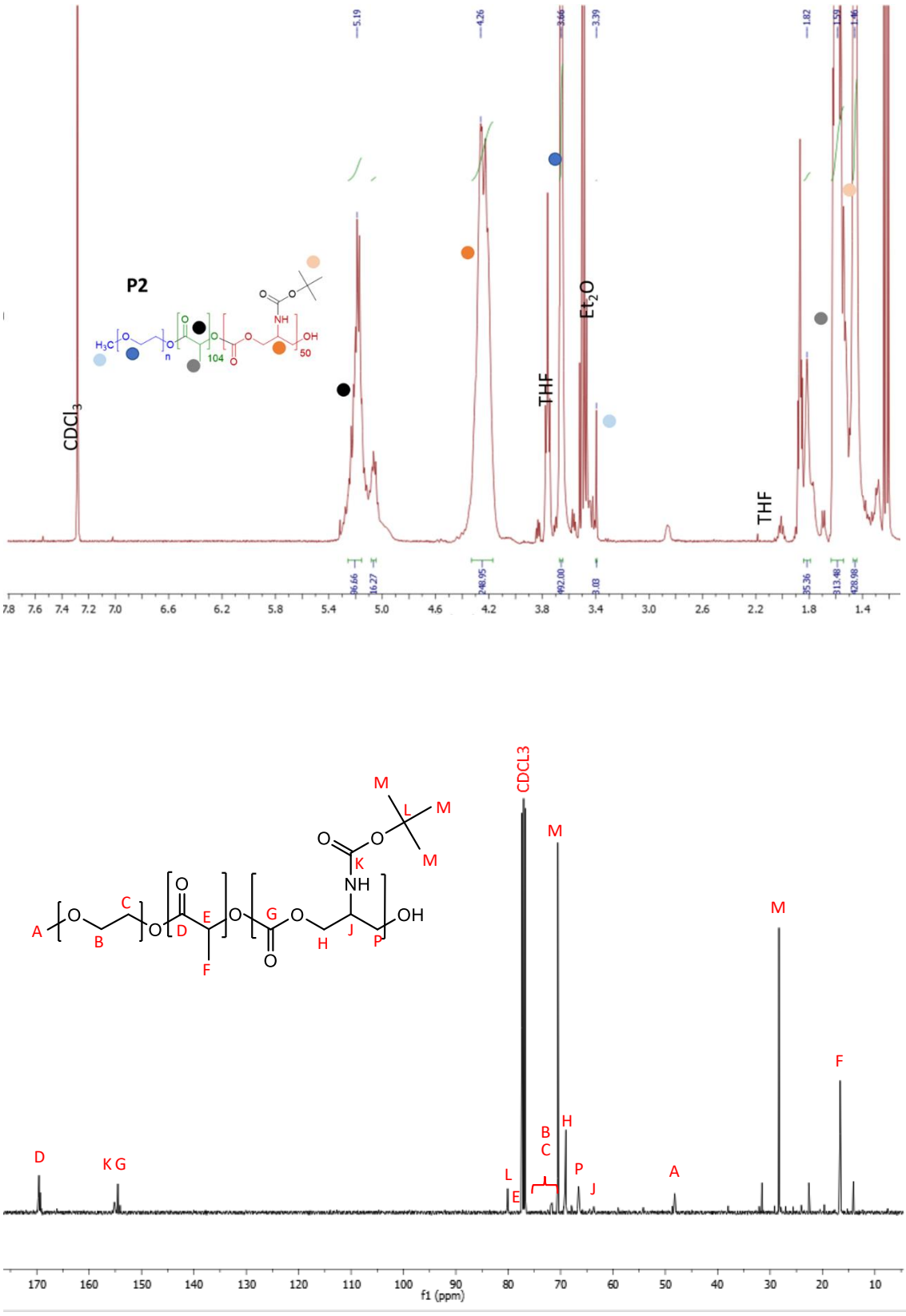


Figure A 2 *^{1}H-NMR and ^{13}C-NMR spectrum with integrations of P2 ($mPEG_{5000}$-$(LA)_{50}$-$(tBSC)_{50}$) as model polymer.*

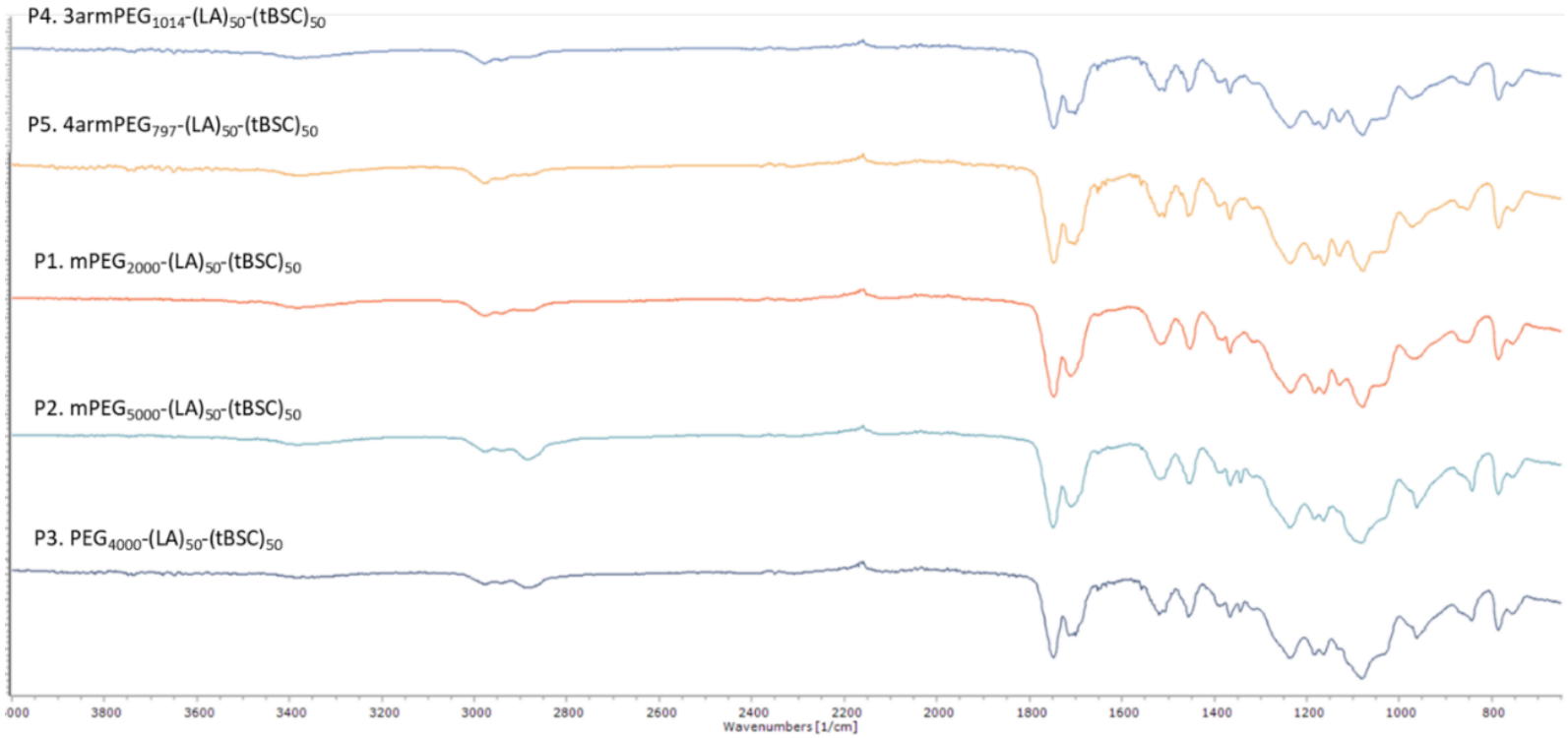


Figure A 3 ATR-IR spectra of the five PEGylated ester-carbonate co-polymers showing typical peaks of both ester and carbonate functionalities. In particular, C-H stretching in the region between 2900 -2800, $C=O_{ester}$ and $C=O_{carbonate}$ in the region of 1750 -1680 and the C-O-C bending of the ester and ether (PEG) functionalities at 1100 cm^{-1}.

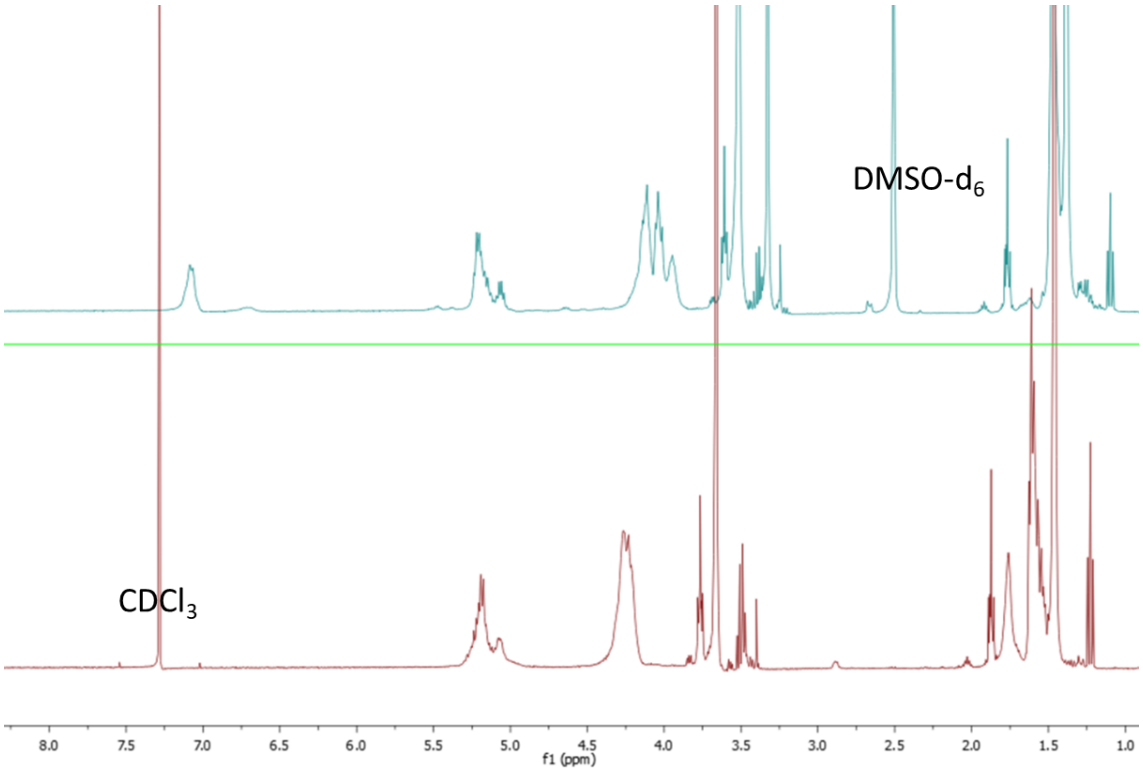


Figure A 4 *^{1}H-NMR spectra of P2 co-polymer in deuterated chloroform (bottom) and deuterated DMSO (top) in order to show peak variations in the two solvents.*

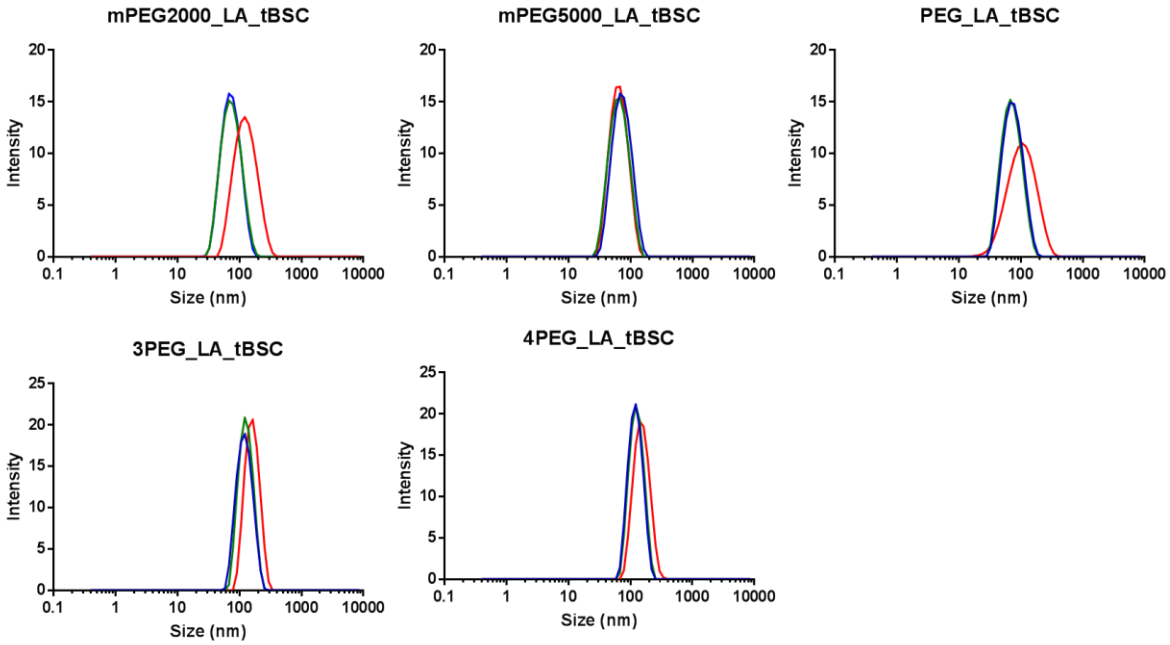


Figure A 5 *DLS trace of the five PEGylated ester-carbonate co-polymers in nanoparticle form, showing uniform size across the three independent cell viability studies.*

DNA-System	DNA-criteria GIN-8 p11 CL181019_026	DNA-criteria GIN-8 p33 CL181019_026	DNA-criteria T8.3 CL181019_014	DNA-criteria GIN-28 p11 CL181019_026	DNA-criteria GIN-28 p33 CL181019_026	DNA-criteria T28.3 CL181019_025	DNA-criteria GIN-31 p11 CL181019_026	DNA-criteria GIN-31 p31 CL181019_027	DNA-criteria T31.5 CL181019_030
AM	X, X	X, X	X, X	X, Y	X, Y	X, Y	X, X	X, X	X, X
D3S1358	15, 16	15, 16	15, 16	14, 17	14, 17	14, 17	16, 18	16, 18	16, 18
D1S1656	12, 16	12, 16	12, 16	12, 16	12, 16	12, 16	12, 15	12, 15	12, 15
D6S1043	14, 18	14, 18	14, 18	11, 13	11, 13	11, 13	12, 18	12, 18	12, 18
D13S317	12, 12,	12, 12,	12, 12,	11, 12	11, 12	11, 12	11, 13	11, 13	13, 13
Penta E	6, 9	6, 9	6, 9	7, 17	7, 17	7, 17	7, 12	7, 12	7, 12
D16S539	12, 12	12, 12	12, 12	9, 12	9, 12	9, 12	10, 11	10, 11	10, 11
D18S51	16, 17	16, 17	16, 17	14, 17	14, 17	14, 17	17, 18	16, 17, 18	17, 18
D2S1338	17, 19	17, 19	17, 19	19, 23	19, 23	19, 23	19, 25	11, 19, 25	19, 25
CSF1PO	11, 11	11, 11	11, 11	11, 13	11, 13	11, 13	11, 12	11, 12	11, 12
Penta D	12, 13	12, 13	12, 13	12, 14	12, 14	12, 13, 14	11, 12	11, 12	11, 12
TH01	9, 9	9, 9	9, 9	6, 9.3	6, 9.3	6, 9.3	6, 9	6, 9	6, 9
vWA	17, ?	17, 17	17, 17	14, 15	14, 15	14, 15	14, 18	14, 15, 18, 21	14, 18
D21S11	30, 30	30, 30	30, 30	27, 33	27, 33	27, 33	29, 29	29, 29	29, 29
D7S820	9, 10	9, 10	9, 10	8, 10	8, 10	8, 10	7, 10	7, 10	7, 10
D5S818	12, 13	12, 13	12, 13	11, 12	11, 12	11, 12	11, 12	11, 12	11, 12
TPOX	8, 11	8, 11	8, 11	8, 11	8, 11	8, 11	9, 9	9, 9	9, 9
D8S1179	10, 13	10, 13	10, 13	10, 14	10, 14	10, 14	11, 13	11, 13, 14.1	11, 13
D12S391	18, 18	18, 18	18, 18	20, 21	20, 21	20, 21	17, 23	16, 17, 22.3, 23	23, 23
D19S433	13, 13	13, 13	13, 13	14, 14	14, 14	13, 14	12, 15	12, 13.1, 15	12, ?
FGA	21, 22	21, 22	21, 22	23, 25	23, 25	23, 25	22, 26	19.3, 22, 26	22, 26

Figure A 6 ***Single tandem repeat genotyping of patient-derived GBM cell lines.*** *Cell line authentication of the GIN-8, GIN-28, and GIN-31 patient-derived primary lines isolated from the GBM invasive edge. DNA was isolated from each sample and genetic characteristics determined by PCR-single-locus-technology, utilizing 21 independent DNA loci. The GIN-8 line compared across two passages (p11 and p33), showed identical STR genotypes, which fully matched the STR genotype from primary invasive margin GBM tissue (T8.3) from which the cells were derived. The GIN-28 line compared across two passages (p11 and p33), showed identical STR genotypes, with 20/21 DNA systems matching the STR genotype from primary invasive margin GBM tissue (T28.3) from which the cells were derived. STR genotypes for the GIN-31 line compared across two passages (p11 and p33), showed 19/21 (90.5%) p11 and 14/21 (66.7%) p33 similarity to primary invasive margin GBM tissue (T31.5) from which the cells were derived. Minimal genotypic changes between p11 and p33 likely reflect the acquisition of DNA variants as cells adapt to an in vitro culture environment as passages increase. Collectively these results confirm that the cell lines utilised in this study have not been cross-contaminated with any other cell line and the primary lines derived from the GBM invasive margin broadly retain the genotype of the tumour.*